

LEVEL #

12



RADC-TR-79-359
Final Technical Report
January 1980

AN ANALYTICAL STUDY OF WAVE PROPAGATION THROUGH FOLIAGE

Applied Science Associates, Inc.

Dr. Gary S. Brown
William J. Curry

ADA 084348

APPROVED FOR PUBLIC RELEASE; DISTRIBUTION UNLIMITED

SDIC
ELECTE
MAY 20 1980
A

ROME AIR DEVELOPMENT CENTER
Air Force Systems Command
Griffiss Air Force Base, New York 13441

FILE COPY

80 5 19 198

This report has been reviewed by the RADC Public Affairs Office (PA) and is releasable to the National Technical Information Service (NTIS). At NTIS it will be releasable to the general public, including foreign nations.

RADC-TR-79-359 has been reviewed and is approved for publication.

APPROVED: *Harry H. Godlewski, Jr.*
HARRY GODLEWSKI, Jr., 1LT, USAF
Project Engineer

APPROVED: *Allan C. Schell*
ALLAN C. SCHELL
Chief, Electromagnetic Sciences Division

FOR THE COMMANDER: *John P. Huss*
JOHN P. HUSS
Acting Chief, Plans Office

If your address has changed or if you wish to be removed from the RADC mailing list, or if the addressee is no longer employed by your organization, please notify RADC (EEC), Hanscom AFB MA 01731. This will assist us in maintaining a current mailing list.

Do not return this copy. Retain or destroy.

UNCLASSIFIED

SECURITY CLASSIFICATION OF THIS PAGE (When Data Entered)

REPORT DOCUMENTATION PAGE		READ INSTRUCTIONS BEFORE COMPLETING FORM	
1. REPORT NUMBER	2. GOVT ACCESSION NO.	RECIPIENT'S CATALOG NUMBER	
18) RADC TR-79-359	AD-A084348		
3. TITLE (and Subtitle)		4. TYPE OF REPORT AND PERIOD COVERED	
AN ANALYTICAL STUDY OF WAVE PROPAGATION THROUGH FOLIAGE.		9) Final Technical Report. 9 Sep 78 - 30 Sep 79	
7. AUTHOR(s)		14) PERFORMING ORG. REPORT NUMBER	
3) Gary S. Brown William J. Curry		ASA-79(AF)-1	
9. PERFORMING ORGANIZATION NAME AND ADDRESS		15) CONTRACT OR GRANT NUMBER(s)	
Applied Science Associates, Inc. 105 East Chatham Apex NC 27502		F19628-78-C-0159	
11. CONTROLLING OFFICE NAME AND ADDRESS		10. PROGRAM ELEMENT, PROJECT, TASK AREA & WORK UNIT NUMBERS	
Deputy for Electronic Technology (RADC/EEC) Hanscom AFB MA 01731		62702F 46001529	
14. MONITORING AGENCY NAME & ADDRESS (if different from Controlling Office)		12. REPORT DATE	
Same		17) 15) 11) January 1980	
16. DISTRIBUTION STATEMENT (of this Report)		13. NUMBER OF PAGES	
Approved for public release; distribution unlimited		200	
17. DISTRIBUTION STATEMENT (of the abstract entered in Block 20, if different from Report)		15. SECURITY CLASS. (of this report)	
Same		UNCLASSIFIED	
18. SUPPLEMENTARY NOTES		15a. DECLASSIFICATION/DOWNGRADING SCHEDULE	
RADC Project Engineer: Harry H. Godlewski, 1LT, USAF (EEC)		N/A	
19. KEY WORDS (Continue on reverse side if necessary and identify by block number)			
Synthetic Aperture Radar Wave Propagation Foliage Penetration			
20. ABSTRACT (Continue on reverse side if necessary and identify by block number)			
A model is developed for the effect of foliage on the average or coherent field propagating in the foliage and parallel to the foliage-air or foliage-ground interfaces. The model is based upon a number of assumptions which considerably reduce its complexity to the point where it can be used by systems designers in evaluating the effect of foliage on Synthetic Aperture Radars operating near grazing incidence. The model is hypothesized to be valid in the frequency range of about 0.1 to 1.5 GHz for deciduous trees and from 0.1 to about 3 GHz for needle bearing trees. Comparisons with available measurements indicate			

S/C 394248

Handwritten signature

UNCLASSIFIED

SECURITY CLASSIFICATION OF THIS PAGE(When Data Entered)

a surprisingly high degree of agreement considering the simplicity of the model. Suggestions for future analytical and experimental efforts are presented.

Accession For	
NTIS Grant	<input checked="" type="checkbox"/>
DDC TAB	<input type="checkbox"/>
Unannounced	<input type="checkbox"/>
Justification	
By _____	
Distribution/	
Availability Codes	
Dist.	Avail and/or special
A	

UNCLASSIFIED

SECURITY CLASSIFICATION OF THIS PAGE(When Data Entered)

TABLE OF CONTENTS

	Page
1.0 INTRODUCTION	1
1.1 Summary of Results.	3
2.0 BACKGROUND	6
2.1 Continuous vs. Discrete Media Approaches.	7
2.1.1 General Propagation Assumptions.	8
2.2 Relevant Foliage Characteristics and Simplifications.	11
3.0 RAYLEIGH-EFFECTIVE VOLUME (REV) MODEL.	12
3.1 Model Rationale	13
3.2 Model Development	19
3.2.1 Propagation Through Small Cylinders and Discs.	21
3.2.2 Inclusion of Scattering Losses	35
3.2.3 The Effective Fractional Volume Of Foliage	45
3.2.4 The Dielectric Constant And Loss Factor For Wood	50
3.3 REV Model Calculations.	64
4.0 MEASUREMENTS AND MODEL COMPARISONS	73
4.1 Review of Measurements.	73
4.1.1 Jansky and Bailey [15]	74
4.1.2 Saxton and Lane [16]	78
4.1.3 Stutzman, <u>et al.</u> [6]	80
4.1.4 Georgia Institute of Technology [17]	81
4.2 A Comparison of the Model with Measurements	83
5.0 CONCLUSIONS AND SUGGESTED FUTURE INVESTIGATIONS.	86
5.1 Modeling.	87
5.2 Measurements.	89
REFERENCES.	95
APPENDIX A: COHERENT WAVE PROPAGATION THROUGH A SPARSE RANDOM COLLECTION OF SPHERICAL PARTICLES.	A-1
APPENDIX B: DERIVATION OF A RELATIONSHIP REQUIRED IN SECTION 3.2.2	B-1
APPENDIX C: ESTIMATION OF MODEL PARAMETERS FROM FOLIAGE STATISTICAL DATA	C-1

TABLE OF CONTENTS

	Page
APPENDIX D: DIELECTRIC PROPERTIES OF TREES AT RADIO FREQUENCIES. . . .	D-1
APPENDIX E: DIELECTRIC CONSTANT MEASUREMENT METHODS WITH APPLICATION TO GREEN WOOD AT GHz FREQUENCIES	E-1
APPENDIX F: THE MEASUREMENT OF APPLICABLE FOLIAGE STATISTICS	F-1

EVALUATION

This document contains the results of an analytical study conducted between 9 September 1978 and 30 September 1979. The study effort was initiated in address to the Foliage Screening problem (ref: TPO R11B, Radar). The expected application is to the development of a complete, reliable and practical analytical tool for the prediction and evaluation of foliage penetration radar performance. The study has significantly extended the horizons of theoretical understanding with regard to wave propagation through random medium with specific application to foliage penetration. Study results indicate a strong need for further theoretical and field measurement work in this area in order to meet the intended goal.

Harry H. Godlewski, Jr.

HARRY H. GODLEWSKI, Jr., 1LT, USAF
Project Engineer

1.0 INTRODUCTION

The quantitative description of the effects of the natural environment on electromagnetic wave propagation and scattering represents a research area where much work remains to be accomplished. Since electromagnetic theory is a particularly detailed subset of boundary value mathematics and physics, electromagnetic problems are not easily solved in the presence of a hodge-podge of objects or surfaces such as is typical of natural terrain or vegetation. However, since most radiating systems must operate near to or in the presence of such an environment, it is essential that we attempt to understand the effects of these perturbing media. Within the last twenty or so years, significant advances have been made in combining probabilistic mathematics with asymptotic electromagnetic theory to obtain insight into this very difficult problem. In fact, it appears that this is truly the only feasible approach to the environmental effects problem.

This particular study comprises an effort to solve or model one of the more difficult of these environmental effects problems. More specifically, this investigation is concerned with obtaining a model for the effects of foliage upon the target detection and imaging capabilities of a Synthetic Aperture Radar (SAR). This problem has obvious military applications and it is also of interest to the remote sensing of terrain and water resources. Since the successful operation of a SAR is based upon the coherency of the transmitted and the received field over the spatial and temporal extent of the synthesized aperture, we must direct our attention toward the effects of foliage on the average or coherent field. The coherent field is defined as follows. Any electromagnetic field \vec{E} which fluctuates about some mean value $\langle \vec{E} \rangle$ may be written as the sum of its mean value and its zero mean fluctuation \vec{E}_f , i.e.

$$\vec{E} = \langle \vec{E} \rangle + \vec{E}_f$$

The power in this field averaged over all possible values is given by $\langle |\vec{E}|^2 \rangle$

or

$$\langle |\vec{E}|^2 \rangle = |\langle \vec{E} \rangle|^2 + \langle |\vec{E}_f|^2 \rangle$$

since $\langle \vec{E}_f \rangle = 0$. The average field $\langle \vec{E} \rangle$ is the coherent field and $|\langle \vec{E} \rangle|^2$ is the coherent power. The term $\langle |\vec{E}_f|^2 \rangle$ is the incoherent power or the variance of the field. It should be noted that if the coherent power is small with respect to the incoherent power, the total average power is nearly equal to the incoherent power. In a lossless random medium, the attenuation of the coherent power represents a transfer of power to the incoherent term since energy must be conserved. It should be noted that the coherent field is not a random variable; rather it is the mean or first moment of the random field.

Before continuing it is worthwhile addressing at this point a question that is often asked about the operation of a SAR in the presence of foliage masking a target. This question is as follows; is it ever possible that the total target scattered field received by a SAR is sufficiently correlated over the spatial extent of the synthetic aperture to be useful in forming the image? This question is equivalent to asking if \vec{E}_f is sufficiently correlated over the extent of the synthesized aperture as to appear as a coherent field. To answer the question we need to know the correlation between the target scattered fields at the beginning and end of the synthesized aperture. This correlation is determined by the correlation of these two fields as they exit the foliage which, in turn, is determined by the spatial separation of the exit point of these fields, the wavelength, and the scattering medium. Ishimaru [1, vol. 1] has shown that when the random medium comprises discrete particles or objects which are small in terms of the electromagnetic wavelength, the

fluctuating component of the random field decorrelates within a wavelength separation. Thus, only for relatively low frequencies will the total field be correlated over the full extent of the synthesized aperture. Actually the situation is somewhat worse than this because if the target is large in terms of a wavelength, the total field will not even be correlated over the full extent of the target. In fact this appears to be more of a limitation than field correlation over the synthetic aperture especially for SAR's operating at long ranges and near grazing incidence, e.g. where the spatial separation between the two extreme fields forming the aperture as they exit the foliage is possibly small in terms of a wavelength.

From the above discussion we can conclude that it is not reasonable to expect that the total target scattered field will be coherent over the full synthetic aperture of the SAR. Thus, we should direct our attention toward the effects of the foliage on the average or coherent field scattered by the target since this is the field that the SAR will use to image the target. The remainder of this report is devoted to obtaining a simple model for the attenuation and phase retarding effects of foliage on the coherent field.

1.1 Summary of Results

The primary result of this study is a model for the attenuation and phase retarding effects of foliage on the average or coherent field propagating through the foliage. The model, which we call the Rayleigh-Effective Volume or REV model, is based upon the hypothesis that it is the smaller components of the forest or foliage which have the greatest impact upon the coherent field. This model is not based entirely upon supposition because there are foliage propagation data which indicate that it is the smaller foliage components which are most effective in the attenuation process. Using these measured results we conclude that the fractional volume of wood that is important

to attenuation consists of those cylindrical components having a diameter to wavelength ratio of less than one-half. We also assume that these effective scatterers/absorbers can be electromagnetically modeled using Rayleigh or quasi-static techniques.

We next approximately solve the Foldy-Twersky integral for the propagation constant of the coherent field passing through a random collection of Rayleigh cylinders. In the vicinity of 100 MHz, we conclude that all the woody components of the forest may be considered as Rayleigh in their scattering characteristics. Due to the large vertically oriented trunks, we conclude that the probability density function for the orientation of the cylinders representing the woody components is skewed toward the vertical. This is shown to give rise to a larger attenuation rate for vertically polarized fields than horizontally polarized ones. In the neighborhood of 500 MHz (based upon propagation measurements), we conclude that a sufficient number of large tree trunks have been eliminated from the effective fractional volume as to cause the orientation density function to become uniform over the upper hemisphere. Thus, above 500 MHz all polarization differences disappear in the model.

Because of the limitations imposed by the Rayleigh or quasi-static field approximation, it is necessary to make an ad hoc correction for the scattering effects of the small foliage components and this is accomplished. We also present a relatively crude model for estimating the effective fractional volume of wood based upon forest stand table data and the criterion of cylinder diameter to wavelength ratio of less than one-half. Finally, we also develop a model for the complex dielectric constant of green wood over the frequency range of interest to this study, i.e. 0.1 to 3 GHz.

At this point in the development, the model accounts for all of the woody components in the forest and needles in the case of needle bearing trees. We

show how leaves can be formally accounted for but we were unable to estimate the effective volume of leaves and our analysis indicates that leaves should start to become important near 1.5 GHz. Thus for leaf bearing trees the model is limited to less than 1.5 GHz; for needle bearing trees, the model fails above 10 GHz because the effective fractional volume rapidly approaches zero.

When we compare the absorption dependent part of the propagation constant with total average power measurements, we obtain rather surprisingly good agreement. In reviewing some of the measurements, we detect the distinct possibility of a lateral wave contribution which causes an error in the measurement, i.e. it leads to a smaller attenuation constant. Those measurements which are suspect do, in fact, fall below the model predictions. In general, the model shows much better agreement with measurements than we had anticipated.

We purposely approached this problem using a very simple theory which combined some of the early work of Pounds and Lagrone [2] with random wave propagation theory [1]. We did this for two reasons. First, we hoped to provide systems designers with a relatively simple model which would enable them to obtain reasonable estimates of the effects of foliage on SAR (and other types of radars) performance. Second, we did not feel that the time allotted to this study was sufficient to develop a completely rigorous model nor were we convinced that all the input data required by such a model would ever practically be available. As a consequence, the Rayleigh-Effective-Volume Model has a number of analytical shortcomings which eventually should be resolved. To this end, we have suggested an extensive experimental program to obtain basic data on the attenuation of the coherent field. Before such a program can be initiated there are a number of problems that must be solved and we have suggested a feasibility study to resolve these issues. We feel very strongly

about the need for a measurements program because of the analytical complexity of the problem. That is, we feel that experimental results should guide the theorist and not just provide a benchmark against which theories are tested.

We also suggest further analytical efforts and we start on this problem by obtaining an exact solution of the Foldy-Twersky integral equation for the propagation constant of the average field in a sparsely populated volume containing spherical objects. The approach used can be easily applied to any collection of similarly aligned objects which individually do not depolarize the incident field. The extension to randomly oriented objects is more difficult but we feel that is certainly worth further study.

In short, we feel that the Rayleigh-Effective Volume model can provide engineering estimates of the attenuation and phase retarding effects of foliage. However, because of certain shortcomings of the model, we strongly urge further experimental and analytical studies of this problem.

2.0 BACKGROUND

In order to accurately predict the impact of a foliated environment on the performance of a synthetic aperture radar (SAR), one must first understand the effect of the foliage upon the propagation and scattering of an electromagnetic field. Because of the complexity of the foliage, this latter problem is best addressed using the techniques of random wave propagation theory. This means that, at best, the propagating electromagnetic field can be described by a probability density function and a spatial-temporal correlation function or, more practically, a few of the statistical moments of the field such as the mean and variance. This of course does not help the systems designer who is looking for pulse-by-pulse behavior; however, it does provide performance bounds which can be effectively used during systems design and evaluation.

Bearing in mind the fundamental characteristics of a SAR, there are four general means by which an intervening layer of foliage can effect the detection of targets. The primary one is the attenuation of the transmitted and target scattered field; the second is the dispersive characteristics of the foliage, the third is the spatial decorrelation distance of a field propagating in or through foliage, and the last is the ratio of the signal strength backscattered from the embedded target to the signal strength backscattered from the range-distributed foliage. The first and last of the above properties determine, to a large degree, the minimum detectable target size or type for a given depth of foliage. The second property impacts the accurate location of the target while the third determines the maximum synthesized aperture available for full and complete coherent integration. The work reported here is concerned primarily with estimating the attenuation and phase delay imparted to the average field by the foliage. As noted in Section 1, we do not feel that the total target scattered field will be sufficiently coherent over the full synthetic aperture to be useful except at very low frequencies. Even in this case, we question the coherency properties of the incident and scattered fields over the full extent of the target. Thus, the attenuation and phase characteristics appear to be the most useful in estimating the performance of a SAR when viewing targets immersed in foliage.

2.1 Continuous vs. Discrete Media Approaches

Having isolated attenuation and phase delay of the mean or average field as the parameters of interest, it is necessary to establish a realistic mathematical model for the propagation and scattering of an electromagnetic field by a foliated environment. As a first step one must choose between models for propagation through continuous or discrete random media. Although foliage is a discrete random medium, there are some valid reasons for modeling it as a

medium having a continuously varying dielectric constant. Most of these reasons center around the fact that propagation through continuously varying random media is better developed from an analytical point of view and possibly better understood also. In fact, one often finds discrete theories referenced to equivalent continuous theories in order to take advantage of the level of understanding of continuous problems. Koth and Elachi [3] have even used continuous theory to predict the attenuation of the mean field propagating in a discrete collection of rocks. Collin [4] has shown that when a plane wave is incident upon a half-space having a dielectric constant which fluctuates in one dimension and is characterized by an exponential spatial correlation, two propagating waves can be excited at the interface. Collin's work is particularly attractive in view of its similarity to the problem considered here.

The primary difficulty with using continuous theories for discrete problems is that the continuous theory assumes that one has knowledge of the mean, variance, and spatial correlation function of the complex dielectric constant. In actual fact these quantities are completely unknown and one can only guess at their true value. For example, in the case of the spatial correlation function of the complex dielectric constant fluctuations, one often finds that this electro-physical property of the medium is chosen more for analytical convenience than physical realizability. Thus, although the theories dealing with propagation through continuous media are at a more advanced stage of development and understanding, the inputs to these theories are not known for the discrete problem. Consequently, the models used in this analysis will adhere to the discrete nature of the foliage.

2.1.1 General Propagation Assumptions

Having decided that this problem is most meaningfully approached using the theories governing the propagation of electrognetic fields through discrete

random media, it is next necessary to determine exactly what is needed to derive the attenuation and phase delay of the mean field. Since the complex propagation constant is primarily governed by the constituents of the medium and not the boundaries, the infinite boundary problem can shed light on the behavior of the propagation constant of the mean field. That is, as a first step, the foliage is assumed to fill all space and the propagation constant of the mean field in this environment is determined. Then, if the free space-to-foliage interface can be considered to be planar and if there are no secondary propagating waves excited at the interface (such as in the continuous medium problem [4]), one can estimate the reduction in the mean field amplitude across the planar interface via conventional Fresnel theory. The average complex dielectric constant of the random medium is determined from the propagation constant of the average field in the medium.

Implicit in the above approach are two subtle points which require further consideration. The first has to do with the assumption of a planar free space-to-foliage interface while the second is that the propagation constant may well depend upon the direction of propagation or the angle of incidence. The assumption of a planar free space-to-foliage interface is one of mathematical simplification whereas the actual boundary is anything but planar. The difficulty associated with estimating boundary effects in a problem of this nature stems primarily from the fact that the foliage boundary is diffuse as opposed to a distinct surface separating two well defined continuous media such as the ocean surface. Thus, conventional rough surface scattering phenomenon such as specular point reflection and Bragg resonance scattering are difficult to apply to this problem. If, however, the equivalent complex dielectric constant for the average field is not much different from free space, the boundary effects cannot be too important simply because there is not a significant change in the

constitutive parameters across the boundary. This means that backscatter from the foliage will be due primarily to incoherent scattering within the medium and will not result from the free space-to-foliage interface. This hypothesis is confirmed to a degree by the measurements of scattering from crop foliage by the University of Kansas in which volume scattering was estimated to be the primary mechanism. In summary, the assumption of a planar boundary is not considered to be unreasonable primarily because of the low dielectric contrast between free space and the average medium, i.e. the medium pertaining to the mean or average field.

The fact that the propagation constant may depend upon the direction of travel and polarization of the mean field is due to the anisotropic properties of the average medium. For foliage, anisotropy in the mean will be a result of either the shape, orientation, or complex dielectric constant of the constituents comprising the foliated environment. This point will be discussed in more detail later in the report. In view of the conventional usage of SAR systems, it is not unreasonable to assume that the SAR is operating very near grazing incidence. For the analysis to follow, it will be assumed that the SAR is operating, for all intents and purposes, at grazing incidence. This means that the random propagation problem can be treated as if the direction of travel of the incident field within the foliage is parallel to the free space-to-foliage planar boundary. An additional advantage of this simplification is that analytical results can be compared with point-to-point communication attenuation measurements. Certainly the few degrees difference between near grazing incidence and exact grazing incidence should not drastically alter the computed values of the propagation constant of the average field, so this would appear to be a reasonable simplification.

At this point it is probably wise to summarize the general approach and

assumptions that will be employed in this analysis. First, theories pertaining to the propagation of the average field in a discrete random medium will be used. Second, propagation in an infinite unbounded medium comprising typical foliage constituents will be analyzed to determine the propagation constant of the average field. Free space-to-foliage boundary effects on the average field will be ignored although they can be easily accounted for if it is assumed that the boundary is planar and no secondary propagating fields are excited at the interface. Finally, it is assumed that propagation in the medium is parallel to the free space-to-foliage interface or sufficiently close to the actual direction of propagation of a SAR transmitted field to be the only direction of interest.

As this report progresses additional hypotheses and assumptions will be employed. However, the above are considered special because they are common to all of the analyses to follow.

2.2 Relevant Foliage Characteristics and Simplifications

The previous sections have dealt with the general approach and assumptions that will be employed in analyzing the propagation of the average electromagnetic field in a foliated environment. To a large degree, specific analytical approaches to this problem will be dictated by the characteristics of the foliage. That is, since it is not possible to solve the problem exactly, certain simplifying assumptions will have to be made and these should be based on the physical and electrical characteristics of the foliage. The foliage parameters that are of importance to the propagation problem can be grouped into the three following categories; the physical statistics of the foliage constituents, the shape of the constituents, and the complex dielectric constant of the constituents. The term constituent, as used above, refers to the physical components that make up the foliage such as the leaves, stems, branches,

tree trunks, bark, etc. The physical statistics category refers to such parameters as the average fractional volume occupied by the foliage, the spatial homogeneity of the foliage, and the statistical distribution of the size and orientation of the foliage constituents.

The average fractional volume occupied by the foliage and the spatial homogeneity of the foliage are very important because they will dictate, to a large degree, the complexity of the random wave propagation model. The statistical distribution of the foliage constituent sizes will impact the variation of the average or coherent field with frequency. The actual shapes and permittivity of the foliage constituents will be most important in determining the absorption and scattering properties of the average medium. In regard to the shapes of the foliage constituents, it is obviously not possible to model exactly every detail of a leaf or branch. Consequently, it will be necessary to replace these exact shapes by simplified or canonical forms. For example, leaves will be replaced by thin discs while branches, stems, and trunks will be approximated by cylinders. Obviously, this approximation ignores the curling of leaves, the crookedness of branches, and certainly the roughness of the surface bark of branches and trunks. Whether or not these characteristics are important remains to be evaluated.

3.0 RAYLEIGH-EFFECTIVE VOLUME (REV) MODEL

The purposes of the previous section were to define the problem as it applies to an SAR, establish the basic analytical approach, and state certain simplifying assumptions. This section will be devoted to obtaining a model which predicts the attenuation and phase delay of the average or coherent field propagating through foliage. Before getting into the details of the derivation, it is necessary to explain the assumption that will be employed herein.

It should be clearly obvious that a full-blown, detailed, rigorous approach to this problem is well outside the time constraint imposed upon this study. Conversely, the modeling effort should comprise more than just empirical extrapolation. In point of fact, what is really desirable is a model which adheres as closely as possible to basic scattering principles, contains insight into the basic problem, provides straightforward and simple results which can be used by system designers, and, most important of all, agrees with measured results. If all of these criteria cannot be simultaneously satisfied, which then are the most important? From an analytical point of view and certainly for the purposes of future studies, it would be desirable to obtain as much insight into the general problem as possible. However, for the purposes of system design and evaluation it is more important to generate a relatively simple model which agrees with measured data.

For the purposes of this study, we have chosen the latter criterion as a guide. That is, attention has been specifically directed toward generating a relatively simple model which can be used by systems engineers and one which exhibits a great deal of agreement with measured data. This approach was selected for the following reasons. First, this approach is in consonance with the end goal of the study, i.e. providing an engineering tool for estimating SAR performance. Second, this approach provides a "strawman" model which can be studied more thoroughly and improved upon in future studies. Finally, we feel very strongly that in problems as complex as this it is more important to generate a model that agrees with measurements than to derive a model which requires so many input variables as to be essentially impractical.

3.1 Model Rationale

This section is very important because it presents a justification of the particular approach used in this model. A forest may be considered to comprise

three basic constituents; tree trunks, branches, and leaves. In the case of pine or needle bearing trees, there are no leaves and the needles may be broadly categorized as branches by virtue of the cylindrical shape. Tree trunks may be so classified by their size, vertical orientation, and relatively small number density. Although the tree trunks are few in number density, they have a large enough average volume to comprise anywhere from 60 to 90% of the total fractional volume occupied by the foliage. Branches are characterized by their smaller average size, random orientation, and relatively high number density. In spite of their high number density, branches only comprise from 10 to 30% of the fractional volume of the foliage. Both the trunks and the branches will be modeled as cylinders. Leaves are similar to very thin discs with a random orientation and a relatively high number density. Like branches, they only comprise a very small percentage of the total fractional volume of the foliage, say, less than 10%.

It is intuitively obvious that at very low frequencies, the tree trunks are the dominant foliage constituent in determining the propagation characteristics of the coherent or average field. That is, since all of the foliage constituents are Rayleigh scatterers/absorbers and the tree trunks have the largest volume, they will dominate the process. At or near optical frequencies, the leaves dominate the attenuation of the coherent field because of their high number density and their geometric cross sectional area. The transition from low frequency volume dependent attenuation to high frequency area dependent attenuation is well understood from single scatter random propagation theory. What is really important, for the purposes of this study, is the transition in the roles of importance of the foliage constituents. In fact, we conjecture that each of the three primary foliage constituents (trunks, branches, and leaves) is dominant in only a limited range of frequencies and

as each constituent transitions from a Rayleigh or volume dependent scatterer/absorber to a number density/cross sectional area dependent scatterer/absorber it dwarfs, in impact, the effect of the much larger volume (but fewer in number) obstacles.

This statement can be proven if it is assumed that single or independent scattering theory [5] provides a reasonably accurate expression for the attenuation constant of the coherent field. According to single scattering theory, the attenuation constant of the average or coherent field is given by [1, Vol II]

$$\text{Im}(k) = \rho(\sigma_s + \sigma_a)$$

where ρ is the number of scattering/absorbing objects per unit volume and σ_s and σ_a are the scattering and absorption cross sections of a single object. Ignoring the complex dielectric constant dependence, since it is not germane to the argument, the absorption cross sections for trunks and branches are proportional to $\rho_t V_t = \rho_t \pi a_t^2 L_t$ and $\rho_b V_b = \rho_b \pi a_b^2 L_b$, respectively, when the frequency is sufficiently low that the objects are Rayleigh scatterers. V is the volume, a is the radius, and L is the length of the cylinders representing the trunks and branches; the subscripts b and t denote branches and trunks, respectively. Because of the significant size difference between trunks and branches, $a_b \ll a_t$ and $L_b \ll L_t$; however, the number density of branches is much larger than that of the trunks, i.e. $\rho_b \gg \rho_t$, so that $\rho_t V_t$ is at most larger than $\rho_b V_b$ by a factor of ten. In the optical limit, $\sigma_a \rightarrow \sigma_g$ where σ_g is the geometric cross section of the scatterer/absorber. For the trunks $\sigma_g = 2a_t L_t$ because they are all represented as similarly oriented cylinders. The branches comprise a collection of randomly oriented cylinders with all orientations assumed equally likely. Van de Hulst [10] has shown that the geometric cross section of a randomly oriented object is

one-fourth the total surface area; thus, for the branches $\sigma_g \approx \pi a_b L_b / 2$. Consequently, in the optical limit the attenuation constant due to the trunks only is proportional to $2\rho_t V_t / \pi a_t$ while the attenuation constant due to branches only is proportional to $\rho_b V_b / 2a_b$. The ratio of these two attenuation constants is given by the following;

$$\frac{\text{Im}(k_b)}{\text{Im}(k_t)} = \frac{\pi a_t}{4a_b} \frac{\rho_b V_b}{\rho_t V_t}$$

As noted previously, $\rho_b V_b / \rho_t V_t \lesssim 10$ however the ratio of the trunk radius to the branch radius is significantly larger than ten. Thus, in the optical limit, the attenuation due to the branches can be significantly larger than the attenuation due to the trunks. This difference is even more drastic in the case of leaves versus branches because the volume of a leaf depends on its very small thickness while its geometric cross section is determined by the surface area of the leaf. Once again it should be pointed out that the reasons for the transition in the dominant scattering/absorbing objects from trunks to branches to leaves as the frequency increases is due to the change from volume to area dependence and the much larger number density of the branches and the leaves.

Having established the relative importance of trunks, branches and leaves as a function of frequency and assuming that they act essentially as independent scatterers, one could use classical boundary value techniques to accurately compute $\sigma_a + \sigma_s$ for a single object (trunk, branch, or leaf). The attenuation constant could then be estimated from the single scattering approximation, i.e. $\text{Im}(k) = \rho(\sigma_a + \sigma_s)$. The problem with this approach is that the size parameters for each of the three primary canonical objects (trunks, branches, and leaves) are random variables with unknown distribution functions. That is, even though the problem can be solved formally, it is doubtful that measurements

of the required size distribution functions are practical; this is especially true for the branches and the leaves.

One way of overcoming this need for detailed statistics on the trunks, branches, and leaves would be to assume that those foliage constituents which are primarily important to the propagation problem are the ones which are Rayleigh scatterers/absorbers. That is, only those constituents which are small in terms of a free space wavelength are significant in determining the attenuation of the coherent or average field. If this were the case, the problem could be analyzed using low frequency or Rayleigh approximation techniques. This, in turn, would mean that the attenuation constant is dependent upon an effective fractional volume of foliage, i.e. $\{\rho V_p\}_e$ where ρ is the number density of Rayleigh foliage constituents, V_p is their volume, and the subscript e denotes effective. Such an assumption, if true, would certainly be a great simplification because there are approximate means and data available for estimating $\{\rho V_p\}_e$ as a function of frequency. However, does such an assumption have any analytical foundation or is it justified by measurements? First it should be noted that the use of an effective fractional volume is in agreement with the above reasoning that as the scatterers become electrically larger they become less influential in the attenuation of the coherent field. That is, by using an effective fractional volume comprising only those foliage constituents whose characteristic dimensions are small in terms of a wavelength, the influence of electrically large constituents is eliminated. The problem that remains to be solved is the electrical size of a constituent where it transitions from an effective to an ineffective scatterer/absorber relative to the attenuation of the coherent field. If this transition occurs in or near the Rayleigh region, the use of Rayleigh scattering/absorbing approximation and an effective fractional volume is justified. If, on the other hand,

the transition occurs well into the resonance or optical region, the approach is totally invalid.

The only analytical or experimental results that have a bearing on this problem which we have been able to find are the recent measurements by Stutzman, et al., [6]. In this experiment, an attempt was made to correlate the attenuation of an X-band signal with the weight and size of the intervening foliage (pine trees in particular). They found the highest correlation to depend upon the green or dry weight of those foliage constituents having a diameter of less than one half a free space wavelength. That is, they found that the attenuation correlated more strongly with the smaller foliage constituents than with all the foliage. Unfortunately, they did not attempt a correlation with even smaller constituents so the exact point of maximum correlation is unknown. In any case, we consider that these experimental results do show that the use of an effective fractional volume comprising only Rayleigh constituents has some degree of justification.

The purpose of this section is to provide some degree of rationale for the Rayleigh assumption. We know that it must fail beyond some frequency because all foliage constituents will eventually no longer be Rayleigh scatterers or absorbers, i.e. $\{\rho V\}_{p_e}$ goes to zero. Conversely, we feel that there is some frequency range for which it is valid because it has some analytical justification and it is in reasonable agreement with measurements. In addition, it has the added benefit of being very simple in terms of the number of required input variables. For these reasons, we have developed a model based upon the Rayleigh-effective volume assumption and it will be called the Rayleigh-Effective Volume (REV) model.

3.2 Model Development

The Rayleigh-Effective Volume (REV) model is based upon the approximation that only those foliage components having a diameter to wavelength ratio of less than one half are the major contributors to the attenuation of the average or coherent field. Furthermore, it is assumed that all foliage components in this category may be considered to be Rayleigh in their scattering and absorbing characteristics. With these model characteristics in mind, it is now appropriate to direct attention toward the determination of the propagation constant of the average or coherent field.

Having already decided that we will use a discrete medium formulation to solve this problem, the choice of approach essentially boils down to three; single scattering, the Foldy-Twersky integral equation, or the Lax-Twersky integral equation. Single or independent scattering [5] completely ignores any multiple scattering between particles or objects in the medium. It provides a very simple result but one does not know for what range of object parameters the solution is accurate. If the medium is sparsely populated with scattering/absorbing objects, the Foldy-Twersky integral equation provides a reasonably accurate description of the process provided the objects comprising the medium are not strong backscatterers relative to scattering in other directions [1, Vol II]. (A good counter example is the case of small Rayleigh spheres which are perfectly conducting.) If the medium is so densely populated with scatterers/absorbers that the positions of the particles are not mutually independent, then the Lax-Twersky approach must be used.

The choice between the Foldy-Twersky and the Lax-Twersky formulation depends primarily upon the fractional volume occupied by the scattering/absorbing objects. In most forests, the fractional volume occupied by the wood and leaves or needles seldom exceeds 0.1%. There are exceptions to this figure

especially for managed forests in Europe where the fractional volume can be as large as 0.5%. However, even in this case the fractional foliage volume is sufficiently small as to indicate that the Foldy-Twersky integral equation is an adequate description of the process. Another very practical reason for choosing the Foldy-Twersky formulation is that we have no idea as to how the positions of the foliage constituents are correlated; consequently, we do not have adequate information to solve the Lax-Twersky equation.

During the latter phase of this study, we were able to obtain an exact solution of the Foldy-Twersky integral equation. This solution for the case of spherical objects or particles is given in Appendix A. Unfortunately, this exact solution was obtained so late in the study that we were unable to apply it to arbitrarily shaped objects having all orientations equally likely. In fact there is some indication that the solution presented in Appendix A is strictly only applicable to objects which do not give rise to depolarization of the forward scattered wave even though this depolarized wave may go to zero when averaged over all orientation angles. However, in the case of Rayleigh scatterers the problem simplifies somewhat and it is possible to obtain an approximate solution.

In the Foldy-Twersky formulation, the total average field outside the particles is also the field incident upon any one object or particle. Using this fact and assuming that the volume enclosing all the particles or objects is infinite, Appendix A shows that the average field outside of the particles $\langle \vec{E}_o(\vec{r}_a) \rangle$ and the average field inside the particles $\langle \vec{E}_i(\vec{r}_a) \rangle$ are related as follows;

$$(-k^2 + k_o^2) \langle \vec{E}_o(\vec{r}_a) \rangle = -k_o^2 \rho V_p (\epsilon_r - 1) \langle \vec{E}_i(\vec{r}_a) \rangle \quad (1)$$

where it has been assumed that the average field outside the particles is a

plane wave, i.e.

$$\langle \vec{E}_0(\vec{r}_a) \rangle = \vec{E} \exp(-j \vec{k} \cdot \vec{r}_a)$$

In (1), k is the unknown propagation constant of the average or coherent field, $k_0 = 2\pi/\lambda_0$ is the free space propagation constant or wavenumber. ρ is the number of particles or objects per unit volume, V_p is the volume of a particle or object, $\epsilon_r = \epsilon_r' - j\epsilon_r''$ is the complex dielectric constant of the material comprising the objects, and an $\exp(j\omega t)$ time convention is assumed. In order to solve (1) for the unknown propagation constant, it is necessary to obtain the relationship between $\langle \vec{E}_0 \rangle$ and $\langle \vec{E}_1 \rangle$ and this is difficult to do in general. However, in the case of Rayleigh particles or objects, such as assumed in the foliage case, the quasi-static approximation can be used to find an approximate relationship of the form

$$\langle \vec{E}_1 \rangle \approx g(\epsilon_r, P) \langle \vec{E}_0 \rangle \quad (2)$$

because $\langle \vec{E}_0 \rangle$ is also the incident field. The constant of proportionality in (2) depends upon the dielectric constant of the object or particle and the shape of the object. Substituting (2) in (1) yields the following expression for k ;

$$k^2 = k_0^2 + k_0^2 \rho V_p (\epsilon_r - 1) g(\epsilon_r, P) \quad (3)$$

Thus, in order to determine the propagation constant of the average or coherent field it is necessary to use the quasi-static approximation to estimate $g(\epsilon_r, P)$.

3.2.1 Propagation Through Small Cylinders and Discs

There are a number of different ways to obtain approximate expressions for $g(\epsilon_r, P)$ and the approach presented here should not be considered as the only valid one. The advantages of this approach are that it is analytically

simple, intuitively appealing, and it makes use of measured data to determine certain unknowns in the problem. As noted previously, the three major scattering/absorbing constituents in a forest are the trunks, branches, and leaves.* The only essential differences between branches and trunks are their sizes and orientations; the branches are smaller in diameter than the trunks and they are randomly oriented whereas the trunks are vertically oriented. This suggests that we might consider lumping the branches and trunks together and, in addition to dealing with an effective volume of the total, treat the probability density function for their orientation as frequency dependent. That is, for low frequencies where the bulk of the effective fractional volume is concentrated in the trunks, the probability density function for the orientation of the trunks and branches should be significantly skewed toward the vertical. As the frequency increases and the trunks no longer contribute to the effective fractional volume, the probability density for the orientation of the constituents comprising the effective fractional volume should approach a more uniform behavior, i.e. all orientations are equally likely.

We can easily construct probability density functions for the orientation of the trunks and branches which are either skewed toward the vertical or are uniform. What we do not know is at what frequency the transition from skewed toward the vertical to uniform occurs. Fortunately, we can estimate this transition frequency by examining multifrequency propagation data through foliage. That is, at lower frequencies one should expect a significant difference between the attenuation constant of vertically and horizontally polarized waves and this difference should disappear as the frequency is increased.

*In the case of trees having needles rather than leaves, the needles may be considered to be in the branch class by virtue of their similarity in shape and random orientation.

Surprisingly enough, most of the relevant data we have examined indicates that the transition in polarization dependence always occurs near 500 MHz. This does not tell us how the orientation density function changes in the vicinity of the transition; however, as demonstrated below, this problem can be overcome to a great extent by properly choosing the analytic form of the skewed orientation density function.

Figure 1 illustrates an arbitrarily oriented cylinder and the defining geometry. The (x,y,z) coordinate system is fixed while the angles θ and ϕ describe the orientation of the cylinder. In consonance with the Rayleigh-Effective Volume (REV) model, we shall assume that the cylinder representing the branches and trunks is long and thin and that the internal field may be approximated by quasi-static techniques. Thus, if \vec{E}^i is the incident field, the internal field along the axis of the cylinder is given by

$$\vec{E}_i \cdot \hat{r} = \hat{r} \cdot \vec{E}^i \quad (4)$$

whereas the internal field orthogonal to the axis is [8]

$$\hat{r} \times \vec{E}_i = \hat{r} \times \vec{E}^i \left[\frac{2}{\epsilon_r + 1} \right] \quad (5)$$

where \hat{r} is a unit vector along the axis of the cylinder. Equations (4) and (5) give the internal field components in terms of a unit vector which changes direction as θ and ϕ vary. Before these field components can be averaged, they must be converted back to the fixed (x,y,z) coordinate system. This entire process is greatly facilitated by noting that the direction parallel to the cylinder axis is given by the unit radius vector \hat{r} of a spherical coordinate system^⓪ while $\hat{\theta}$ and $\hat{\phi}$ of the same system specify the directions orthogonal to the axis of the cylinder. One then merely needs the relationships between

^⓪This is an approximation which is true only in the thin cylinder limit.

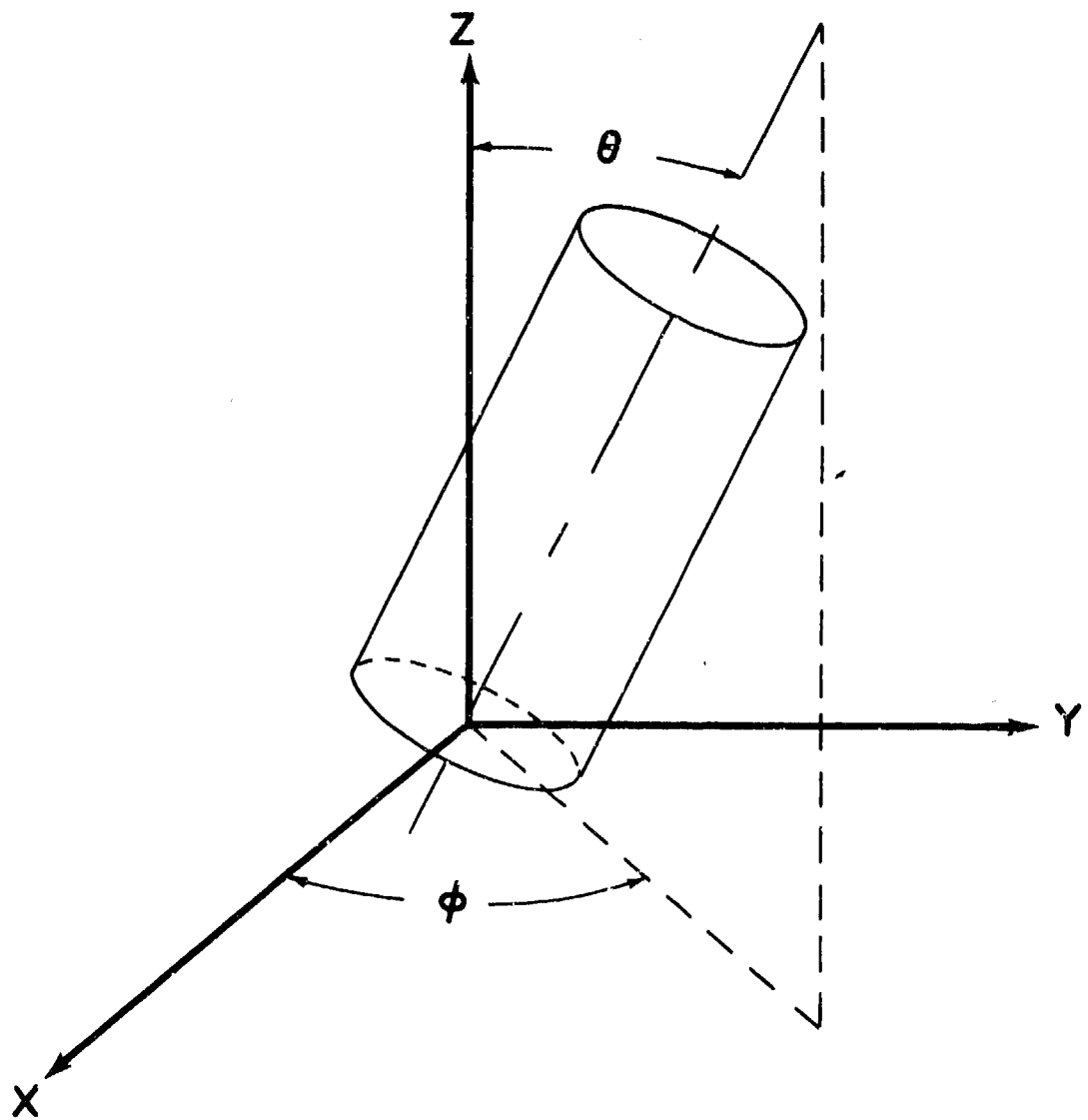


Figure 1. Coordinates and geometry for the cylindrical representation of the woody components of a forest. The angles θ and ϕ are random variables.

the spherical coordinate system unit vectors $(\hat{r}, \hat{\theta}, \hat{\phi})$ and the cartesian unit vectors $(\hat{x}, \hat{y}, \hat{z})$, e.g.

$$\begin{aligned} \hat{x} \cdot \hat{r} &= \sin\theta \cos\phi & \hat{x} \cdot \hat{\theta} &= \cos\theta \cos\phi & \hat{x} \cdot \hat{\phi} &= -\sin\phi \\ \hat{y} \cdot \hat{r} &= \sin\theta \sin\phi & \hat{y} \cdot \hat{\theta} &= \cos\theta \sin\phi & \hat{y} \cdot \hat{\phi} &= \cos\phi \\ \hat{z} \cdot \hat{r} &= \cos\theta & \hat{z} \cdot \hat{\theta} &= -\sin\theta & \hat{z} \cdot \hat{\phi} &= 0 \end{aligned}$$

Thus, if the incident field is z-polarized (vertical), then

$$\vec{E}^i = E^i \hat{z} = E^i [\cos\theta \hat{r} - \sin\theta \hat{\theta}]$$

and the internal field is

$$\vec{E}_i = E^i \left[\cos\theta \hat{r} - \frac{2}{\epsilon_r + 1} \sin\theta \hat{\theta} \right]$$

which in terms of the fixed cartesian unit vectors is

$$\begin{aligned} \vec{E}_i &= E^i \left\{ \sin\theta \cos\theta \cos\phi \hat{x} + \sin\theta \cos\theta \sin\phi \hat{y} + \cos^2\theta \hat{z} \right. \\ &\quad \left. - \frac{2}{\epsilon_r + 1} \left[\cos\theta \sin\theta \cos\phi \hat{x} + \cos\theta \sin\theta \sin\phi \hat{y} - \sin^2\theta \hat{z} \right] \right\} \quad (6) \end{aligned}$$

The z-component of \vec{E}_i in (6) is the principally polarized component of the internal field while the x and y-components are the cross polarized parts.

If the incident field is y-polarized (horizontal), then

$$\vec{E}^i = E^i \hat{y} = E^i \left[\sin\theta \cos\phi \hat{r} + \cos\theta \sin\phi \hat{\theta} + \cos\phi \hat{\phi} \right]$$

and the internal field is

$$\vec{E}_i = E^i \left\{ \sin\theta \sin\phi \hat{r} + \frac{2}{\epsilon_r + 1} \left[\cos\theta \sin\phi \hat{\theta} + \cos\phi \hat{\phi} \right] \right\}$$

which in terms of the fixed cartesian unit vectors is

$$\begin{aligned} \vec{E}_1 = E^i \left\{ \sin^2 \theta \cos \phi \sin \phi \hat{x} + \sin^2 \theta \sin^2 \phi \hat{y} + \sin \theta \cos \theta \sin \phi \hat{z} \right. \\ \left. + \frac{2}{\epsilon_r + 1} \left[(\cos^2 \theta \cos \phi \sin \phi - \sin \phi \cos \phi) \hat{x} + (\cos^2 \theta \sin^2 \phi + \cos^2 \phi) \hat{y} \right. \right. \\ \left. \left. - \sin \theta \cos \phi \hat{z} \right] \right\} \end{aligned} \quad (7)$$

For this polarization of the incident field, the y-component of \vec{E}_1 is the principally polarized component of the internal field while the x and z-components are the cross polarized parts.

Equations (6) and (7) give the quasi-static internal field inside an arbitrarily oriented thin cylinder for vertically and horizontally polarized incident fields, respectively. We must now choose a probability density function for the orientation of the cylinder which is representative of the trunks and branches. In selecting the density function, we will use measured data as our guide. For example, near 100 MHz, measurements have shown [15,16] that a vertically polarized field is attenuated at twice the rate of a horizontally polarized field. A probability density function which will produce this behavior is as follows;

$$P_w(\theta, \phi) d\theta d\phi = \begin{cases} \frac{d\theta d\phi}{(2\pi)(\pi/2)} & \theta \in (0, \pi/2) \\ & \phi \in (0, 2\pi) \\ 0 & \text{all other angles} \end{cases} \quad (8)$$

That is, averaging (6) and (7) over all angles θ and ϕ using (8) yields

$$\langle \vec{E}_1 \rangle = \frac{1}{2} \left[1 + \frac{2}{\epsilon_r + 1} \right] \vec{E}^i \quad (9)$$

for a vertically polarized incident field, and

$$\langle \vec{E}_1 \rangle = \frac{1}{2} \left[\frac{1}{2} + \frac{3}{2} \left(\frac{2}{\epsilon_r + 1} \right) \right] \vec{E}^i \quad (10)$$

for a horizontally polarized incident field. Substituting the above results in (2) and then in (3) gives the following results for the propagation constants of the coherent fields

$$k_v^2 = k_o^2 + k_o^2 \{\rho V_p\}_{ew} (\epsilon_r - 1) \left\{ \frac{1}{2} \left[1 + \left(\frac{2}{\epsilon_r + 1} \right) \right] \right\} \quad (11)$$

$$k_h^2 = k_o^2 + k_o^2 \{\rho V_p\}_{ew} (\epsilon_r - 1) \left\{ \frac{1}{2} \left[\frac{1}{2} + \frac{3}{2} \left(\frac{2}{\epsilon_r + 1} \right) \right] \right\} \quad (12)$$

where the subscripts denote the polarization of the average or coherent field and $\{\rho V_p\}_{ew}$ denotes the effective fractional volume of the woody (trunks and branches) constituents of the forest. Since the second terms on the right hand sides of (11) and (12) are small with respect to k_o^2 and because $|\epsilon_r| \gg 1$ for wood in the frequency range of interest to this study (see Section 3.2.4 and Appendix C), (11) and (12) simplify to

$$k_v \approx k_o + k_o \{\rho V_p\}_{ew} (\epsilon_r - 1) / 4 \quad (13)$$

$$k_h \approx k_o + k_o \{\rho V_p\}_{ew} (\epsilon_r - 1) / 8 \quad (14)$$

and the attenuation of the vertically polarized wave is twice that of the horizontally polarized wave.

It may appear, at first glance, that the probability density function in (8) does not, in fact, represent an orientation density function that is skewed toward the vertical. This apparent error is easily understood if it is realized that the uniformity or skewness of the orientation density is only obvious when the density is expressed in terms of the solid angle[⊙]. That is, in terms of

[⊙]One author (GSB) is indebted to Dr. R. L. Fante for pointing this fact out.

the differential solid angle $d\Omega$ and with $d\Omega = \sin\theta d\theta d\phi$, equation (8) becomes

$$p_w(\Omega)d\Omega = \begin{cases} \frac{d\Omega}{\pi^2 \sin\theta} & 0 \leq \Omega \leq 2\pi \\ 0 & 2\pi \leq \Omega \leq 4\pi \end{cases} \quad (15)$$

Clearly, the density function expressed in terms of the solid angle Ω by (15) is skewed toward the vertical; in fact, when $\theta = 0$ the density is infinite.

Before leaving this subject, there are two other points that should be addressed. When the trunks are included in the effective fractional volume, we do not know a priori the probability density function for the cylinders representing the woody components of the forest. We do, however, know from measurements that the attenuation constant for a vertically polarized field is twice as large as that for a horizontally polarized field. In our model, this observation means that the average vertically polarized field inside the cylinder must be twice as large as the horizontally polarized internal field for $\epsilon_r \gg 1$. That is,

$$\begin{aligned} \int_0^{\pi/2} \int_0^{2\pi} \vec{E}_i(\theta, \phi | \hat{z}) \hat{p}_w(\theta, \phi) d\phi d\theta \\ = 2 \int_0^{\pi/2} \int_0^{2\pi} \vec{E}_i(\theta, \phi | \hat{y}) \hat{p}_w(\theta, \phi) d\phi d\theta \end{aligned} \quad (16)$$

where $\vec{E}_i(\theta, \phi | \hat{z})$ is the internal field for a z-polarized (vertical) incident field, $\vec{E}_i(\theta, \phi | \hat{y})$ is the internal field for a y-polarized (horizontal) incident field, and $\hat{p}_w(\theta, \phi)$ is the probability density function for the orientation of the cylinders. Assuming that $\hat{p}_w(\theta, \phi)$ is functionally independent

of ϕ over $(0, 2\pi)$, it can be shown using (6) and (7) that (16) reduces to the following;

$$\int_0^{\pi/2} \cos^2 \theta \hat{p}_w(\theta) d\theta = \int_0^{\pi/2} \sin^2 \theta \hat{p}_w(\theta) d\theta \quad (17)$$

Using some straightforward trigonometric substitutions, (17) reduces to

$$\int_0^{\pi} \cos \theta \hat{p}_w(\theta/2) d\theta = 0 \quad (18)$$

Thus, any function $\hat{p}_w(\theta)$ which satisfied (18) and is a valid probability density function is a solution to our problem. There is, however, one other point which may have some practical significance. When we transform $\hat{p}_w(\theta, \phi)$ to $\hat{p}_w(\Omega)$, it would seem reasonable to require that $\hat{p}_w(\Omega)$ should be everywhere finite. The density function given by (8) does not satisfy this condition because, as shown by (15), it is singular at $\theta = 0$. However, another choice of the density function is as follows;

$$\hat{p}_w(\theta, \phi) d\theta d\phi = \begin{cases} \frac{\sin 2\theta}{\pi} d\theta d\phi & \left\{ \begin{array}{l} 0 \leq \theta \leq \pi/2 \\ 0 \leq \phi \leq 2\pi \end{array} \right. \\ 0 & \text{all other angles} \end{cases} \quad (19)$$

This density function satisfies (18), is a valid probability density function, and is not singular when transformed to $\hat{p}_w(\Omega)$. Thus, although (8) and (19) lead to the same results for the attenuation constant, (19) is preferable since it does not have any singularities when transformed into solid angle space. The important point of this discussion is that equation (16) can be satisfied by a large number of functional forms for $\hat{p}_w(\theta, \phi)$, and so if we had

measured data on $\hat{p}_w(\theta, \phi)$, we could construct a function which matched the data and satisfied (16). This is most encouraging because it means that the model is not locked to a specific functional form for $\hat{f}_w(\theta, \phi)$.

The above paragraphs present the details of the REV model for frequencies below roughly 500 MHz. The larger rate of attenuation of the vertically polarized average or coherent field is attributed to an orientation probability density function that is significantly skewed toward the vertical; this skewing of the density function is attributed to the vertically oriented tree trunks. Above 500 MHz, measurements have shown that the attenuation constant of the vertically and horizontally polarized average fields are nearly equal [9, 15, 16]. These results are completely consistent with the REV model because as the frequency increases the effective fractional volume of wood, $\{\rho V\}_{p_{ew}}$, decreases, i.e. only those cylindrical shapes having a diameter to wavelength ratio of less than one half comprise $\{\rho V\}_{p_{ew}}$. Since the tree trunks are the largest wood components in the forest, they are the first to be eliminated from $\{\rho V\}_{p_{ew}}$. As the tree trunks are deleted from $\{\rho V\}_{p_{ew}}$, the remaining woody components represent the smaller tree trunks and nearly all of the branches. These components would appear to be oriented in a more or less random fashion. That is, for frequencies above 500 MHz the probability density function for the orientation of the canonical cylinders representing $\{\rho V\}_{p_{ew}}$ is probably best described by a function which is uniform in the upper hemisphere.^① In terms of the angles θ and ϕ , a hemispherically uniform probability density function is given by

^①Since cylinders have end-for-end symmetry, their orientation need only encompass the upper hemisphere.

$$P_w(\theta, \phi) d\theta d\phi = \begin{cases} \frac{\sin\theta}{2\pi} d\theta d\phi & \begin{cases} 0 \leq \theta \leq \pi/2 \\ 0 \leq \phi \leq 2\pi \end{cases} \\ 0 & \text{all other angles} \end{cases} \quad (20)$$

Averaging (6) and (7) over the upper hemisphere using (20) yields the following results for k_v and k_h ;

$$\begin{aligned} k_v &\approx k_o + k_o \{ \rho V_p \}_{ew} (\epsilon_r - 1) / 6 \\ k_h &\approx k_o + k_o \{ \rho V_p \}_{ew} (\epsilon_r - 1) / 6 \end{aligned} \quad (21)$$

since $|\epsilon_r| \gg 1$ for wood in the range of frequencies of interest to this study. Comparing (21) with k_v and k_h for a skewed orientation density function, i.e. (13) and (14), shows that the uniform orientation density gives rise to a smaller value of k_v and a larger value of k_h .

The above expressions are valid for those constituents of a forest which can be canonically represented by cylinders. They can essentially be used for all the woody parts of a forest and the needles of pine, fir, or spruce trees; they cannot, however, be used for leaves. We assume that the effects of the leaves can be computed independently and then added to (21) in order to arrive at the net effect of the wood and the leaves. It is not necessary to account for the leaves below about 500 MHz because they comprise such a small effective fractional volume $\{ \rho V_p \}_{e\ell}$ relative to the wood. As noted previously, the leaves are modeled as very thin discs which need not be circular. In the quasi-static limit, if the incident field is parallel to the flat face of the disc, the internal field is equal to the incident field. If the incident field is orthogonal to the flat face of the disc, the internal field is equal to the incident field divided by the relative dielectric permittivity of the leaf [8]. The geometry of the disc representation of the

leaves is shown in Figure 2. Recognizing that the unit vectors $\hat{\theta}$ and $\hat{\phi}$ are parallel to the flat face of the thin disc while \hat{r} is perpendicular to the face, we can proceed exactly as with the cylinder to determine the average internal field. It should be noted, however, that there is a distinct difference between the internal fields in a disc and a cylinder; for a disc the $\hat{\theta}$ and $\hat{\phi}$ -components of the incident field couple strongly to the internal field while for a cylinder it is the \hat{r} -component of the incident field that exhibits a strong coupling to the internal field.

If the incident field is z-polarized (vertical), the internal field is given by;

$$\vec{E}_i = E^i \left[\frac{\cos\theta}{\epsilon_r} \hat{r} - \sin\theta \hat{\theta} \right] \quad (22)$$

and if the incident field is y-polarized (horizontal), the internal field is given by;

$$\vec{E}_i = E^i \left[\frac{\sin\theta \cos\phi}{\epsilon_r} \hat{r} + \cos\theta \sin\phi \hat{\theta} + \cos\phi \hat{\phi} \right] \quad (23)$$

where E^i is the amplitude of the incident field. Converting (22) and (23) back to cartesian coordinates and averaging over all orientations, assuming all orientations equally likely, i.e. equation (20), yields the following relation for the average internal field;

$$\langle \vec{E}_i \rangle = \left(\frac{1}{3\epsilon_r} + \frac{2}{3} \right) \vec{E}^i \quad (24)$$

for a z-polarized (vertical) incident field and

$$\langle \vec{E}_i \rangle = \left(\frac{1}{3\epsilon_r} + \frac{2}{3} \right) \vec{E}^i \quad (25)$$

for a y-polarized (horizontal) incident field. Substituting this result in (2) and then into (1) results in the following propagation constant for the

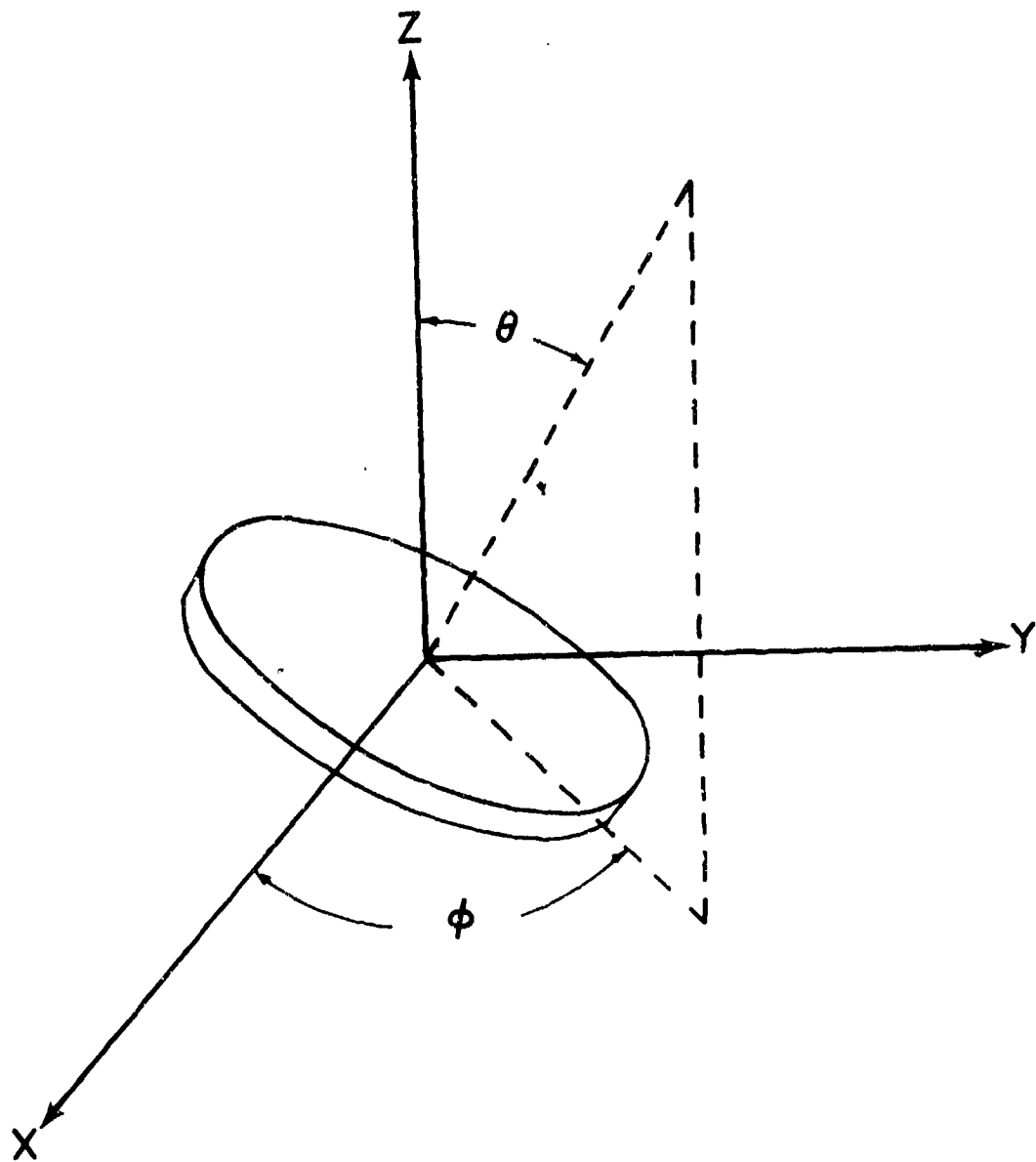


Figure 2. Coordinate system and geometry for the canonical model of leaves. Note that the leaf need not be a perfectly circular disc, but may have an arbitrarily shaped broadside cross section.

average field propagating through leaves only;

$$k_{\frac{y}{h}} \approx k_o + k_o \{ \rho V_{p_{el}} \} (\epsilon_r - 1) / 3 \quad (26)$$

where $\{ \rho V_{p_{el}} \}$ is the effective fractional volume occupied by the leaves and ϵ_r is the permittivity of the leaves. If it is assumed that the effects of the leaves and the woody components of the forest add independently, equations (21) and (26) can be combined to yield the following result for the propagation constant above 500 MHz;

$$k_{\frac{y}{h}} \approx k_o + k_o (\epsilon_r - 1) \left[\{ \rho V_{p_{ew}} \} / 6 + \{ \rho V_{p_{el}} \} / 3 \right] \quad (27)$$

where it has been assumed that the permittivities of the green wood and the leaves are essentially equal. It should be noted that for equal effective fractional volumes of wood and leaves, the leaves have a greater effect on the propagation constant of the coherent field. This is a consequence of the manner in which the incident field couples to the internal field.

In the above derivation, we assumed that the normal to the flat face of leaves in a forest was uniformly distributed in orientation over the upper hemisphere. In certain situations this assumption may not be completely valid. Leaves orient themselves in such a manner as to intercept a maximum of solar radiation. Thus, leaves on trees at the edge of a forest tend to be tilted at an angle of $\pi/4$ or more with respect to the vertical. Inside a dense forest, the leaves usually intercept maximum direct solar radiation when the sun is overhead. Thus, these leaves tend to have their normals oriented perpendicular to the ground. In this case the density function for the orientation of the normals to the leaves flat faces will be skewed toward the vertical. If we use a skewed (toward the vertical) density in computing the average internal field, the average internal field for horizontal polarization will

exceed that for the vertical polarization. Consequently, the attenuation constant for the average horizontally polarized field will be larger than that for the vertically polarized field; how much larger will depend upon how skewed toward the vertical the density function is. The important point is that for very dense forests, one may find the attenuation rate of the horizontally polarized field to be slightly larger than the vertically polarized field. It should be noted that Jansky and Bailey [15] did find a measurable (but small) difference between the attenuation rates for the two polarizations above 550 MHz and in the jungle. Furthermore, they found the horizontal field attenuation rate to be larger.

3.2.2 Inclusion of Scattering Losses

It should be noted from the expressions for the average propagation constant, e.g. (13) and (14) for frequencies below about 500 MHz and (27) for frequencies greater than 500 MHz, that the imaginary part of k is entirely dependent upon the loss factor ϵ_r'' of the complex dielectric constant. That is, if the material comprising the particles or objects in the medium is lossless then $\text{Im}(k) = 0$ and there is no attenuation of the average or coherent field. This, of course, is a physical absurdity that is a direct consequence of the Rayleigh or quasi-static approximation for the field inside an object. It is a mathematical oddity that is well known and is also well understood [1, Vol I]. If one is only interested in the scattering cross section of a Rayleigh object, it is also easy to overcome the limitations of the quasi-static approximation [1, Vol I]. However, for the problem addressed here, we need to obtain a better approximation for the internal field than is provided by the quasi-static technique. This makes the problem somewhat more difficult and we therefore present a rather detailed approach below. It should be remembered that we are trying to obtain a first order correction field (to

the zeroth order quasi-static approximation) which will yield a non-zero value of $\text{Im}(k)$ as the dielectric loss factor of the perturbing objects goes to zero, i.e. $\epsilon_r'' \rightarrow 0$.

We take the incident field as follows;

$$\vec{E}^i = E \hat{e} \quad (28)$$

where E is the complex amplitude and \hat{e} is a unit vector indicating the polarization of the incident field. It is first necessary to obtain the field inside an arbitrarily oriented cylinder (the canonical model of the wood in the forest). This is accomplished as in Section 3.2.1; the incident field is expressed first in terms of unit vectors along the axis of the cylinder (\hat{r}) and orthogonal to the axis ($\hat{\theta}$ and $\hat{\phi}$), i.e.

$$E^i = E [(\hat{e} \cdot \hat{r})\hat{r} + (\hat{e} \cdot \hat{\theta})\hat{\theta} + (\hat{e} \cdot \hat{\phi})\hat{\phi}]$$

The zeroth order or Rayleigh approximation to the field inside the cylinder is given by

$$\vec{E}_i^0 = E \left\{ (\hat{e} \cdot \hat{r})\hat{r} + \frac{2}{\epsilon_r + 1} [(\hat{e} \cdot \hat{\theta})\hat{\theta} + (\hat{e} \cdot \hat{\phi})\hat{\phi}] \right\}$$

or

$$\vec{E}_i^0 = E \vec{\xi} \quad (29)$$

where

$$\vec{\xi} = \left\{ (\hat{e} \cdot \hat{r})\hat{r} + \frac{2}{\epsilon_r + 1} [(\hat{e} \cdot \hat{\theta})\hat{\theta} + (\hat{e} \cdot \hat{\phi})\hat{\phi}] \right\} \quad (29a)$$

Since \hat{r} , $\hat{\theta}$, and $\hat{\phi}$ change direction with the angles defining the orientation of the cylinder (θ, ϕ) , it is necessary to convert (29) back to the cartesian unit vector base; that is

$$\vec{E}_1^0 = E \left\{ (\hat{x} \cdot \vec{\xi}) \hat{x} + (\hat{y} \cdot \vec{\xi}) \hat{y} + (\hat{z} \cdot \vec{\xi}) \hat{z} \right\} \quad (30)$$

Equation (30) represents the field inside the dielectric cylinder to the order of approximation inherent in the Rayleigh or quasi-static approximation, i.e. the zeroth order approximation. It is known that this zeroth order field is only approximate since if $\epsilon_r'' \rightarrow 0$, the forward scattering theorem [1, Vol I] predicts a zero scattering cross section. The problem is that the Rayleigh approximation ignores a small field component inside the cylinder which is in phase quadrature to the field given by (30). In the limit of $\epsilon_r'' \rightarrow 0$, the zeroth order or Rayleigh approximation for the internal field is real and the correction field is purely imaginary. This correction field gives rise to the non-zero scattering cross section of the cylinder which may be determined by the forward scattering theorem. In order to properly account for scattering in the results obtained in Section 3.2.1, it is necessary to obtain the small correction to the internal field for the cylinder.

If $\delta\vec{E}$ is the correction field, then the first order approximation to the field inside the cylinder is given by

$$\vec{E}_1^1 = \vec{E}_1^0 + \delta\vec{E}$$

or

$$\begin{aligned} \vec{E}_1^1 = E \left\{ [(\vec{\xi} + \delta\vec{E}/E) \cdot \hat{x}] \hat{x} + [(\vec{\xi} + \delta\vec{E}/E) \cdot \hat{y}] \hat{y} \right. \\ \left. + [(\vec{\xi} + \delta\vec{E}/E) \cdot \hat{z}] \hat{z} \right\} \end{aligned} \quad (31)$$

The scattering pattern of the cylinder with (31) as an internal field is given by the following [1, Vol I];

$$\vec{f}(\hat{k}_s, \hat{k}_i) = \frac{k_o^2}{4\pi} \int_{V_p} \left\{ -\hat{k}_s \times \left[\hat{k}_s \times \vec{E}_i^1 / E \right] \right\} (\epsilon_r - 1) \exp(j \vec{k}_s \cdot \vec{r}') d\vec{r}' \quad (32)$$

where $k_o = 2\pi/\lambda_o$, \hat{k}_s is a unit vector in the direction of scattering, $\vec{k}_s = k_o \hat{k}_s$, \hat{k}_i is a unit vector in the direction of incidence, and $d\vec{r}'$ is a differential volume element inside V_p . Assuming that V_p is so small that \vec{E}_i^1 / E is constant and

$$\exp(j \vec{k}_s \cdot \vec{r}') \approx 1,$$

then

$$\vec{f}(\hat{k}_s, \hat{k}_i) \approx \frac{k_o^2}{4\pi} (\epsilon_r - 1) V_p \left\{ -\hat{k}_s \times \left[\hat{k}_s \times \vec{E}_i^1 / E \right] \right\} \quad (33)$$

According to the forward scattering theorem, the total cross section σ_t is the sum of the absorption and scattering cross sections, σ_a and σ_s , respectively, and

$$\sigma_t = \sigma_a + \sigma_s = -\frac{4\pi}{k_o} \text{Im} \left\{ \vec{f}(\hat{k}_i, \hat{k}_i) \cdot \hat{e} \right\} \quad (34)$$

The total cross section averaged over all possible orientations and random dimensions of the cylinder is $\langle \sigma_t \rangle$ where

$$\langle \sigma_t \rangle = \langle \sigma_a \rangle + \langle \sigma_s \rangle = -\frac{4\pi}{k_o} \text{Im} \left\{ \langle \vec{f}(\hat{k}_i, \hat{k}_i) \rangle \cdot \hat{e} \right\} \quad (35)$$

Assuming that the orientation and volume of the cylinder are independent random variables and substituting (33) in (35) yields

$$\langle \sigma_a \rangle + \langle \sigma_s \rangle = -k_o \langle V_p \rangle \text{Im} \left\{ (\epsilon_r - 1) \left[-\hat{k}_i \times \left(\hat{k}_i \times \langle \vec{E}_i^1 / E \rangle \right) \right] \cdot \hat{e} \right\} \quad (36)$$

In Section 3.2.1 it was shown that the cross polarized components average to zero, thus $\langle \vec{E}_i^1 / E \rangle$ is in the direction of \hat{e} and

$$\langle \vec{E}_i^1 / E \rangle = \left[\langle \vec{E}_i^0 / E \cdot \hat{e} \rangle + \langle \delta \vec{E} / E \cdot \hat{e} \rangle \right] \hat{e}$$

or using (29)

$$\langle \vec{E}_i^1 / E \rangle = \left[\langle \vec{\xi} \cdot \hat{e} \rangle + \langle \delta \vec{E} / E \cdot \hat{e} \rangle \right] \hat{e} \quad (37)$$

Since $-\hat{k}_i \times [\hat{k}_i \times \hat{e}] = \hat{e} - \hat{k}_i (\hat{k}_i \cdot \hat{e})$ and because the incident field is orthogonal to the direction of incidence ($\hat{k}_i \cdot \hat{e} = 0$), (36) reduces to

$$\langle \sigma_a \rangle + \langle \sigma_s \rangle = -k_o \langle V_p \rangle \text{Im} \left\{ (\epsilon_r - 1) \left[\langle \vec{\xi} \cdot \hat{e} \rangle + \langle \delta \vec{E} / E \cdot \hat{e} \rangle \right] \right\} \quad (38)$$

where $\vec{\xi}$ is given by (29a).

The definition of $\langle \sigma_a \rangle$ is as follows;

$$\langle \sigma_a \rangle = k_o \epsilon_r'' \left\langle \int_{V_p} |\vec{E}_i^1 / E|^2 dV \right\rangle \quad (39)$$

however since

$$\vec{E}_i^1 = \vec{E}_i^0 + \delta \vec{E} \approx \vec{E}_i^0 \quad (40)$$

it can be shown by using (40) in (39) that

$$\langle \sigma_a \rangle = -k_o \langle V_p \rangle \text{Im} \left\{ (\epsilon_r - 1) \langle \vec{\xi} \cdot \hat{e} \rangle \right\} \quad (41)$$

The proof of this statement is given in Appendix B. From the expression for $\vec{\xi}$ (the equation (29a)), it is noted that for either $|\epsilon_r + 1| \gg 2$ or $\epsilon_r' \gg \epsilon_r''$ the normalized field $\vec{\xi}$ is predominantly real. Consequently, the

normalized correction field $\delta\vec{E}/E$ in (38) must be nearly pure imaginary because it must be in phase quadrature to $\vec{\xi}$. Using this fact and (41) in (38) shows that

$$\langle \sigma_s \rangle \approx k_o \langle v_p \rangle (\epsilon_r' - 1) \text{Im} \left\{ \left\langle \frac{\delta\vec{E}}{E} \cdot \hat{e} \right\rangle \right\} \quad (42)$$

because $j\epsilon_r'' \left\{ \left\langle \frac{\delta\vec{E}}{E} \cdot \hat{e} \right\rangle \right\}$ is real. We can determine $\left\langle \frac{\delta\vec{E}}{E} \cdot \hat{e} \right\rangle$ from (42) if we have an alternate evaluation of $\langle \sigma_s \rangle$. The alternate expression for $\langle \sigma_s \rangle$ is given by

$$\langle \sigma_s \rangle = \int_{4\pi} \left\langle |f(k_s, k_i)|^2 \right\rangle d\Omega_s \quad (43)$$

where $d\Omega_s$ is the differential solid angle centered on the direction \hat{k}_s . In the computation of (43), we ignore the contribution of the correction field since it is assumed to be small with respect to the zeroth order field, see (40). Using (31) in (33) results in the following

$$\begin{aligned} \vec{f}(\hat{k}_s, \hat{k}_i) \approx & \frac{k_o^2}{4\pi} (\epsilon_r - 1) v_p \left\{ (\vec{\xi} \cdot \hat{x}) \left[-\hat{k}_s \times (\hat{k}_s \times \hat{x}) \right] + (\vec{\xi} \cdot \hat{y}) \left[-\hat{k}_s \times (\hat{k}_s \times \hat{y}) \right] \right. \\ & \left. + (\vec{\xi} \cdot \hat{z}) \left[-\hat{k}_s \times (\hat{k}_s \times \hat{z}) \right] \right\} \end{aligned}$$

or

$$\begin{aligned} \vec{f}(\hat{k}_s, \hat{k}_i) = & \frac{k_o^2}{4\pi} (\epsilon_r - 1) v_p \left\{ (\vec{\xi} \cdot \hat{x}) \left[\hat{x} - \hat{k}_s (\hat{k}_s \cdot \hat{x}) \right] + (\vec{\xi} \cdot \hat{y}) \left[\hat{y} - \hat{k}_s (\hat{k}_s \cdot \hat{y}) \right] \right. \\ & \left. + (\vec{\xi} \cdot \hat{z}) \left[\hat{z} - \hat{k}_s (\hat{k}_s \cdot \hat{z}) \right] \right\} \quad (44) \end{aligned}$$

The function $|\vec{f}|^2$ can be simplified somewhat if it is realized that the following identities hold;

$$\left[\hat{n}_i - \hat{k}_s (\hat{n}_i \cdot \hat{k}_s) \right] \cdot \left[\hat{n}_i - \hat{k}_s (\hat{n}_i \cdot \hat{k}_s) \right] = 1 - (\hat{k}_s \cdot \hat{n}_i) = \sin^2 \chi_{si}$$

$$\left[\hat{n}_i - \hat{k}_s (\hat{n}_i \cdot \hat{k}_s) \right] \cdot \left[\hat{n}_j - \hat{k}_s (\hat{n}_j \cdot \hat{k}_s) \right] = -(\hat{n}_i \cdot \hat{k}_s) (\hat{n}_j \cdot \hat{k}_s) = -\cos \chi_{si} \cos \chi_{sj}$$

where \hat{n}_i represents any of the unit vectors \hat{x} , \hat{y} , or \hat{z} and χ_{si} is the angle between \hat{n}_i and \hat{k}_s . Thus $|\vec{f}|^2$ becomes

$$\begin{aligned} |\vec{f}|^2 = & \frac{k_o^4}{(4\pi)^2} |\epsilon_r - 1|^2 v_p^2 \left\{ |\vec{\xi} \cdot \hat{x}|^2 \sin^2 \chi_{sx} + |\vec{\xi} \cdot \hat{y}|^2 \sin^2 \chi_{sy} + |\vec{\xi} \cdot \hat{z}|^2 \sin^2 \chi_{sz} \right. \\ & - 2 \operatorname{Re} \left[(\vec{\xi} \cdot \hat{x}) (\vec{\xi} \cdot \hat{y}) \right] \cos \chi_{sx} \cos \chi_{sy} - 2 \operatorname{Re} \left[(\vec{\xi} \cdot \hat{x}) (\vec{\xi} \cdot \hat{z}) \right] \cos \chi_{sx} \cos \chi_{sz} \\ & \left. - 2 \operatorname{Re} \left[(\vec{\xi} \cdot \hat{y}) (\vec{\xi} \cdot \hat{z}) \right] \cos \chi_{sy} \cos \chi_{sz} \right\} \end{aligned} \quad (45)$$

Substitution of (45) in (43) and integration over the 4π solid angle causes the $\cos(\cdot) \cos(\cdot)$ terms to go to zero while the integration of the $\sin^2(\cdot)$ terms will yield $8\pi/3$. Thus, the average scattering cross section is given by

$$\langle \sigma_s \rangle = \left(\frac{8\pi}{3} \right) \frac{k_o^4 \langle v_p^2 \rangle}{(4\pi)^2} |\epsilon_r - 1|^2 \left\langle |\vec{\xi} \cdot \hat{x}|^2 + |\vec{\xi} \cdot \hat{y}|^2 + |\vec{\xi} \cdot \hat{z}|^2 \right\rangle \quad (46)$$

From equations (29a) and (30), it is noted that

$$|\vec{\xi} \cdot \hat{x}|^2 + |\vec{\xi} \cdot \hat{y}|^2 + |\vec{\xi} \cdot \hat{z}|^2 = |\hat{e} \cdot \hat{r}|^2 + \left| \frac{2}{\epsilon_r + 1} \right|^2 \left\{ |\hat{e} \cdot \hat{\theta}|^2 + |\hat{e} \cdot \hat{\phi}|^2 \right\}$$

where \hat{e} is the polarizator direction of the incident field. Thus

$$\langle \sigma_s \rangle = \left(\frac{8\pi}{3} \right) \frac{k_o^4 \langle v_p^2 \rangle}{(4\pi)^2} |\epsilon_r - 1|^2 \left\{ \langle |\hat{e} \cdot \vec{r}|^2 \rangle + \left| \frac{2}{\epsilon_r + 1} \right|^2 \left[\langle |\hat{e} \cdot \hat{\theta}|^2 \rangle + \langle |\hat{e} \cdot \hat{\phi}|^2 \rangle \right] \right\} \quad (47)$$

and the alternate expression for $\langle \sigma_s \rangle$ has been found.

Equating (47) to (42) yields

$$\text{Im} \left\{ \langle \delta \vec{E} / E \cdot \hat{e} \rangle \right\} = \left(\frac{8\pi}{3} \right) \frac{k_o^3 \langle v_p^2 \rangle}{(4\pi)^2 \langle v_p \rangle} \frac{|\epsilon_r - 1|^2}{(\epsilon_r' - 1)} \left\{ \langle (\hat{e} \cdot \hat{r})^2 \rangle + \left| \frac{2}{\epsilon_r + 1} \right|^2 \left[\langle (\hat{e} \cdot \hat{\theta})^2 \rangle + \langle (\hat{e} \cdot \hat{\phi})^2 \rangle \right] \right\}$$

or since $\delta \vec{E} / E$ is pure imaginary

$$\langle \delta \vec{E} / E \cdot \hat{e} \rangle = j \left(\frac{8\pi}{3} \right) \frac{k_o^3 \langle v_p^2 \rangle}{(4\pi)^2 \langle v_p \rangle} \frac{|\epsilon_r - 1|^2}{(\epsilon_r' - 1)} \left\{ \langle (\hat{e} \cdot \hat{r})^2 \rangle + \left| \frac{2}{\epsilon_r + 1} \right|^2 \left[\langle (\hat{e} \cdot \hat{\theta})^2 \rangle + \langle (\hat{e} \cdot \hat{\phi})^2 \rangle \right] \right\} \quad (48)$$

Equation (48) is the expression for the average correction field that must be added to the quasi-static internal field in order to obtain the proper average scattering cross section of the cylinders. It should be noted that this field goes to zero as $k_o \rightarrow 0$ as it must since in this limit only the static field remains. The total average first order approximate field inside the randomly oriented dielectric cylinder is given by combining (48) with (29), i.e.

$$\langle \vec{E}_i^1 \cdot \hat{e} \rangle = E \left\{ \langle (\hat{e} \cdot \hat{r})^2 \rangle + \frac{2}{\epsilon_r + 1} \left[\langle (\hat{e} \cdot \hat{\theta})^2 \rangle + \langle (\hat{e} \cdot \hat{\phi})^2 \rangle \right] \right\} + j E \left(\frac{8\pi}{3} \right) \frac{k_o^3 \langle v_p^2 \rangle}{(4\pi)^2 \langle v_p \rangle} \frac{|\epsilon_r - 1|^2}{(\epsilon_r' - 1)} \left\{ \langle (\hat{e} \cdot \hat{r})^2 \rangle + \left| \frac{2}{\epsilon_r + 1} \right|^2 \left[\langle (\hat{e} \cdot \hat{\theta})^2 \rangle + \langle (\hat{e} \cdot \hat{\phi})^2 \rangle \right] \right\} \quad (49)$$

It is important at this point to determine under what conditions the average correction field is small compared to the zeroth order average field. Ignoring terms the order of $1/\epsilon_r$ in (49), since ϵ_r is large, results in the following criterion;

$$\left(\frac{8\pi}{3}\right) \frac{k_o^3 \langle v_p^2 \rangle}{(4\pi)^2 \langle v_p \rangle} \frac{|\epsilon_r - 1|^2}{(\epsilon_r' - 1)} \ll 1$$

or

$$\frac{4\pi^2}{3} \frac{\langle v_p^2 \rangle}{\lambda_o^3 \langle v_p \rangle} \left[(\epsilon_r' - 1) + \frac{(\epsilon_r'')^2}{(\epsilon_r' - 1)^2} \right] \ll 1 \quad (50)$$

This is the criterion that must be satisfied by a small cylinder if the Rayleigh approximation is to hold.

If (49) is now substituted into (i) of Section 3.2.1 for $\langle \vec{E}_1 \cdot \hat{e} \rangle$ and with $\langle \vec{E}_o \cdot \hat{e} \rangle = \langle \vec{E}^1 \cdot \hat{e} \rangle$, the following result for the propagation constant of the average coherent field is obtained;

$$\begin{aligned} k^2 = k_o^2 \left\{ 1 - \left\{ \rho \langle v_p \rangle \right\}_{ew} (\epsilon_r - 1) \left[\langle (\hat{e} \cdot \hat{r})^2 \rangle + \frac{2 \langle (\hat{e} \cdot \hat{\theta})^2 \rangle}{\epsilon_r + 1} + \frac{2 \langle (\hat{e} \cdot \hat{\phi})^2 \rangle}{\epsilon_r + 1} \right. \right. \\ \left. \left. + j \frac{k_o^3 \langle v_p^2 \rangle}{6\pi \langle v_p \rangle} \frac{|\epsilon_r - 1|^2}{(\epsilon_r' - 1)} \left(\langle (\hat{e} \cdot \hat{r})^2 \rangle + \left| \frac{2}{\epsilon_r + 1} \right|^2 \langle (\hat{e} \cdot \hat{\theta})^2 \rangle \right. \right. \right. \\ \left. \left. \left. + \left| \frac{2}{\epsilon_r + 1} \right|^2 \langle (\hat{e} \cdot \hat{\phi})^2 \rangle \right) \right] \right\} \quad (51) \end{aligned}$$

Ignoring terms the order of $1/\epsilon_r$ and $1/\epsilon_r^2$ relative to one yields

$$k^2 \approx k_o^2 \left\{ 1 - \left\{ \rho \langle v_p \rangle \right\}_{ew} (\epsilon_r - 1) \langle (\hat{e} \cdot \hat{r})^2 \rangle \left[1 + j \frac{k_o^3 \langle v_p^2 \rangle}{6\pi \langle v_p \rangle} \frac{|\epsilon_r - 1|^2}{(\epsilon_r' - 1)} \right] \right\} \quad (52)$$

The imaginary term in (52) represents the contribution due to scattering. Unfortunately it is difficult to evaluate for a forest because we only know $\{\rho\langle V_p \rangle\}_{ew}$; however, if we take it to be small relative to one then we will have satisfied (50). Thus, if we take

$$\frac{k_o^3 \langle V_p^2 \rangle}{6\pi \langle V_p \rangle} \frac{|\epsilon_r - 1|^2}{(\epsilon_r' - 1)} \approx 0.1 \quad (53)$$

then the average correction field will be small compared to the quasi-static internal field and the analysis will be self consistent. Substituting (53) in (52) yields

$$k^2 \approx k_o^2 \left\{ 1 - \{\rho\langle V_p \rangle\}_{ew} (\epsilon_r - 1) \langle (\hat{e} \cdot \hat{r})^2 \rangle (1 + j/10) \right\} \quad (54)$$

The imaginary part of the propagation constant determines the attenuation rate of the average coherent field. From (54) it is given by

$$\text{Im}(k) \approx -\frac{1}{2} k_o \{\rho\langle V_p \rangle\}_{ew} \langle (\hat{e} \cdot \hat{r})^2 \rangle [\epsilon_r'' + (\epsilon_r' - 1)/10] \quad (55)$$

Of particular note in (55) is the fact that the contribution to $\text{Im}(k)$ from the nonzero scattering cross section of the cylinder depends upon the real part of the dielectric constant or ϵ_r' . It is also possible that the scattering contribution is larger than the absorption effects, i.e.

$$(\epsilon_r' - 1)/10 > \epsilon_r''$$

This result, however, in no way violates (53) but is simply a condition involving the relative magnitudes of the real and imaginary parts of the dielectric constant.

For frequencies below about 500 MHz, $\langle (\hat{e} \cdot \hat{r})^2 \rangle = 1/2$ for vertically polarized fields and $\langle (\hat{e} \cdot \hat{r})^2 \rangle = 1/4$ for horizontally polarized fields (see Section 3.2.1). This difference is due to the dominance of the (vertically

oriented) tree trunks. For frequencies above 500 MHz, the dominance of the trunks disappears and $\langle (\hat{e} \cdot \hat{r})^2 \rangle = 1/3$ due to the branches. In this frequency range, the effect of the leaves must be included also. The above field perturbation analysis applies to the disc representation for the leaves except that $\langle (\hat{e} \cdot \hat{r})^2 \rangle$ is replaced by the sum $\langle (\hat{e} \cdot \hat{\theta})^2 \rangle + \langle (\hat{e} \cdot \hat{\phi})^2 \rangle = 2/3$; thus, the imaginary part of the propagation constant including wood and leaves is given by

$$\text{Im}(k_{y_h}) \approx -k_o \left[\epsilon_r'' + (\epsilon_r' - 1)/10 \right] \left\{ \frac{1}{6} \{\rho V_p\}_{ew} + \frac{1}{3} \{\rho V_p\}_{el} \right\} \quad (56)$$

This section has presented a very detailed derivation of how the quasi-static average field inside a Rayleigh particle having a random size and orientation can be corrected to properly reflect the non-zero scattering cross section of the particle. Unfortunately, the result of this correction and its impact upon the propagation constant of the average coherent field, (52), gives rise to a dependency upon characteristics of the foliage constituents which are not normally known, i.e. $\langle V_p \rangle$ and $\langle V_p^2 \rangle$. However, by requiring the correction field inside the particle or foliage constituent to be one-tenth the quasi-static or Rayleigh field, it is possible to obtain a relatively simple result for the effects of particle scattering upon the propagation constant of the average coherent field. By approximating the internal correction field as one tenth the zeroth order field, we are certainly making a gross assumption. However, the assumption is consistent with the Rayleigh-Effective Volume (REV) model and it does lead to a simple result which can be compared with measurements.

3.2.3 The Effective Fractional Volume Of Foliage

The Rayleigh-Effective Volume (REV) model equation for the propagation constant of the average or coherent field were developed in the previous

section. In order to evaluate this model one must know the complex dielectric constant of green wood and the effective fractional volume of the wood, $\{\rho V\}_{P_{ew}}$, and the leaves, $\{\rho V\}_{P_{el}}$, comprising the foliage in a forest. This section will be concerned with estimating the effective fractional volume of wood.

The effective fractional volume of the wood or needles in a forest comprises those cylindrically shaped components having a diameter to free space wavelength ratio of less than one half, i.e. $D/\lambda_0 \leq 1/2$. This particular criterion is based upon the experimental results presented in [6]. The estimation of $\{\rho V\}_{P_{ew}}$ as a function of D/λ_0 is a most difficult task because there are no extensive foliage measurements which directly apply to this problem. However, using some limited data on the percentage volume of wood of greater than 7 cm in diameter as a function of tree height [7], forest stand table data, and a model which we developed for estimating the total fractional volume of wood (see Appendix C) it is possible to estimate the behavior of $\{\rho V\}_{P_{ew}}$ as a function of D . A detailed description of the estimation technique is given in Appendix C along with details of how it might be applied to any forest. The results of this model and data are shown in Figure 3. The vertical axis is the effective fractional volume of the foliage remaining after all components of the forest having a diameter greater than a point on the horizontal axis are removed. Using the criterion of $D \leq 0.5 \lambda_0$, the horizontal axis has also been converted to frequency. Thus, for a specified frequency this fixes the point on the horizontal axis and one moves up vertically until the curve is intersected; the value of $\{\rho V\}_{P_{ew}}$ at the intersection is the effective remaining fractional volume for the specified frequency. When the curve flattens out, this indicates that all components of the forest satisfy $D \leq 0.5 \lambda_0$ and the value for $\{\rho V\}_{P_{ew}}$ is then equal to the total

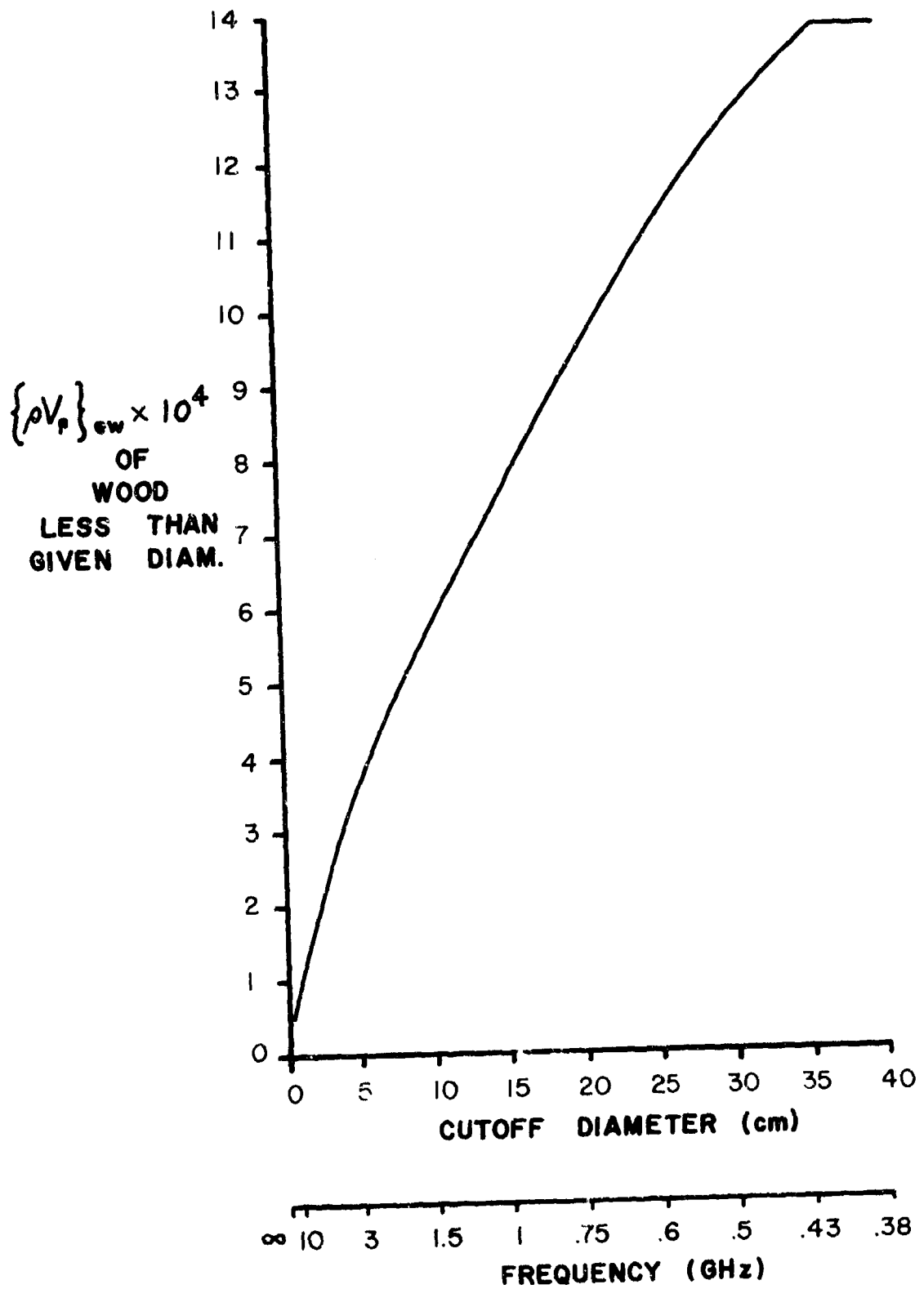


Figure 3. The effective fractional volume of the woody components of a forest based upon the criterion of $D/\lambda_0 \leq 0.5$.

fractional volume of the wood. It should be noted that we have developed the model for this curve to the point where we can estimate its shape based upon conventional forest stand table data. The curve will certainly change based upon the primary constituents of the forest, i.e. a small number of large diameter trees or a large number of small diameter trees. It should be emphasized that the curve in Figure 3 is based upon forest stand table data taken from a site in the Clear Creek Forest Experimental area in Anderson County, Tennessee. This site was described as a "fair" quality site with approximately 15 year old dominant tree growth comprising 60 square feet per acre of basal area density. A total of 1154 trees were counted to form the stand table data. The species of trees in this area were as follows; oak, yellow poplar, dogwood, and a few pines. We will use this curve to obtain estimates of the behavior of $\text{Im}(k)$ as a function of frequency in our model comparisons with measurements (see Section 4.2). However, if stand table data for a forested area are available, the techniques presented in Appendices C and F should be used to generate the appropriate equivalent of Figure 3. We did not do this in our comparisons because there were no stand table data reported with the propagation measurements.

Figure 3 shows that $\{\rho V\}_{p_{ew}}$ decreases as the frequency increases; thus, according to (55) and/or (56), the attenuation constant resulting from this model will increase at a less than linear rate with frequency. That is, since both $\text{Im}(k_v)$ and $\text{Im}(k_h)$ depend upon $k_o \{\rho V\}_{p_{ew}}$, the increase due to k_o is partially offset by the decrease in $\{\rho V\}_{p_{ew}}$ as the frequency becomes larger.

It should be noted from Figure 3 that at a frequency of 500 MHz only about 10% of the total fractional volume has been eliminated from $\{\rho V\}_{p_{ew}}$. According to the REV model, 500 MHz is the frequency at which the large tree

trunks are no longer effective in the attenuation of the coherent field. However, we should expect that the large tree trunks comprise more than 10% of the total fractional volume occupied by the woody components; thus there appears to be an inconsistency between the REV model and the approximate physical foliage data in Figure 3. This paradox may be due either to the approximate nature of Figure 3 or it may be that we have overestimated the amount of vertical structure that has to be eliminated from $\{\rho V\}_{p_{ew}}$ before the remaining woody components appear as randomly oriented cylinders. It may also be possible that Figure 3 should be based upon the more rigorous Rayleigh criterion involving the dielectric constant of the material, i.e. $k_0 \sqrt{\epsilon_r'} D \ll 1$. If, for example, this criterion were used to develop Figure 3, it would be found that for $\epsilon_r' \approx 50$ and at 500 MHz, $\{\rho V\}_{p_{ew}}$ only comprises ten percent of the total fractional volume of wood. In short, essentially no woody components of the forest are Rayleigh scatterers or absorbers and, in fact, nearly all components are sufficiently large in terms of a free space wavelength to be considered electrically large. This would explain the polarization insensitivity above 500 MHz because electrically large objects have scattering and absorbing cross sections which are equal to the geometric cross section of the object irrespective of polarization. We reject this logic for the following reasons. First, the transition frequency between polarization sensitivity and insensitivity should be a function of the dielectric constant ϵ_r' , i.e. because of the criterion $k_0 \sqrt{\epsilon_r'} D \ll 1$. However, foliage propagation measurements in Asian jungles [15] and western hardwoods [9] indicate that the transition frequency does not change with dielectric constant. Second, if the great majority of the woody components are electrically large, the attenuation constant should be independent of frequency (see Appendix A) yet total average power measurements do not show this. Finally, if the great majority of the

woody components are electrically large then the attenuation constant should be sensitive to the presence or absence of leaves and Trevor's measurements [9] at 540 MHz do not corroborate this hypothesis. Thus, we do not feel that the "large body" hypothesis is a viable alternative to the REV model and the inconsistencies between the REV model and Figure 3 are due to factors which we have yet to understand.

Unfortunately, we were not able to generate a curve similar to Figure 3 for leaves for two reasons. First, we do not have a size criterion to classify the leaves as Rayleigh scatterers such as the case with the woody components. Second, we found no data on leaves which could be used to estimate Figure 3. Thus, for the remainder of this report we will ignore the effect of the leaves on the attenuation constant of the coherent field. Fortunately, we can estimate at what frequency the leaves should start to be significant in their effect upon the attenuation constant. We know that leaves comprise no more than 10% of the total fractional volume of a forest. According to Figure 3, $\{\rho V\}_{p_{ew}}$ is down to 10% of its maximum value at about 3 GHz. However, according to equation (56) the effect of the leaves is magnified by a factor of two relative to the woody components. Thus, as a crude estimate we should expect the leaves to become significant at about 1.5 GHz. This frequency should be considered to be a crude estimate because the accuracy of the curve in Figure 3 is certainly open to question above 1.5 GHz.

3.2.4 The Dielectric Constant And Loss Factor For Wood

The remaining unknowns in the Rayleigh Effective Volume (REV) model are the dielectric constant ϵ_r' and the loss factor ϵ_r'' of live or green wood. A very comprehensive discussion of this topic is presented in Appendix D. The purpose of this section is to summarize the parts of Appendix D which are directly applicable to the propagation problem.

Figure 4 is a sketch of a section of trunk or branch of a tree; the purpose of this sketch is to define some nomenclature that is often encountered when dealing with dielectric constant measurements of trees. There are three primary directions that are used when referring to the dielectric constant of wood; longitudinal is equivalent to the z-axis of a cylindrical coordinate system, tangential is equivalent to a unit vector in the $\hat{\phi}$ -direction, and radial corresponds to a unit vector in the $\hat{\rho}$ -direction. The term parallel orientation is also used and this corresponds to the longitudinal direction while perpendicular orientation corresponds to any combination of radial and/or tangential directions. The terms perpendicular and parallel are obviously referenced to the direction of the wood grain.

Green wood is characterized by extremely large values of permittivity and loss factor at low frequencies. This unusual behavior is not well understood but is thought to be related to the complex molecular structure of cellulose and water and the manner in which they combine in wood. It is difficult to obtain dielectric constant measurements of wood in a natural state and many of the reported results have started with dried wood and they injected pure distilled water into the dry sample. How well these results predict the dielectric constant for natural wood is not known.

Figures 5 and 6 show measured values for the real part of the dielectric constant for the electric field oriented parallel and perpendicular to the grain, respectively. Broadhurst's [11] measurements were performed on cut samples of poplar having different moisture contents while James' [12] results were from dried and then water soaked samples of oak and Douglas fir. Of particular note here are the relatively large values of permittivity and the fact that it is relatively constant over the frequency range of interest to this study. Figures 7 and 8 present corresponding results for the loss factor

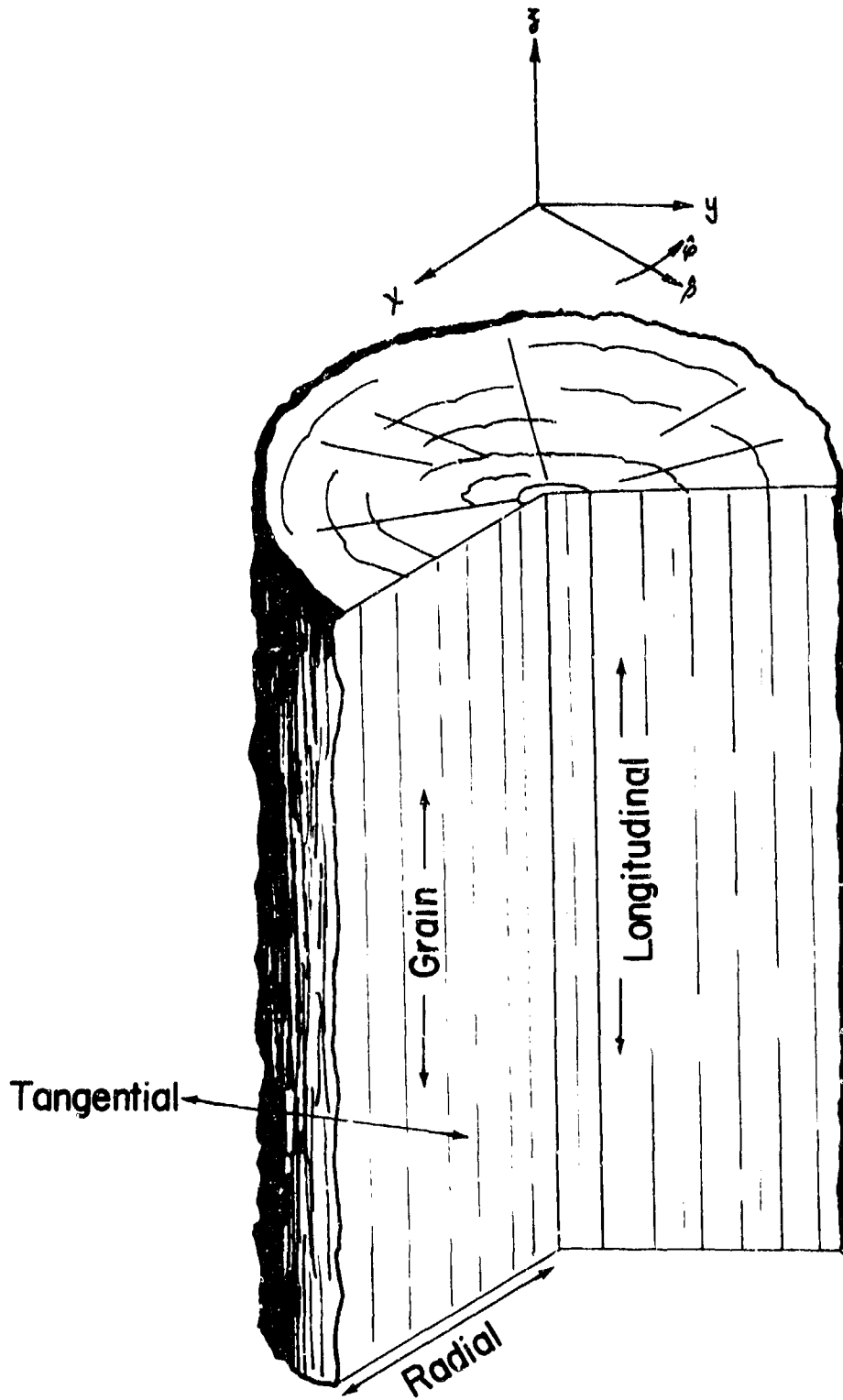


Figure 4. Schematic representation of a tree trunk, branch or twig defining commonly used directional nomenclature.

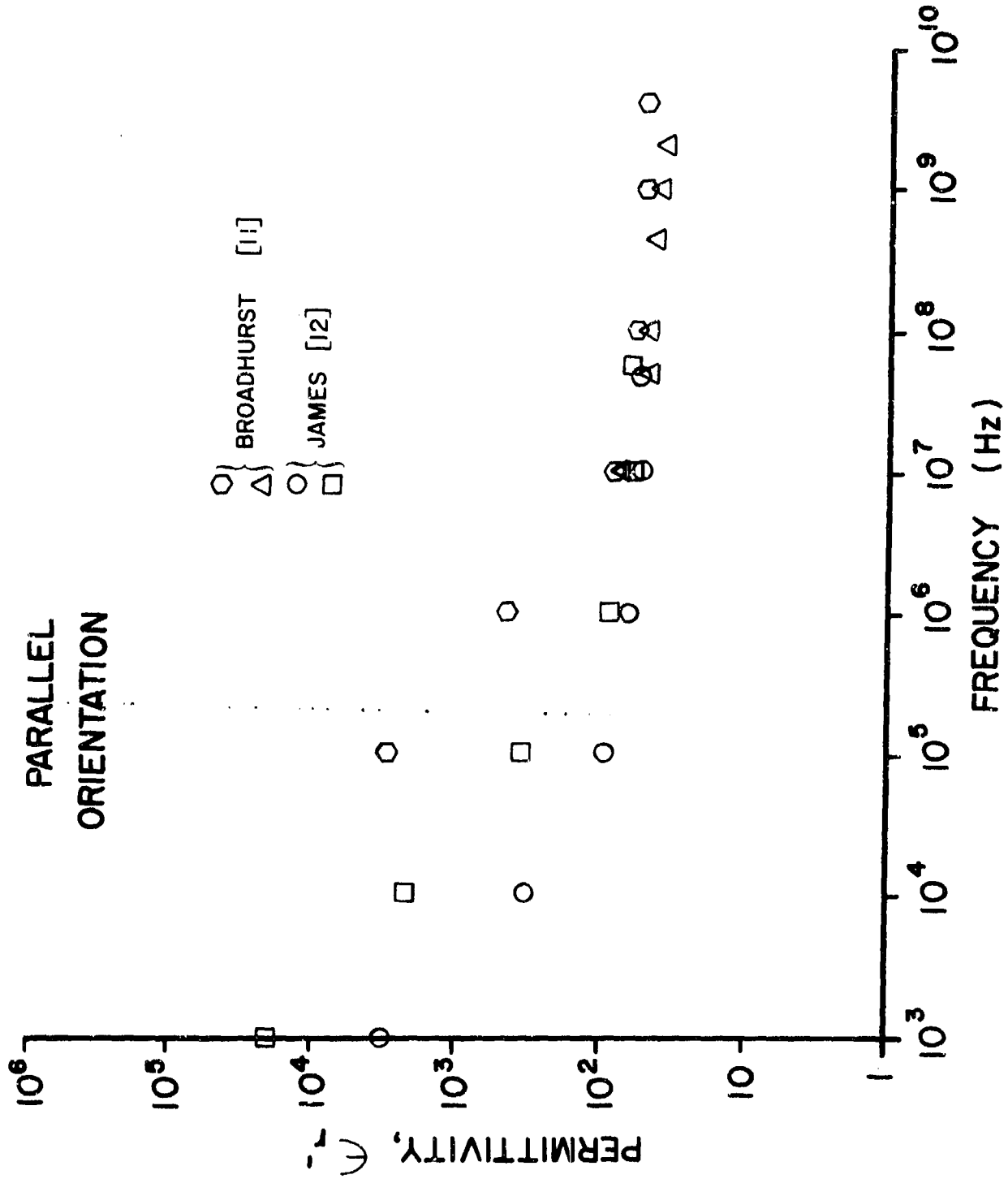


Figure 5. Measurements of the permittivity of wood for parallel (longitudinal/tangential) orientation of the electric field relative to the grain. (○ & △ poplar; ○ Douglas fir; □ oak)

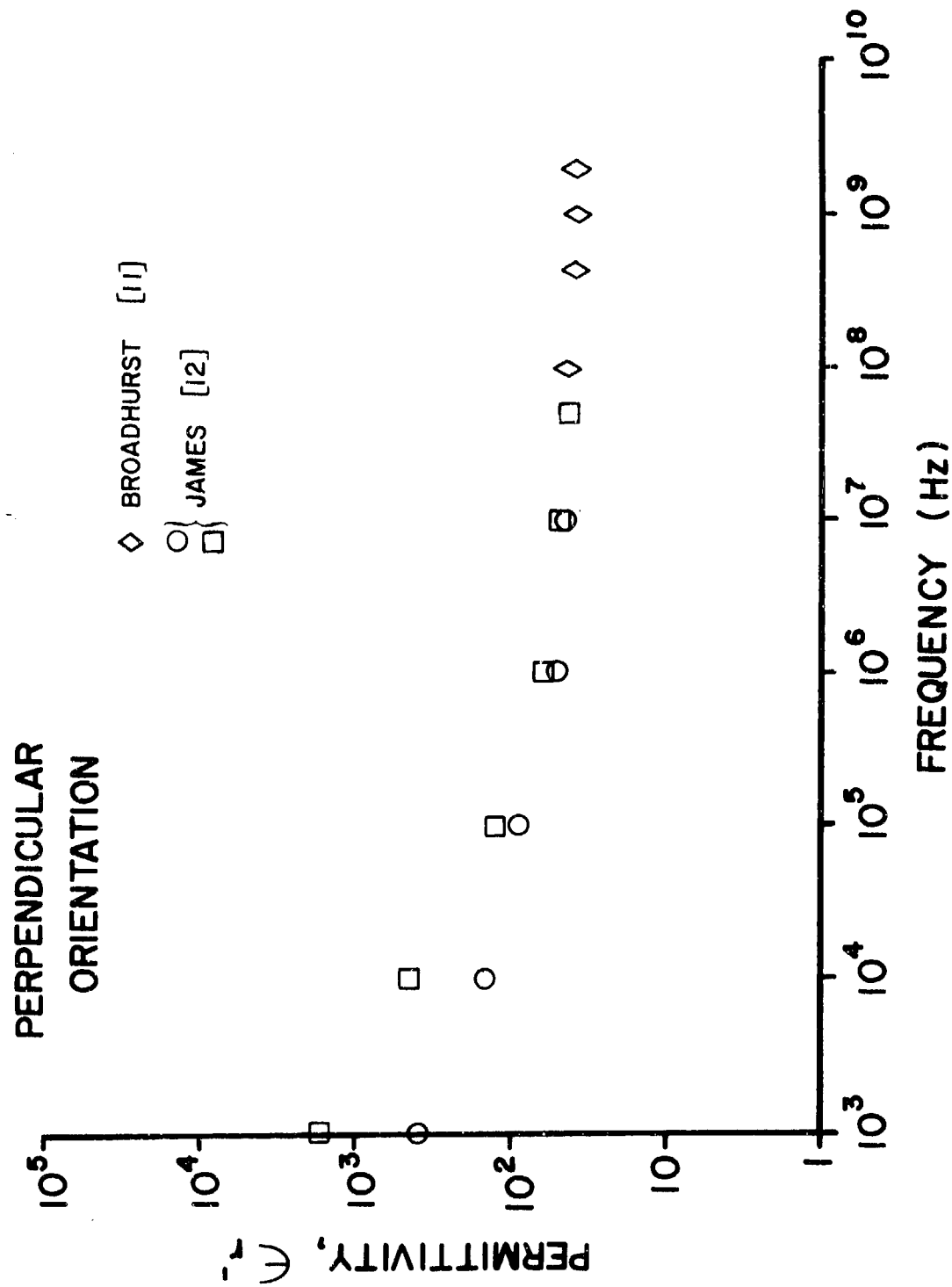


Figure 6. Measurements of the permittivity of wood for perpendicular (radial) orientation of the electric field relative to the grain. (◇ poplar; ○ Douglas fir; □ oak)

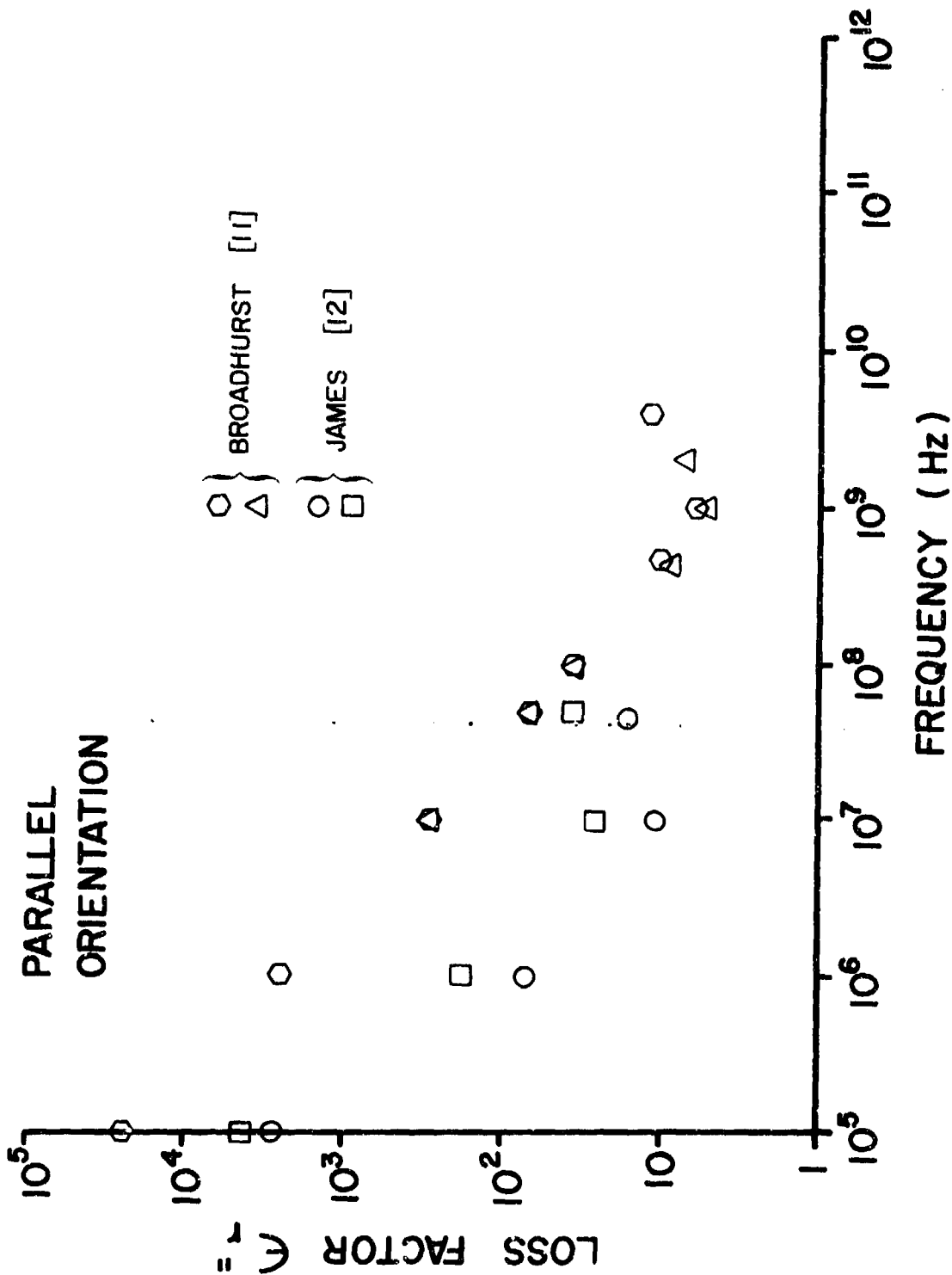


Figure 7. Measurements of the loss factor of wood for parallel (longitudinal/tangential) orientation of the electric field relative to the grain. (\circ Δ poplar; \circ Douglas fir; \square oak)

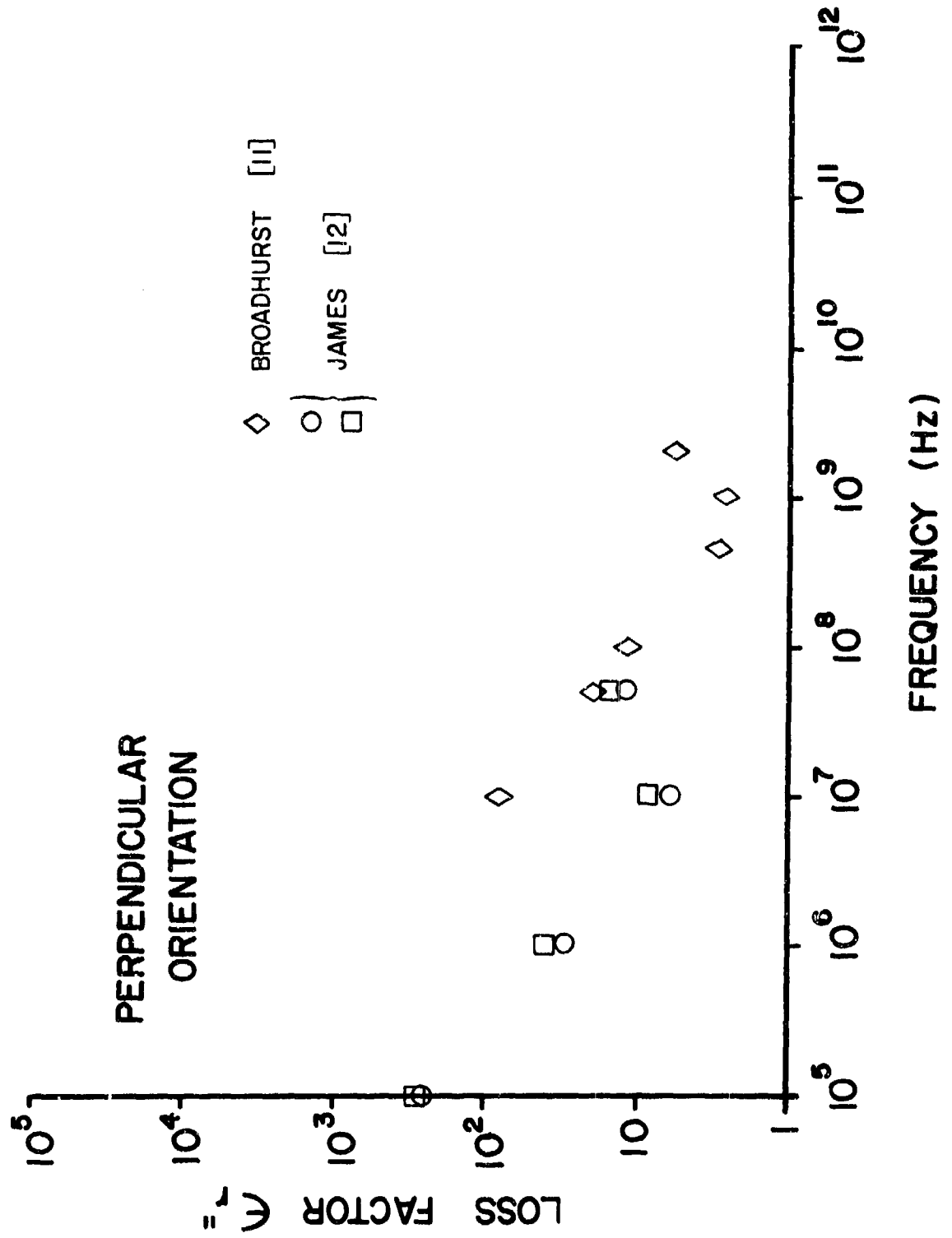


Figure 8. Measurements of the loss factor of wood for perpendicular (radial) orientation of the electric field relative to the grain. (◇ poplar; ○ Douglas fir; □ oak)

The variation of the loss factor with frequency shows an upturn near 1 GHz for Broadhurst's results while James' measurements indicate an upturn near 10 MHz. It is felt that Broadhurst's measurements are more representative of natural wood.

Figures 9 and 10 present estimates of the possible range of permittivity for hardwoods and softwoods as a function of frequency for parallel and perpendicular orientation, respectively. The range of values given in these Figures are primarily for summer months. For winter, the permittivity will decrease but it is not completely known by how much.

Variation of the loss factor with frequency, time of year and tree type is less well known. For frequencies below 10 MHz, the loss factor is dominated by ionic conductivity due to salts and other minerals in the tree sap. The variation with frequency appears to be something like $1/f$, but this depends to a degree upon the density of the wood. That is, there is also some effect resulting from high frequency cellulose relaxation loss. Above 10 MHz the situation becomes more complex due to the combined effects of conduction loss and dipolar or Debye relaxation loss. The complexity is a result of the effect of impurities in the water and changes in the Debye effect resulting from mixing water and wood. These factors can give rise to the following changes in the Debye relaxation curve; a shift in the center frequency of the Debye curve, possible multiple resonant-like losses due to the cellulose-water mixture, and a reduction in amplitude and spreading of the basic Debye curve. The situation is further complicated by the fact that there are few measurements of the loss factor in the frequency range of interest to this study; almost none of the limited measurements reported were performed on true green wood, and some of the measurements are contradictory. For example, in Figures 7 and 8 Broadhurst's measurements hint at a normal Debye-like

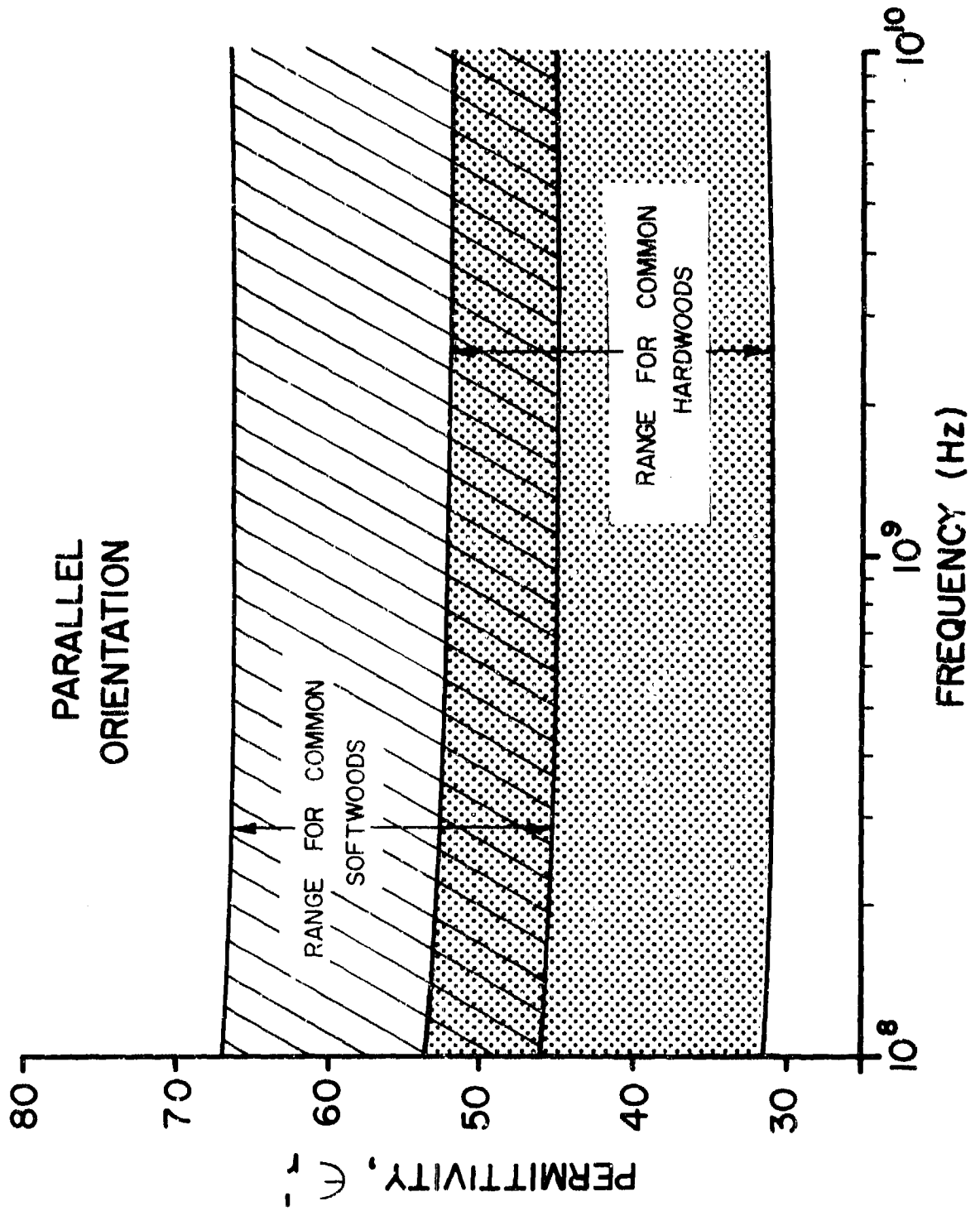


Figure 9. Estimated range of permittivity for green wood, parallel (longitudinal/tangential) electric field orientation, and summer temperatures.

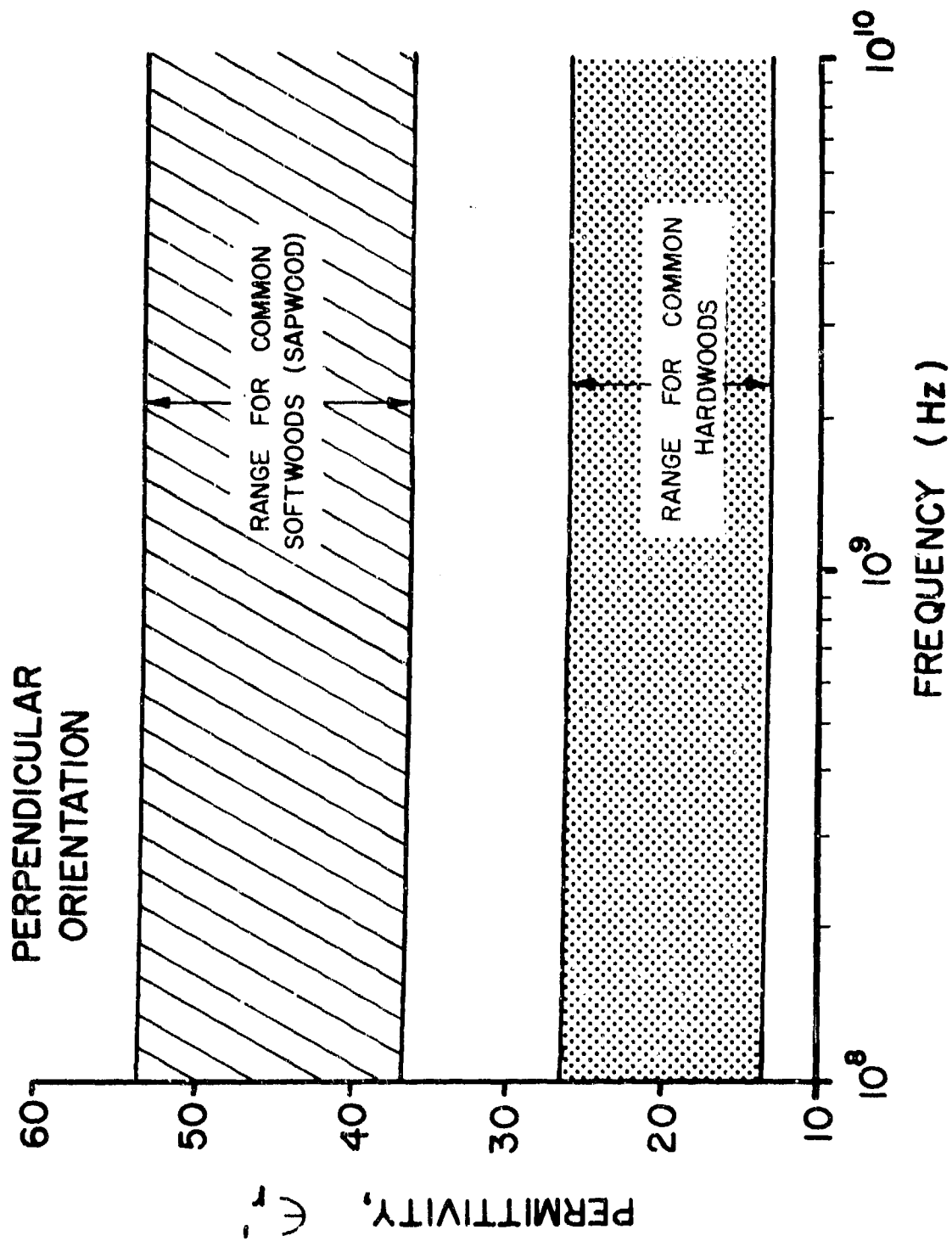


Figure 10. Estimated range of permittivity for green wood, perpendicular (radial) electric field orientation, and summer temperatures.

relaxation loss but his measurements do not go high enough in frequency to completely validate this hypothesis. James' measurements, on the other hand, indicate the initiation of a relaxation type loss at a much lower frequency. Trapp and Pungs [13] cloud the issue further by reporting significantly lower values of loss factor for fir wood.

The above inconsistencies have forced us into a very careful review of the measurement procedures employed in these experiments. It is our opinion that Broadhurst's results are most representative of the true green wood. This opinion is based upon his use of green wood in his experiment and his very scrupulous attention to the error sources (and their minimization) in his experimental apparatus. Based upon Broadhurst's measurements, we are presently using the following relation to estimate the loss factor for wood;

$$\epsilon_r'' = \frac{A}{f^{0.96}} + \frac{B(f/f_c)}{1 + (f/f_c)^2} \quad (57)$$

where

$$A \approx \begin{array}{ll} 1.5 \times 10^9 & \text{(Electric field parallel to grain)} \\ 4 \times 10^8 & \text{(Electric field perpendicular to grain)} \end{array}$$

and

$$f_c = \begin{array}{ll} 20 \text{ GHz} & \text{for summer (25°C)} \\ 10 \text{ GHz} & \text{for winter (0°C)} \end{array}$$

The factor B represents a modification to the magnitude of the basic Debye relaxation loss; it has been assumed that any spreading of the Debye loss is negligible. The data that we used to construct (57) is definitely limited (see Appendix D); these data do however indicate a unique relation between B and the product $\mu\rho$ where μ is the moisture content of the wood and ρ

is the density or specific gravity of the wood. The product $\mu\rho$ is also sometimes called the water volume ratio. A plot of our estimate of the relationship between B and $\mu\rho$ is shown in Figure 11.

It should also be noted that isolating winter effects to only a change in the Debye frequency is very approximate. During extremely cold periods where the temperature is below freezing for a long time, B should also decrease. In fact, if the moisture in the tree freezes, B should approach zero since ice does not exhibit a high frequency Debye effect.

A plot of (57) using the B curve in Figure 11 is shown in Figure 12. The dip in the vicinity of 1 GHz is the transition between conduction loss and Debye relaxation loss. Since the curve is based upon Broadhurst's measurements, it should be most representative of poplar trees. Hardwood trees will probably exhibit greater loss factors at the low end of the frequency band in Figure 12 due to their higher density. Pines, firs and other needle bearing coniferous trees may have a larger Debye loss due to their increased moisture content. At this time there is very little data for extending the results in Figure 12 to a wide variety of trees.

It should be noted that Figures 5 - 8 are presented as a function of the orientation of the incident electric field with respect to the wood grain, i.e. parallel or perpendicular. James, in his measurements, observed this convention. Closer examination of Broadhurst's measurements technique indicate that he deviated from this convention. Instead of aligning the grain of his sample parallel to the electric field, as stated in Figures 5 and 7, he aligned it so that the electric field was in a combination of longitudinal and tangential directions. For the perpendicular cases in Figures 6 and 8, his sample was aligned in the radial direction. Since we have used his measurements to estimate ϵ_r'' , all of our model results are strictly only

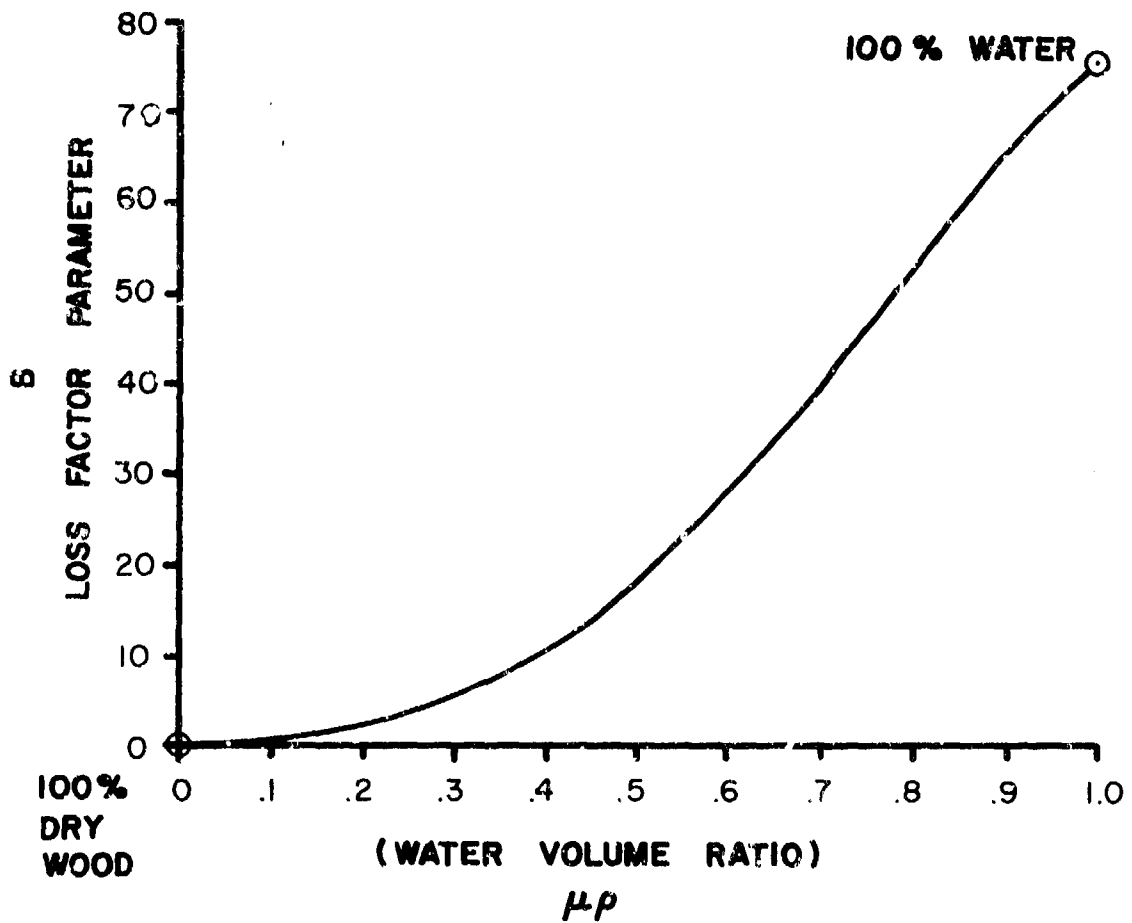


Figure 11. The estimated variation of the Debye loss factor parameter for green wood as a function of the moisture-density product.

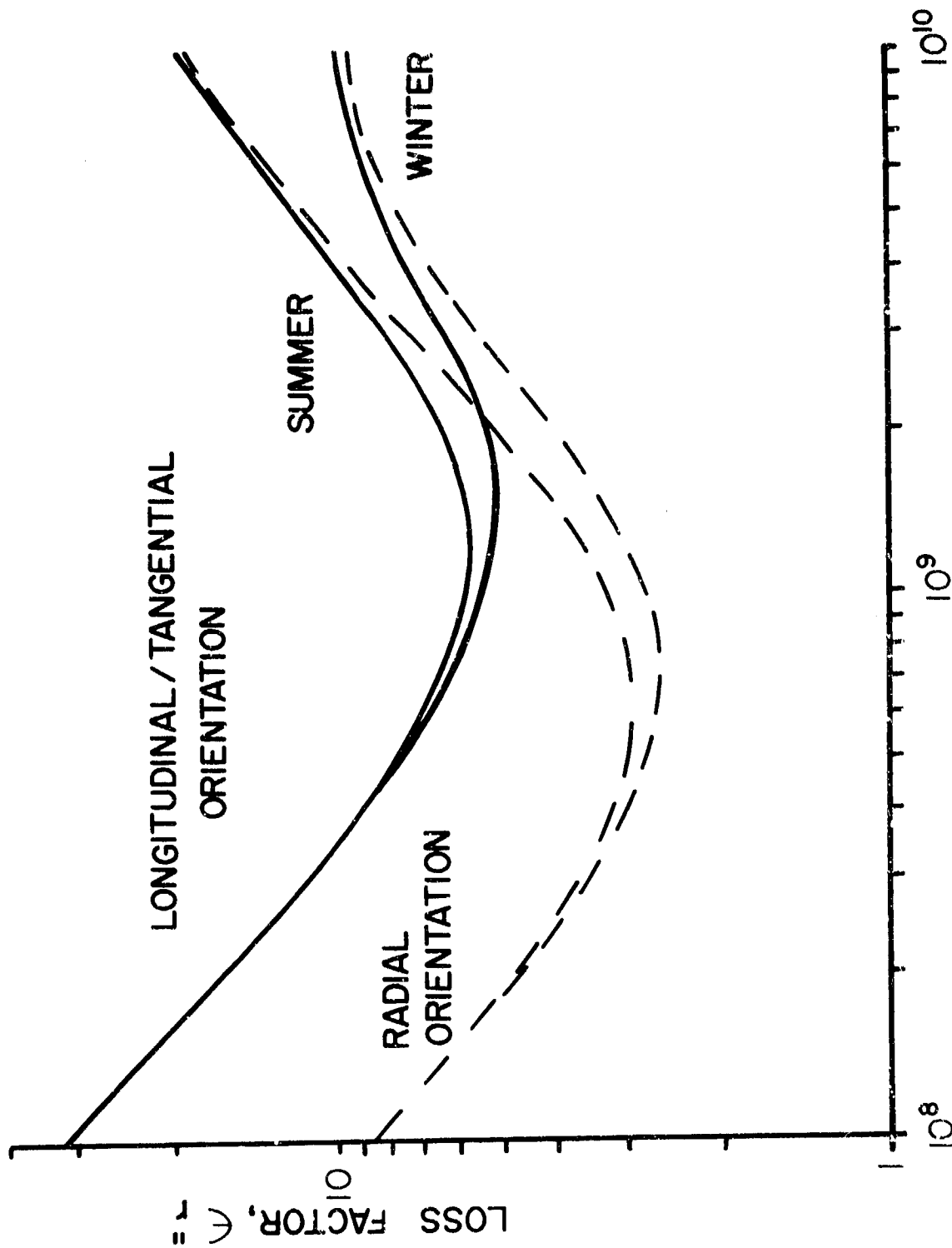


Figure 12. The estimated variation of the loss factor for green wood as a function of frequency, season, and field orientation.

applicable for the electric field in either the longitudinal/tangential direction or the radial direction and we have so labeled our curves. However, we feel that the longitudinal/tangential direction is most nearly equivalent to the parallel orientation while radial is closest to the perpendicular orientation.

3.3 REV Model Calculations

Each of the previous sections of this report have dealt with certain aspects of the model for the propagation constant of the average field propagating through a forest. Although this degree of detail was necessary, it also tended to obscure the end result of the study. The purpose of this section is to combine all the aspects of the model to illustrate the type behavior of the attenuation constant that is predicted by the model. For these results, Figure 3 will be assumed to accurately represent the effective fractional volume of the wood in a well developed forest. Figure 12 will also be assumed to be a reasonable representation for the loss factor of the trees in the forest.

If one ignores the change in probability density function for the orientation of the cylinders representing the wood for frequencies greater than 500 MHz, the attenuation constants due to absorption only for vertical and horizontal polarization are given by (13) and (14) or

$$\begin{aligned} \text{Im}(k_v) &= \frac{1}{4} k_o \epsilon_r'' \{\rho V_p\}_{ew} \\ \text{Im}(k_h) &= \frac{1}{8} k_o \epsilon_r'' \{\rho V_p\}_{ew} \end{aligned} \tag{58}$$

The model contained in (58) is interesting because it illustrates what would happen if there were no change in the orientation statistics as $\{\rho V_p\}_{ew}$ decreases. The inclusion of absorption effects only means that the results can

be compared to total power measurements [1]. Figure 13 is a plot of (58)^⑥ as a function of frequency, polarization, season, and parallel field orientation. The flatness of the curves at the low frequency end results from the inverse dependence of ϵ_r'' on frequency (see Figure 12). The cusps around 400 MHz represents the onset of $\{\rho V\}_{p_{ew}}$ decreasing. The increase in the attenuation beyond 1 GHz is a result of the product $k_o \epsilon_r''$ increasing at a faster rate than $\{\rho V\}_{p_{ew}}$ is decreasing. Figure 14 shows the attenuation constants for the electric field perpendicular to the wood grain. For the perpendicular orientation, the attenuation constant starts off smaller but rises faster so that near 10 GHz both orientations are comparable. It is interesting to note that seasonal effects are most predominant beyond 1 GHz; this is a consequence of the temperature effects on the moisture dependent dielectric losses and is not related to the presence or absence of leaves.

It is wise at this point to reemphasize the frequency limitations of the model. For leaf bearing trees the model is probably not accurate beyond 1.5 GHz. This is because at 1.5 GHz the "magnified" fractional volume occupied by the leaves, see (56), is comparable to the effective fractional volume of the wood and the model does not account for the leaves. For needle bearing trees such as pine, fur and spruce the model should be good up to 10 GHz because the needles can be accounted for by the canonical cylinder representation. However, 10 GHz is really stretching the accuracy of the $\{\rho V\}_{p_{ew}}$ curve shown in Figure 3 and the basic assumptions in the REV model. The actual upper frequency bound on the model is probably most dependent upon when optical reflection and diffraction become important. At the present time, no estimate is available for the frequency at which this occurs.

^⑥The units of (58) are nepers/meter; conversion to dB/m is accomplished by multiplying (58) by 8.686, i.e. $20 \log_{10} e$.

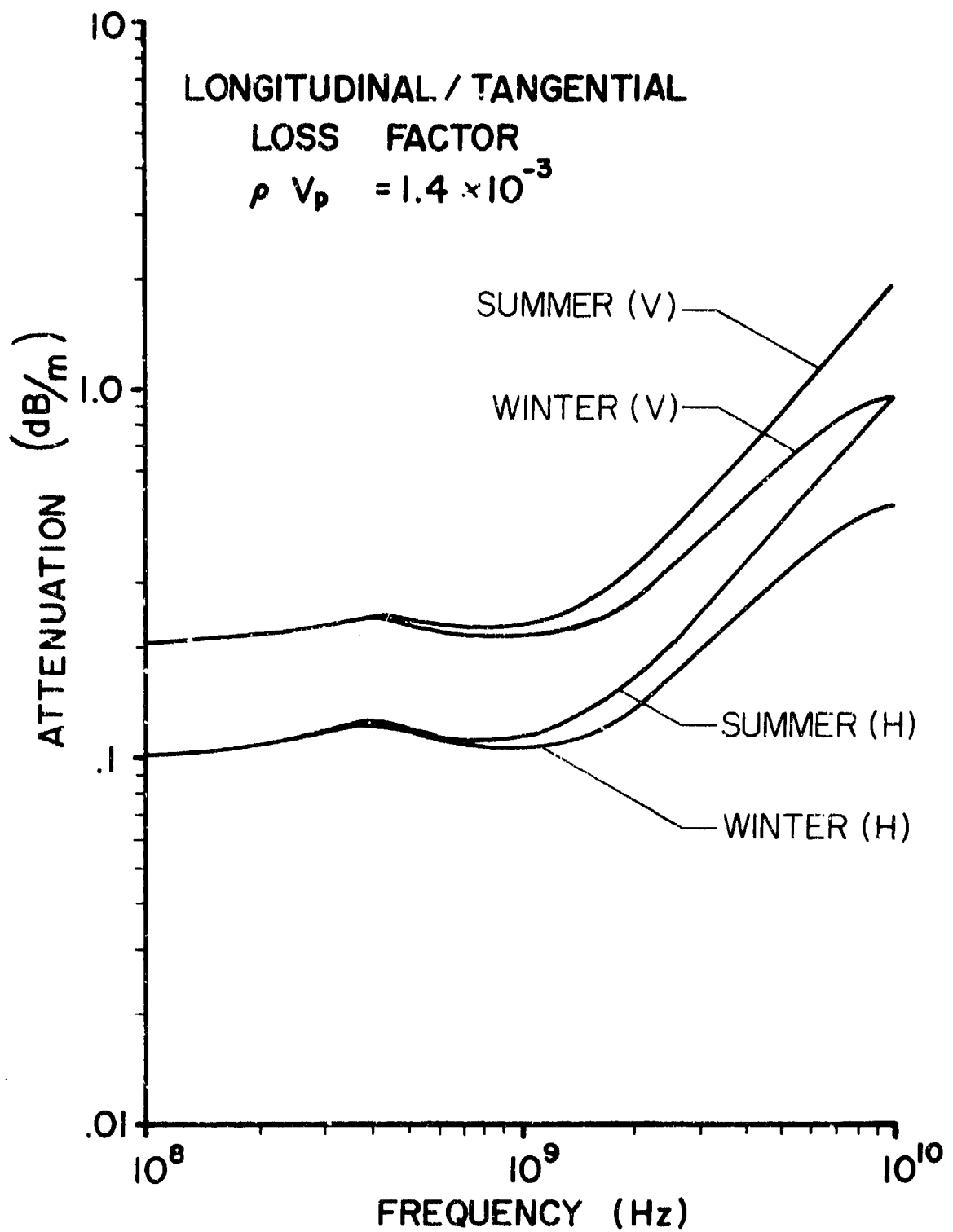


Figure 13. The predicted attenuation constant for the average coherent field oriented parallel to the wood grain, and a skewed orientation of the woody components. Only absorption has been included.

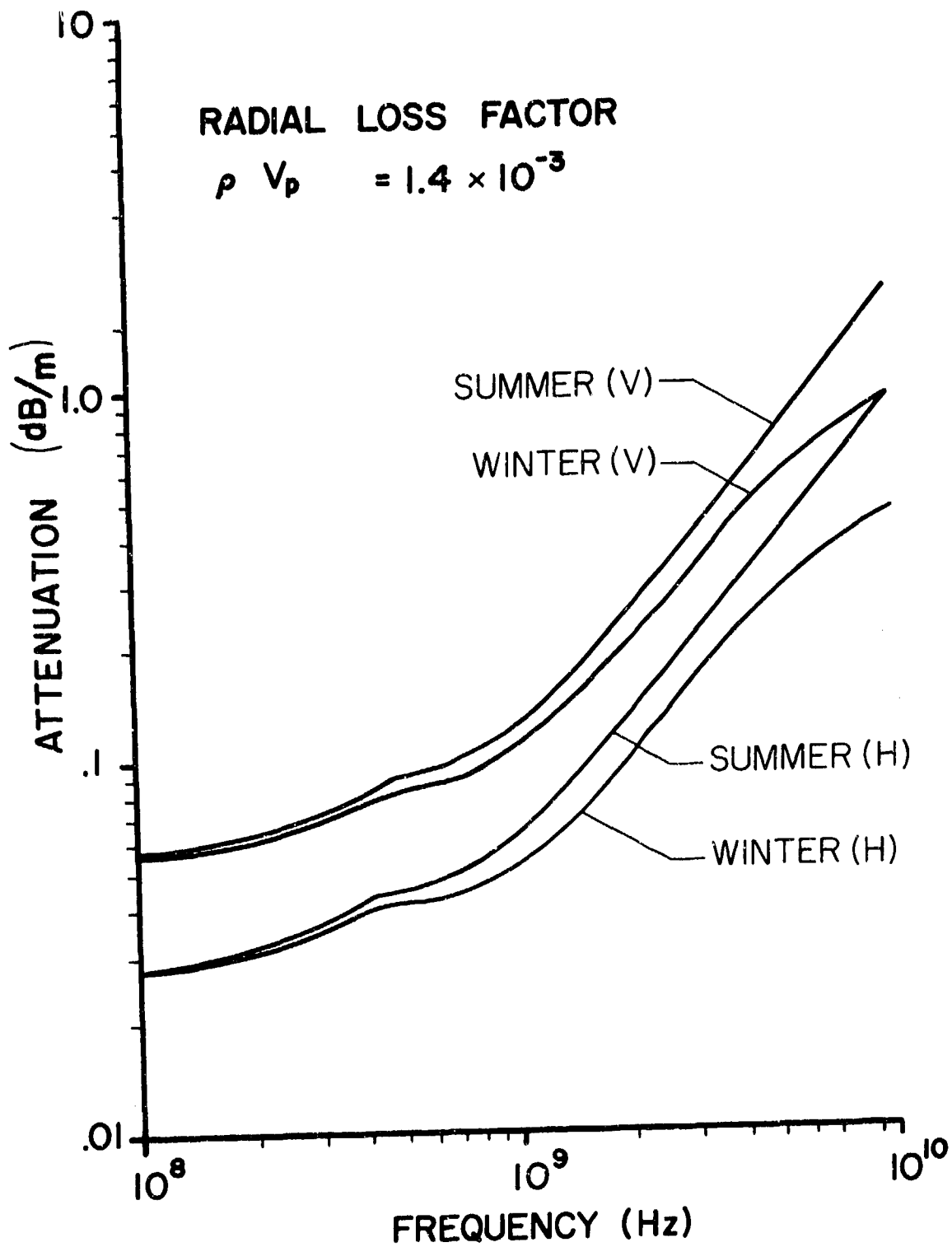


Figure 14. The predicted attenuation constant for the average coherent field oriented perpendicular to the wood grain, and a skewed orientation for the woody components. Only absorption has been included.

If (58) is corrected to include the change in probability of orientation of the cylinders representing the wood, the following result is obtained from (13), (14), and (21);

$$\text{Im}(k_v) = \alpha_v k_o \epsilon_r'' \{\rho V_p\}_{ew} \quad (59)$$

$$\text{Im}(k_h) = \alpha_h k_o \epsilon_r'' \{\rho V_p\}_{ew}$$

where

$$\alpha_v = \begin{cases} 1/4 & f < 500 \text{ MHz} \\ 1/6 & f \geq 500 \text{ MHz} \end{cases} \quad (60)$$

and

$$\alpha_h = \begin{cases} 1/8 & f < 500 \text{ MHz} \\ 1/6 & f \geq 500 \text{ MHz} \end{cases} \quad (61)$$

Figures 15 and 16 show the behavior of the attenuation constants for parallel and perpendicular field orientation with respect to the grain, respectively. The only difference between these results and those shown in Figures 13 and 14 is the change in polarization dependence resulting from the deletion of tree trunks from $\{\rho V_p\}_{ew}$ and the subsequent uniformity in random orientation of the remaining wood foliage components. It should be pointed out that the transition region between 300 and 500 MHz was simply hand sketched since there is no analytical description of this region. Also, in order not to clutter the curve too much, only the summer value of the attenuation constant is shown.

The dip in the attenuation constant for vertical polarization and parallel orientation near 500 MHz is intriguing in that it suggests that 500 MHz may be a better choice than 100 MHz if lower loss is desired. However, it must be remembered that these curves have been based upon a number of approximations and the dip may well reflect inaccuracies in these approximations.

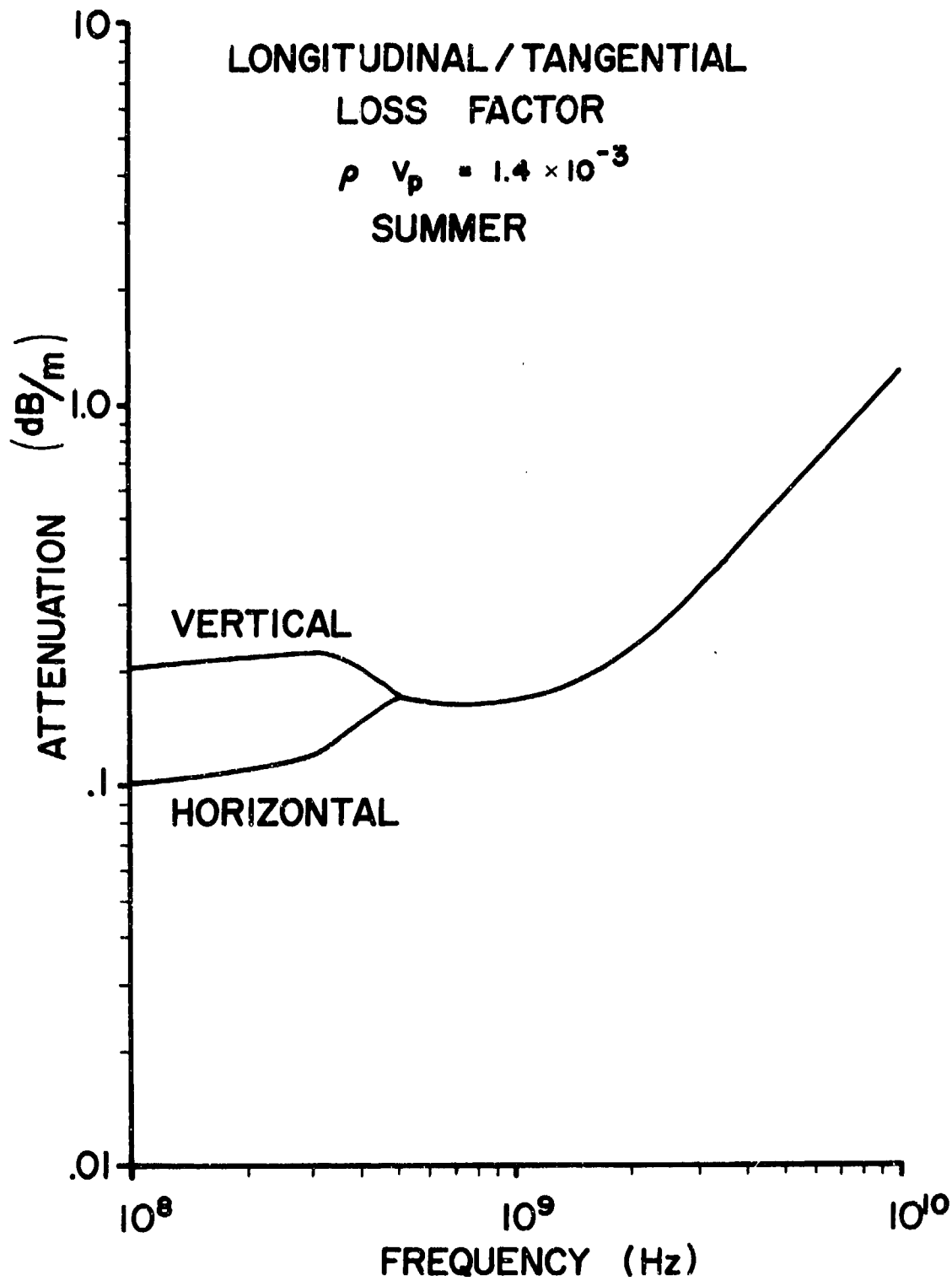


Figure 15. The predicted attenuation constant for parallel field alignment. Only absorption has been included.

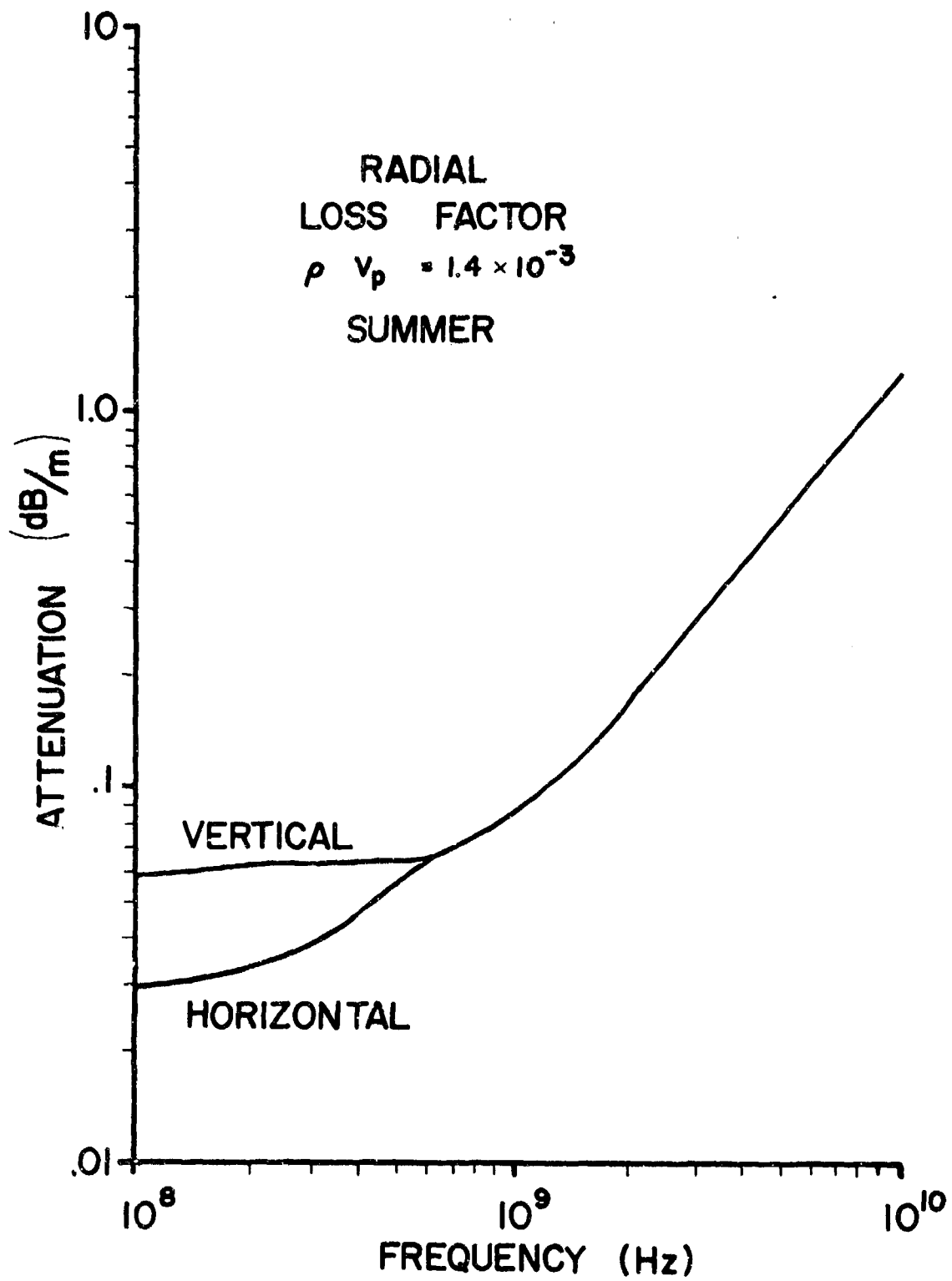


Figure 16. The predicted attenuation constant for perpendicular field alignment. Only absorption has been included.

The lack of a dip for perpendicular orientation may indicate that one must use both orientations, appropriately weighted, to obtain the true polarization dependence of the loss factor. This aspect of the problem has yet to be studied. In any case, Figures 15 and 16 are representative of what the model predicts when one only includes absorption effects. Consequently, the results in Figures 15 and 16 should be comparable to attenuation constant data obtained from average total power measurements acquired at large separation distances [1, Vol II].

The propagation constant for the average field in the foliage must include the effects of particle scattering. Thus, using (55) and the polarization dependent coefficients α_v and α_h for $\langle(\hat{e} \cdot \hat{r})^2\rangle/2$ yields the following result for the attenuation constant of the average field;

$$\begin{aligned} \text{Im}(k_v) &= -\alpha_v k_o \{\rho V_p\}_{ew} \left[\epsilon_r'' + (\epsilon_r' - 1)/10 \right] \\ \text{Im}(k_h) &= -\alpha_h k_o \{\rho V_p\}_{ew} \left[\epsilon_r'' + (\epsilon_r' - 1)/10 \right] \end{aligned} \quad (62)$$

where α_v and α_h are defined in (60) and (61). It is worth noting in (62) that the scattering effects have the same polarization dependence as absorption and this is a consequence of the Rayleigh approximation. Figure 17 compares (62) with (59) for parallel orientation; this illustrates that the inclusion of scattering increases the attenuation. Figure 17 also indicates that the most significant effect occurs near 1 GHz. This results from the decrease in ϵ_r'' in the neighborhood of 1 GHz, see Figure 12, and the relative constant value of ϵ_r' (≈ 50) over the entire frequency range shown in Figure 17. According to (62), the impact of scattering is going to be highly dependent upon the ratio of permittivity to dielectric loss factor. This is also a direct consequence of the Rayleigh assumption. The intriguing point of Figure 17 is

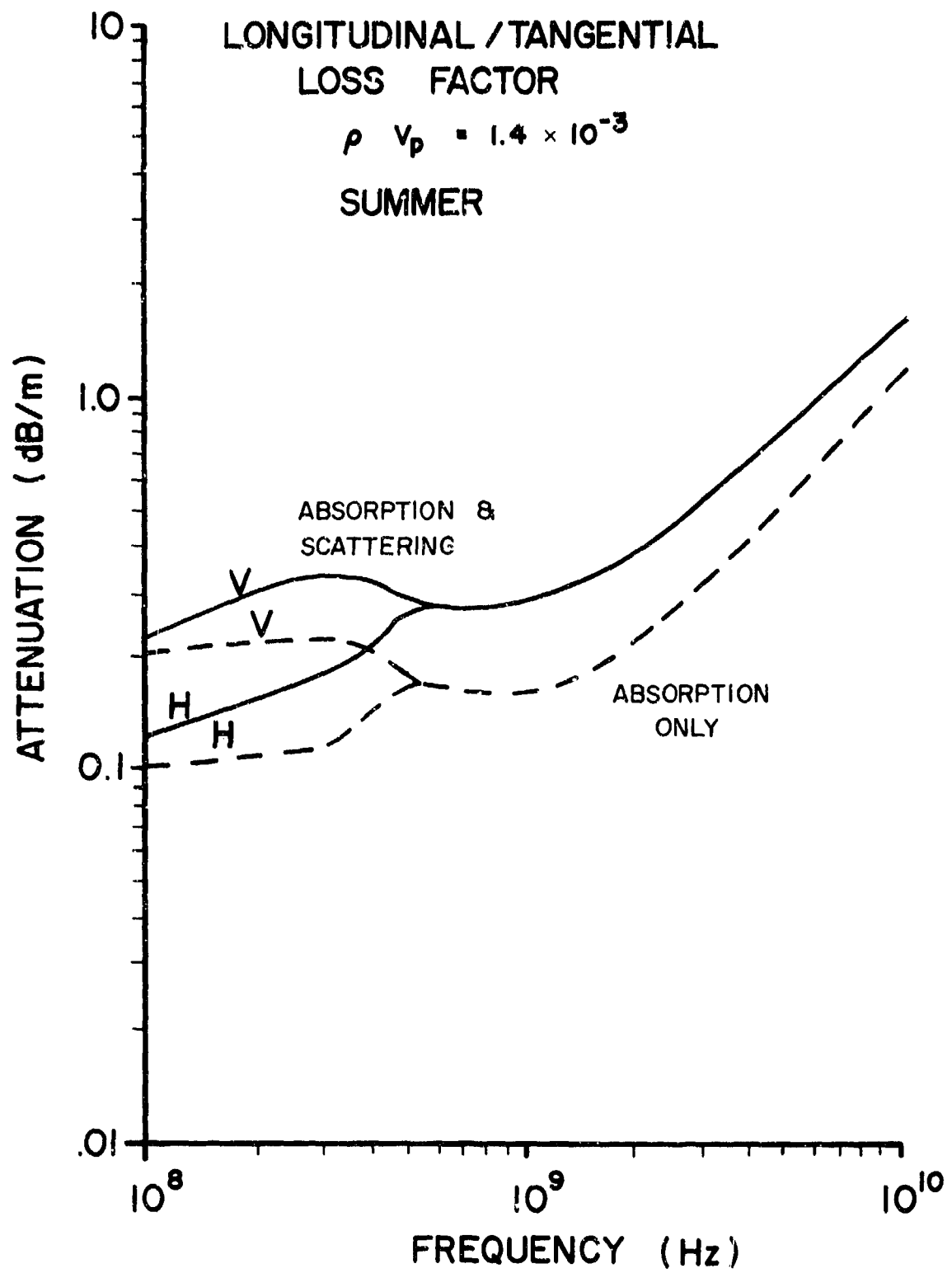


Figure 17. Model predictions based upon absorption only and absorption plus scattering by the woody cylinders comprising the forest.

that scattering increases the attenuation constant by no more than a factor of two. Whether or not this is an accurate model of the actual propagation situation remains to be determined. Unfortunately, there are no data to compare the model with and there are no "rules of thumb" to apply to this situation. Certainly if the absorption only curve in Figure 17 compares favorably with total average power measurements, then one should expect that the scattering model is also reasonably accurate. This is the case because the model has been based upon a self consistent analytical development and it is difficult to see how one result of the model could be correct and another be grossly in error. In any case, a final proof of the model must await the acid test of comparison between theory and measurement.

4.0 MEASUREMENTS AND MODEL COMPARISONS

The previous sections have been concerned with the development of an analytical model for the propagation constant of the average field in a foliated environment. The true test of such a model is its agreement with measurements. However, in all fairness to the model the measurements must also provide estimates of the input variables to the model. In the past, these supporting measurements have been almost nonexistent. Therefore, all we can really hope for in a comparison between theory and past measurement is a reasonable degree of agreement and some logical rationale for large disagreements.

4.1 Review of Measurements

In addition to the above limitation, most past measurements were accomplished before propagation through forests was well understood. It is now reasonably well established that there are at least four mechanisms by which energy launched at point A can be propagated to point B when either A or B or both are immersed in foliage. At low frequencies the primary mechanism is a surface wave which propagates along the foliage-ground interface. As

the frequency increases, it is possible for the energy to be transmitted by ionospheric bounce. Ionospheric bounce usually only occurs for large separations between transmitter and receiver and therefore need not be considered for short transmission paths. As the frequency increases further, it is possible for a lateral wave to become the dominant mode of propagation; the lateral wave propagates along the foliage-air interface. Although much is known about the lateral wave's characteristics [14], there are still some gaps in the theory. For example, it is not really known at what frequency it is no longer of importance and we do not know the minimum separation distance necessary to support the lateral wave. Finally, direct propagation through the foliage is possible; this is the mode that we are attempting to model. Even the measurement of this propagation mechanism is complicated because one must realize the intermixing between coherent and incoherent fields.

The primary consequence of the above considerations is that one simply cannot set up a transmitter and receiver, measure the loss, divide the loss by the distance, and arrive at a meaningful value for the average attenuation constant. One must not only tailor the measurement to isolate and identify the mode of propagation but attention must also be given to obtaining an adequate statistical sample of the propagation process if average values are to be meaningful. These are some of the criteria that have been used in reviewing some of the past measurements.

4.1.1 Jansky and Bailey [15]

Probably the most comprehensive set of measurements ever reported in the open literature were accomplished by the staff of Jansky and Bailey in Thailand during the mid 1960's [15]. Not only did the measurements comprise many frequencies but they also encompassed a number of other important variables such as polarization, antenna height, and terrain effects. The real worth of

these measurements resulted from the experimental attempts to separate the lateral wave from the direct wave. This was accomplished by measuring the attenuation as a function of separation distance between the transmitter and receiver. Since the "through-the-foliage" wave primarily attenuates exponentially with distance and the lateral wave attenuates as d^{-2} , it is possible (though not easy) to isolate the two mechanisms. This technique is especially important in the frequency range of 100 - 500 MHz. Unfortunately, their analysis of the data and subsequent estimation of the attenuation coefficients appear to be in error by a factor of 8.686 for the 100 MHz to 400 MHz data.

They assumed that the loss due to the direct path through the foliage was given by

$$L_D = -20 \log_{10} \left(\frac{A}{d} e^{-1609 \alpha d} \right)$$

where L_D is the loss in dB, A is a constant, α is the attenuation constant in dB/m and d is the separation distance in miles. The factor 1609 is the constant necessary to convert d from miles to meters so that it is dimensionally compatible with α , i.e. 1 mile = 1609 meters. The units of α as it appears above are not dB/m but rather nepers/m; thus the values reported by Jansky and Bailey should be multiplied by 8.686 to obtain the attenuation constant in dB/m. Table I shows the corrected values of α as a function of frequency and polarization. The results reported by Jansky and Bailey also indicated that the transition from the through-the-foliage mode to the lateral wave mode occurred at about 80 to 160 meters separation distance between the transmitter and receiver. The larger separation distance corresponded to the lower frequency of 100 MHz. These results are important because they indicate that the lateral wave can become important at much shorter distances than analytical estimates predict [14].

Although the lateral wave propagates primarily along the foliage-air interface, it does encounter some "through-the-foliage" attenuation in propagating from the transmitter to the interface and from the interface to the receiver. Tamir [14] reported values of the attenuation constant for this "through-the-foliage" path taken by the lateral wave. These data were reportedly obtained from one of the Jansky and Bailey interim reports and are repeated in Table II for the frequencies of interest to this study. The disturbing points of these data are that they are significantly larger than the results in Table I and they do not show the same polarization dependence. It could be that the values in Table II represent the attenuation constant for the average coherent power whereas the Table I values correspond to the attenuation constant of the total average power. Since the attenuation of the coherent power depends upon absorption and scattering while the total power only depends upon absorption, the results in Table II should be larger than those in Table I. However, the differences appear to be too large to be self-consistent. That is, if the frequency is 100 MHz and we assume the total through-the-foliage path length for the lateral wave is 100 m for example then the average coherent power will suffer 10 dB (vertical) and 7.5 dB (horizontal) attenuation due to the foliage. The total average power, according to the results in Table I, will only be attenuated by 3.9 dB (vertical) and 1.7 dB (horizontal) and the received power should therefore be dominated by the lower absorption losses. Thus, it is difficult to understand how the results in Tables I and II can be compatible, and it appears that the results in Table II are somewhat too large. This point certainly bears further investigation.

The Jansky and Bailey report also contains attenuation constant data for the frequency range of 550 MHz to 1.0 GHz. Smoothed estimates of their

TABLE I

Corrected Attenuation Constant Data From Jansky and Bailey

Frequency (MHz)	POLARIZATION	α [*] nepers/meter	α dB/meter
100	V	.045	.391
100	H	.020	.174
250	V	.050	.434
250	H	.025	.217
400	V	.055	.478
400	H	.035	.304

*These values were erroneously reported by Jansky and Bailey to have the units of dB/meter.

TABLE II

Attenuation Constant Obtained From Jansky and Bailey
Lateral Wave Data and Reported by Tamir [14]

Frequency (MHz)	Polarization	α_L (dB/m)
50	V	.69
50	H	.56
100	V	1.0
100	H	.75
250	V	1.08
250	H	1.04

measurements are shown in Figure 18. Area A was characterized by dense underbrush and a large number of double canopy deciduous hardwood trees. Area A is also where the data in Table I were acquired. Area B is dominated by bamboo of various sizes ranging from sticklike to extremely thick clumps. The attenuation data were acquired along three propagation paths in Area A and four paths in Area B. Because of the limited number of measurements used in constructing the curves in Figure 18, it is not clear how representative of the average attenuation characteristics of the foliage the data in Figure 18 are. Also, no histograms of the attenuation constant were presented in the Jansky and Bailey report.

4.1.2 Saxton and Lane [16]

Probably one of the most oft quoted measurements in the open literature are those presented by Saxton and Lane [16]. The Saxton and Lane paper actually summarizes a number of measurements which were obtained earlier but primarily had not been reported. The original Saxton and Lane paper should be consulted for the actual sources of the data.

One reported measurement was accomplished in the summer with deciduous trees in full leaf and at 540 MHz; through 85 meters of foliage, they found the attenuation to be 0.18 dB/m and 0.2 dB/m for horizontally and vertically polarized waves, respectively. Another measurement was accomplished through "four rows of lime trees about 27 m high and with the trunks spaced about 6m in both directions". In this case the attenuation results at 540 MHz were 0.15 dB/m for horizontal and 0.25 dB/m for vertical polarization. For the same stand of lime trees at 1.2 GHz, the attenuation was 0.35 dB/m irrespective of polarization. Saxton and Lane report on measurements at 100 MHz through several hundred meters of mainly deciduous trees in full leaf and with some underbrush; the attenuation constant results were 0.03 dB/m and

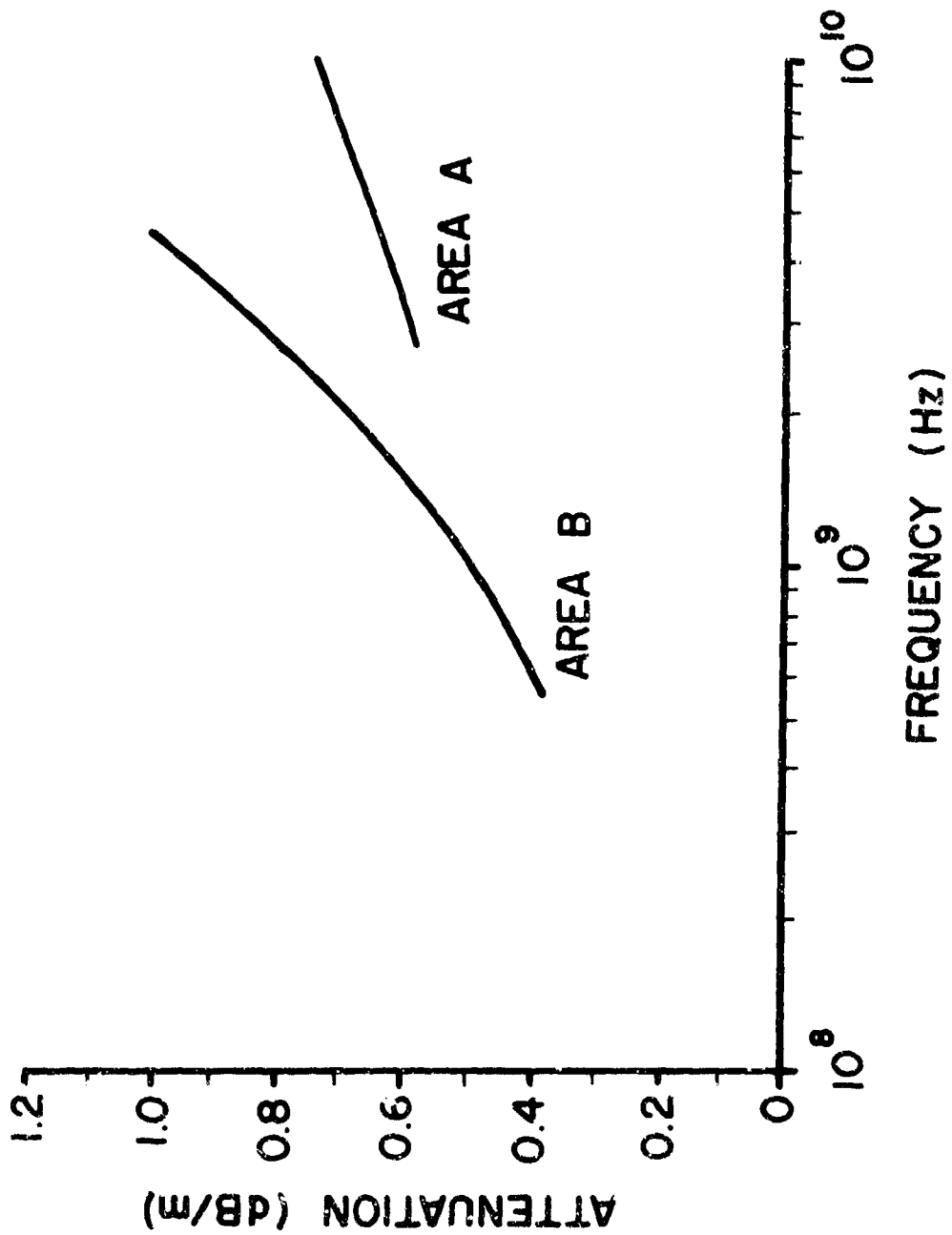


Figure 18. Attenuation constant measurements from Thailand jungles obtained by Jansky and Bailey.

0.06 dB/m for horizontal and vertical polarization, respectively. Saxton and Lane also summarized the measurements of McPetrie and Ford; for a frequency of 3.26 GHz the attenuation constant was 0.63 dB/m irrespective of polarization.

The measurements reported by Saxton and Lane are accompanied by almost no data on the physical characteristics of the foliage of which the attenuation results are representative. Furthermore, no statistics on the attenuation variation are given. Of particular concern is the possibility that some of their measurements could be contaminated by a lateral wave contribution. Based upon the results of Jansky and Bailey, the separation distances reported by Saxton and Lane were certainly sufficiently large in some cases to support a lateral wave; this is particularly true for their 100 MHz measurements.

4.1.3 Stutzman, et al. [6]

Recently Stutzman, Colliver, and Crawford [6] have reported on the attenuation of Virginia pine trees at 10 GHz. Their measurements comprise very short transmission paths, i.e. 5 meters, and their purpose was to determine if a correlation existed between the green weight of the intervening foliage and the attenuation of the electromagnetic wave. The frequency they used is beyond the range of interest to this study; however, we feel that our model may still be applicable since the needles of pine trees conform to our canonical cylinder model. More specifically, we hope to use their data to obtain a better estimate of the B factor in the equation for the dielectric loss factor, see equation (57) and Appendix C.

Professor Stutzman has very kindly provided us with copies of their data and we have reexamined it. One discrepancy that we found in their reported results [6] concerns their so-called correlation coefficient for attenuation versus green or dry weight of the intervening wood. We assumed, based upon

their discussion, that they were computing the correlation of attenuation as a function of green or dry weight. However, the values that they reported seemed to be much larger than one should expect based upon the scatter of the data. Using the data provided us, we computed the correlation coefficient for attenuation versus green and dry weight of wood and found significantly lower values, i.e. in the range of 0.5 to 0.7+. The disparity appears to be a result of a misunderstanding of the statistical computer program they used to compute the correlation. Apparently what they really computed was a correlation coefficient for how good a linear regression curve fitted the data. We feel that the correlation between attenuation and foliage weight is much more meaningful than the correlation of any fitted curve.

In any case, the most important result of their measurements was that the attenuation was most highly correlated with those parts of the pine trees having a diameter of roughly less than one half a free space wavelength. This result lends very strong support to the model hypothesis that only the small scale forest constituents are important to the attenuation process. Unfortunately, no correlations were attempted with even smaller scale components, i.e. $D/\lambda_0 < 0.5$. Another important point that is not completely clear in the experiments of Stutzman, et al. is whether the data are representative of the coherent power or the incoherent power. Since they used relatively short transmission paths, it is not at all obvious which component of power dominated their results.

4.1.4 Georgia Institute of Technology [17]

The Engineering Experiment Station of the Georgia Institute of Technology recently reported foliage attenuation measurements at 9.4, 16.2, 35 and 95 GHz. In our opinion, the Georgia Tech measurements tend to raise more questions than they answer. In the first place, they chose to redefine the foliage path

length. That is, rather than use the total path length from the onset of foliage to the receiver or the reflector, they chose to use the portion of the path that actually comprised foliage. The stated reason for doing this was that it reduced the variability of the measurement. From a practical point of view it is doubtful that one would ever have a reasonable estimate of how much of the total path is actually obscured by trunks, branches, twigs and leaves. On the other hand, one might have a good estimate of the mean height at which the path length starts to become obscured by foliage. Also, the fact that the attenuation has a great deal of variability associated with it is merely a consequence of the statistical nature of the problem. This, in turn, means that a lot of data are required if one is to obtain a low variance estimate of the average attenuation. Thus, redefining the path length to reduce the variability of the measurement helps neither the radar systems designer nor anyone attempting to model the average scattering and absorption effects of the foliage because it introduces a new path length which is probably not known.

Another potential problem with the Georgia Tech measurements is the use of a corner reflector for all of their two way measurements. The corner reflector is primarily an optical-like device which redirects the boresight rays back to the transmitter. The effect of scattering and absorption by the foliage which is off the axis of the transmitter-reflector combination will probably not be properly addressed by this combination. Thus, if the corner reflector were replaced by a diffraction limited receiving antenna or a resonant scatterer, the result should be expected to be different. This same limitation may also apply to targets which are characterized by sharp edge discontinuities. The point of this discussion is that one must consider the specific type of target when determining the impact of the foliage upon its scattering characteristics.

4.1.5 Others

There are two more measurements of attenuation that should be noted. Trevor [9] measured the attenuation of 152 m of hardwood forest with and without leaves at 500 MHz and without leaves at 250 MHz. For 500 MHz and summer, he found the attenuation to be 0.12 dB/m independent of polarization. For 500 MHz and winter, the attenuation was 0.09 dB/m independent of polarization. For 250 MHz and winter, the attenuation was 0.07 dB/m for horizontal polarization and 0.09 dB/m for vertical polarization. Almost no details of the measurement process or the statistics of the attenuation were given. It is not clear from these data whether the reduced attenuation in winter results from the absence of leaves or the possible reduction in dielectric loss factor due to the lower winter temperatures. Furthermore, it should be noted that the separation distance employed by Trevor is sufficient to support a lateral wave. Thus, Trevor's measurements may well represent a mixture of propagating modes and this may explain their rather low value.

Downey [18] employed transmissions by the MARISAT satellite to obtain estimates of the attenuation induced by a forest at 254 MHz. Using a circularly polarized receiving antenna to match the circularly polarized satellite signal, he estimated the foliage induced attenuation to be 0.22 dB/m. Downey obtained his data in forests comprising fir and oak trees accompanied by relatively thick underbrush.

4.2 A Comparison of the Model with Measurements

Figure 19 compares the previously described attenuation measurements with the model predictions for absorption effects only (Figures 15 and 16). The theoretical curves are for the electric field parallel and perpendicular to the grain and they use the loss factor versus frequency curves in Figure 12 and the effective fractional volume curve in Figure 3.

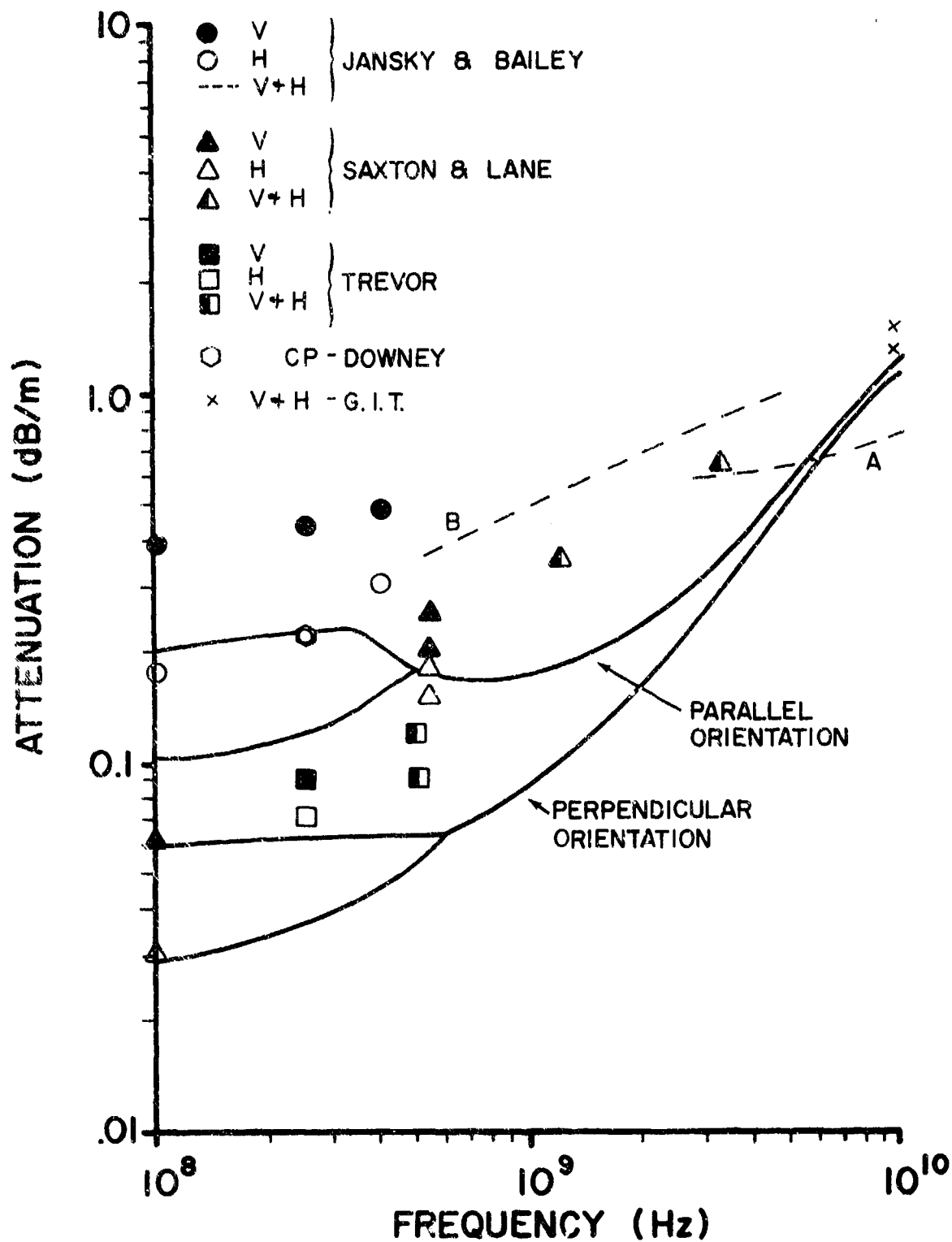


Figure 19. A comparison of model predictions with measured results. The model only includes absorptive effects and is probably most representative of pine, fir or spruce forests.

This figure is included to provide some idea of how the model compares with the measurements. It is also interesting to speculate on the changes that one might expect in the model to reflect the actual forests encountered in the measurements. Comparing the parallel orientation curve with the Jansky and Bailey results indicates that it underestimates the attenuation at the lower frequencies and it increases too fast with frequency beyond 1 GHz. This is felt to be due to inadequate knowledge of the dielectric loss factor for jungle wood. For example, jungle wood is probably denser and less moist than the wood represented by the loss factor in Figure 12. This means that the low frequency end (<1 GHz) of the curve in Figure 12 should be increased while for high frequencies (>1 GHz) the curve should be reduced. This change in the loss factor will translate directly to the model results in Figure 19; that is, the higher density of jungle wood will increase the attenuation at the lower frequencies and the reduced moisture content will lower the loss at the high end of the frequency scale in Figure 19.

One of the most intriguing aspects of the comparisons in Figure 19 is the behavior of the Jansky and Bailey data in the neighborhood of 500 MHz. That is, the Jansky and Bailey data show a dip in the attenuation near 500 MHz for the vertical polarization as predicted by the model. Caution should be exercised in this case because the physical area represented by the solid data points was not quite the same as the area represented by the curve labeled "B". Unfortunately, none of the data acquired below and above 500 MHz were representative of exactly the same area so it is not possible to do more than speculate on the dip near 500 MHz.

Although it remains to be rigorously proven, it is our feeling that the curve labeled parallel orientation is the most representative of the two orientations. This contention is based upon the fact that for either vertical

or horizontal polarization the field is primarily parallel to the wood grain. However, the curve in Figure 19 for perpendicular polarization is interesting in that it shows the effect of a lower dielectric loss factor below 1 GHz (see Figure 12).

The 100 MHz measurements reported by Saxton and Lane and the 250 and 540 MHz results measured by Trevor are disturbing in that they fall considerably below the trend of the other data. Both measurements were reported to have been accomplished in dense forests with some degree of underbrush. Although this is certainly not a precise description, it is doubtful that the forests were any less dense than the one encountered by Downey in his measurements. We tend to feel that the measurements reported by Saxton and Lane at 100 MHz and by Trevor at 250 and 540 MHz may be contaminated by a lateral wave contribution. Certainly, the path lengths used in both measurements were long enough to support a lateral wave, according to the data of Jansky and Bailey. The lateral wave should also be attenuated less than the direct or through-the-foliage mode. Unfortunately, it is not clear that the investigators attempted to separate the effects of these two modes as did Jansky and Bailey.

5.0 CONCLUSIONS AND SUGGESTED FUTURE INVESTIGATIONS

A rather simple model has been developed for the propagation constant of the average coherent field propagating through foliage. It is certainly not based upon completely rigorous theory and in at least one aspect violates classical electromagnetic theory principles. Even this relatively simple theory requires input characteristics which are not usually known for forested environments. Consequently, these characteristics have been estimated based upon extremely sketchy data. However, with all its drawbacks and limitations, the model comes reasonably close to the measured results reported in the literature.

Furthermore, some of the disagreement between the model and the measurements can be attributed to expected variations in the inputs to the model.

The primary conclusion of this study is that a model has been developed which appears to work; however, more measurements and analytical development are required to show that the agreement is something more than just good fortune. That is, we have taken an extremely complex problem and reduced it to a relatively simple equation; does this equation represent the actual physics of the problem or are the input parameters to the equation masking the true behavior? Without further analysis and measurements, these questions cannot be completely answered. The following sections briefly discuss analytical and experimental efforts that might resolve some of these questions.

5.1 Modeling

We feel that the key to any future modeling or analytical efforts is the approach presented in Appendix A. In Appendix A, we have developed an exact solution of the Foldy-Twersky integral equation which, in turn, yields the behavior of the average or coherent field propagating in a sparsely populated random medium. The primary advantage of the Foldy-Twersky integral equation over a single scattering approach is that it retains all chains of multiple scattering except "back and forth" interactions between particles.

The solution shown in Appendix A was obtained at the end of this study so it was not possible to explore its application to this problem. The solution is easily obtained for spheres and any objects which do not depolarize the incident field such as vertically or horizontally oriented cylinders when illuminated by similarly aligned or misaligned incident fields. A solution for cylinders could shed a great deal of light on the effects of the tree trunks since they are vertically aligned. Of particular interest here is the frequency range over which the solution is essentially Rayleigh and its behavior

for large values of the complex dielectric constant.

Some attempt was made toward the very end of this study to extend the approach in Appendix A to arbitrarily shaped objects having all orientations equally likely. Unfortunately, we were unable to do this primarily because the Foldy-Twersky formulation is a scalar formulation and yet the solution requires the internal field for any orientation of an object. It appears at this time that the approach presented in Appendix A may not work in the case of arbitrarily oriented objects having all orientations equally likely. Investigations should be continued on this problem because this is the most reasonable approach to modeling the tree branches and twigs.

Solutions should also be attempted for thin discs since this is a reasonable canonical model for leaves. As above, the purpose of the study would be to identify the frequency range for which the discs may be considered to be Rayleigh even when they have a large dielectric constant.

Finally, the solution in Appendix A clearly shows that when the spheres are large in terms of a wavelength, the propagation constant does not equal the single scattering result, e.g. it is larger. Since this is true even in the case of lossless objects, i.e. $\epsilon_r'' = 0$, the incoherent or total average power must also deviate from the single scattering result, i.e. it will attenuate more rapidly than the single scattering result. Since energy must be conserved, the larger attenuation rate of the incoherent power can only mean that power is being incoherently scattered in directions other than the direction of propagation of the coherent power. What all this means is that we have to reexamine the single scattering solution for the incoherent power or the total average power. It also means that we can no longer say that the total average power, for large separation distances between the transmitter and receiver, attenuates as $\exp(-\sigma_a)$ where σ_a is the average absorption cross section

of a single particle; an assumption that we used to compare the REV model to total average power measurements.

The Rayleigh-Effective Volume or REV model is intended primarily for use by systems design specialists. Its strong point is that it does exhibit a high degree of agreement with limited measurements. Its weak point is that it tends to violate some conventional electromagnetic principles in that the attenuation is attributed to Rayleigh objects rather than electrically large objects. Thus, the aim of further analytical efforts on this problem must be to gain further insight into the basic scattering/absorbing mechanisms involved. Furthermore, we feel very strongly that analytical efforts should be accompanied by a high quality measurements program and that the analysis should always be directed toward understanding these measurements.

5.2 Measurements

One of the greatest hinderances to this study was the lack of a complete set of measurements comprising foliage statistics, the complex dielectric constant of green wood, and the attenuation rate of the coherent and incoherent fields. Appendix E sets forth some concepts and ideas on the measurement of the complex dielectric constant of green wood. Appendix F details the types of foliage measurements that should be accomplished and Appendix C shows how these measurements can be converted into $\{\rho V_p\}_{\text{REV}}$ for use in the REV model.

For the propagation part of this experiment we are primarily interested in the attenuation of the coherent field or power. It is desirable to obtain data of this type over two types of paths; one completely inside the foliage and one from outside the foliage to inside at a number of different incident angles but with emphasis on near grazing. Also, it is desirable to sample the propagating field at a number of different points in the plane orthogonal to

the line of sight path in order to determine the transverse spatial correlation of the total power.

There appear to be only two viable means by which the average or coherent field can be measured. The first uses the fact that the probability density function of a fluctuating field amplitude can be represented by a Ricean function when the mean of field is non-zero. If the mean field is essentially zero, this density function becomes the more familiar Rayleigh function. The practical problems associated with using this approach to estimate the mean field are significant. First of all, a large number of measurements will be required to construct a reliable histogram in order to accurately estimate the true probability density function. More importantly, the dynamic range of this approach is very small. That is, it is doubtful that the coherent power can be estimated reliably once it is greater than 10 dB below the incoherent power. The one advantage of this approach is that it only involves a total power measurement. However, it appears that this approach is not particularly well suited to the foliage problem because of the number of samples required and its inherently small dynamic range.

The other approach to measuring the average or coherent field is the use of in-phase and quadrature detection in the receiver which is also coherent with the transmitter. With this approach, both the amplitude and phase of the received field are measured and recorded for analysis. The greatest difficulty with this approach is maintaining the receiver local oscillator coherent with the transmitter. We have found no obvious way to overcome this problem short of physically connecting the receiver and transmitter by coaxial cable so that both are driven by the same stable local oscillator. This raises the question of how stable is a coaxial cable when it is exposed to bending, curling, and stretching. At the lower frequencies, say less than 1 GHz, it may

be possible to overcome phase changes through the cable by being very careful in moving the cable. One would certainly want to check, in the laboratory, the phase stability of a long run of coaxial cable when exposed to bending, curling, and stretching. It should be noted that if the phase of the signal transmitted through the cable changes randomly as the cable moves, this will introduce phase noise into the measurement which, in turn, will tend to reduce the amplitude of the average or coherent field and increase the incoherent power. We feel that the problem of phase locking the transmitter and receiver to a common stable local oscillator requires much more thought and analysis.

In order to determine the attenuation of the average or coherent field as a function of separation distance between the transmitter and receiver, it is necessary to measure the average field at each fixed separation distance. That is, for a fixed separation distance, it will be necessary to obtain a number of independent measurements of the amplitude and phase of the received field. So as not to confuse the foliage effects with the free-space Green's function, i.e. $\exp(-jk_0 r)/4\pi r$, the fixed distance measurements must be accomplished on a circle centered on the transmitter. If this is not done, the phase factor in the Green's function will cause an additional variation in the measurement which can lead to an error in estimating the average field. Obviously, this is not an easy task because it may not always be easy to stay on a circle or even to define a circular path. This is another aspect of the problem that certainly requires further thought.

At any given separation distance, a large number of measurements will be required to (1) adequately sample the foliated region, (2) insure that the sample mean field has a low sample standard deviation, and (3) obtain measurements which can be used to estimate the spatial correlation properties of the field. How many measurements are adequate at a given separation distance?

This depends entirely upon the sample standard deviation that one is willing to tolerate in the measurement. For example, in the case of a completely incoherent power the probability density function is exponential; this means that the ensemble mean and standard deviation are equal. Thus, the one-sigma error bound on the sample mean is approximately given by the ratio of the mean to the square root of the number of samples and a one-sigma error bound that is ten percent of the measured mean requires 100 samples.

Given the choice of accomplishing the measurements over long or short paths, we feel that it is better to try and acquire the measurements using the shortest possible separation distances between transmitter and receiver. With longer distances and at the lower frequencies, there is the distinct possibility of launching other propagation modes such as the lateral wave and ionospheric bounce modes. Propagation via these modes can yield a completely false measurement of the through-the-foliage effects. One can detect these modes by noting the variation or attenuation of the received field as a function of separation distance but it is most difficult to isolate the through-the-foliage mode. Terrain effects at larger separation distances also become important. Furthermore, using a few long distance paths may also not provide an adequate sample of the foliage because foliage does exhibit a great deal of spatial variability.

In regard to the choice of test site, we feel that it is best to select a conveniently located forest which will be available for measurements at any time. It would also be beneficial if the site were one for which stand table had recently been acquired for this would simplify the foliage statistics problem. It is important to realize that such a measurements program as this is going to involve a great deal of trial and error experimentation to establish and refine measurement techniques. For this reason alone, it is most

desirable to use a site that is close to the laboratory so that new techniques and ideas can be tested and evaluated in a relative short time and with a minimum of expense. After the measurement techniques are refined and the data acquired on the test site are reduced and understood, then other test sites comprising different types or density of foliage can be considered.

In designing the field test hardware, we feel that a great deal of attention should be given to accomplishing as much of the actual data reduction and analysis in the field as possible. That is, along with all the equipment necessary to generate and record the data, emphasis should also be put on using a van-mounted mini-computer to provide near-real-time analysis of the data. Such an approach would eliminate a great deal of remeasurement and it could be designed to indicate problems that would invalidate the data.

In summary, the measurement program that we have suggested is neither easy nor cheap and, in fact, there are some serious questions as to the feasibility of such a program. Consequently, as a first step toward implementing this program, we feel that it is necessary to perform an in-depth feasibility study of the suggested program. Such problems as phase locking a remote receiver to a transmitter, making a field attenuation measurement on a circle centered on the transmitter, and minimizing the generation of other propagation modes are not trivial and they require much more study than we were able to devote to them. It is not unreasonable to conjecture that a feasibility study and the design of a detailed experiment plan would require a good three man-year effort. This manpower estimate depends a great deal on the ability of the researchers to overcome some of the above noted problems. The time required to implement the experiment depends upon the volume and quality of data necessary to validate the analytical models. For the initial phase of the experiment where all the hardware is put together, the complete system is

checked out, and test site is adequately measured the time requirement may be something on the order of four to five man-years of effort. This may seem high but it must be remembered that these measurements should be accomplished when the trees are in full leaf and when they are bare so this is going to stretch the experiment out in time.

A measurements program such as this will require a good deal of time, effort, and funding. However, without it we can never hope to adequately evaluate the accuracy of analytical models nor can we reliably predict the performance of electromagnetic radiating systems in the presence of foliage.

REFERENCES

1. Ishimaru, A., Wave Propagation and Scattering in Random Media, Vols. I & II, Academic Press, New York, 1978.
2. Pounds, D. J. and A. H. LaGrone, "Considering Forest Vegetation as an Imperfect Dielectric Slab," Elect. Engr. Res. Lab., Univ. of Texas, Austin, TX., Report 6-53, May, 1963.
3. Roth, L. E. and C. Elachi, "Coherent Electromagnetic Losses By Scattering From Volume Inhomogeneities," IEEE Trans. on Antennas & Propagation, Vol AP-23, pp. 674-675, Sept., 1975.
4. Collin, R. E., "Coherent Wave Reflection From A Random Half-Space," IEEE Trans. on Antennas & Propagation, Vol. AP-18, pp. 299-301, March, 1970.
5. Jones, D. S., The Theory of Electromagnetism, MacMillian, New York, 1964.
6. Stutzman, W. L., F. W. Colliver, and H. S. Crawford, "Microwave Transmission Measurements for Estimation of the Weight of Standing Pine Trees," IEEE Trans. Antennas & Propagation, Vol. AP-27, pp. 22-26, January, 1979.
7. Assmann, E., The Principles of Forest Yield Study, Pergamon Press, New York, 1970.
8. Harrington, R. F., Time Harmonic Electromagnetic Fields, McGraw-Hill, New York, pg. 324, 1961.
9. Trevor, B., "Ultra-High-Frequency Propagation Through Woods and Underbrush," RCA Rev., Vol. 5, pp. 97-100, July, 1940.
10. Van de Hulst, H. C., Light Scattering By Small Particles, Wiley & Sons, New York, 1957.
11. Broadhurst, M. G., "Complex Dielectric Constant and Dissipation Factor of Foliage," NBS Report 9592, 1970.
12. James, W. L., "Dielectric Properties of Wood and Hardboard: Variation with Temperature, Frequency, Moisture Content, and Grain Orientation,"

REFERENCES (Cont'd.)

- USDA Forest Service Res. Paper FPL 245, USDA Forest Products Lab., Madison, Wisc., 1975.
13. Trapp, W. and L. Pungs, "Influence of Temperature and Moisture on the Dielectric Behavior of Natural Wood in the High Frequency Range," (In German), Holzforschung, Vol. 10, pp. 144-150, 1956.
 14. Tamir, T., "On Radio-Wave Propagation in Forest Environments," IEEE Trans. Antennas & Propagation, Vol. AP-15, pp. 806-817, November, 1967.
 15. Staff, "Tropical Propagation Research, Final Report, Vol. I," Jansky and Bailey, Engineering Dept., Atlantic Research Corp., Alexandria, VA., AD 66031E, June, 1966.
 16. Saxton, J. A. and J. A. Lane, "V.H.F. and U.H.F. Reception, Effects of Trees and Other Obstacles," Wireless World, Vol. 61, pp. 229-232, May, 1955.
 17. Currie, N. C., E. E. Martin and F. B. Dyer, "Radar Foliage Penetration Measurements at Millimeter Wavelengths," Eng. Exp. St., Georgia Inst. Technology, Atlanta, GA., AD A023838, 31 December, 1975.
 18. Downey, M. J., "The Effects of Trees and Foliage on the Propagation of UHF Satellite Signals," Report No. 77017, Royal Signals & Radar Estab., Christchurch, U. K., AD A-048304, May, 1977.

APPENDIX A

COHERENT WAVE PROPAGATION THROUGH A SPARSE RANDOM COLLECTION OF SPHERICAL PARTICLES

The Foldy-Twersky integral equation for the average or coherent field propagating through a medium containing randomly located particles or objects is particularly applicable to the foliage problem because of the small fractional volume comprising foliage. A previous approximate solution of this equation for finite size particles only applies when the dielectric constant of the particles is very near unity, i.e. the particles are nearly transparent. This solution also assumes that the particles are large in terms of the wavelength. In this appendix we first simplify the Foldy-Twersky equation to an algebraic expression which can be approximately solved for Rayleigh particles which either individually or as a group in the mean do not depolarize the field. For spherical particles, we solve the complete equation exactly. Unfortunately, the approach used to solve the spherical particle problem was obtained too late in the study to be of use in the REV model. However, the exact solution for the spherical particles has some very interesting properties. For example, in the case of large spheres we find the attenuation constant to be 33% larger than the single or independent scattering result. We attribute this additional attenuation to multiple scattering.

Introduction and Summary of Results

With the advent of lasers and coherent radar systems there is renewed interest in the propagation of electromagnetic fields through a random collection of particles. In many cases the particle density is sufficiently small that one is tempted to use the so-called single or independent scattering theory [Jones, 1964]. Invariably, the question arises as to the range

of parameters for which single scattering theory is valid. Even if the medium is so sparsely populated with particles that multiple scattering is not expected to be a significant factor, there is still a question concerning the validity of the far-field approximation used in single scattering theory. In the hierarchy of descriptive formulations, one can next turn to the Foldy-Twersky integral equation for a more rigorous solution and, hopefully, more insight into the problem.

If the fractional volume occupied by the particles is very small, if correlations between particles can be ignored, and if the average field in the medium can be represented by scalar equations then the Foldy-Twersky integral equation is a reasonably accurate description for the average field [Beard, et al., 1967]. The Foldy-Twersky integral equation has the following form;

$$\langle \psi(\vec{r}_a) \rangle = \phi_i(\vec{r}_a) + \rho \int_V v_s^a \langle \psi(\vec{r}_s) \rangle d\vec{r}_s \quad (1)$$

where ϕ_i is the incident wave in the absence of the particles, $\langle \psi(\vec{r}_a) \rangle$ is the total average wave outside the particles and evaluated at \vec{r}_a , ρ is the particle density or the ratio of the number of particles N to the enclosing volume V , and $v_s^a \langle \psi(\vec{r}_s) \rangle$ is the average wave at \vec{r}_a due to a particle at \vec{r}_s with $\langle \psi(\vec{r}_s) \rangle$ incident upon it. The Foldy-Twersky representation ignores "back and forth" scattering between particles; however, when the individual particles are strong forward scatterers, this error vanishes as $N \rightarrow \infty$ [Twersky, 1964]. For particles which are not strong forward scatterers, it is not clear what significance this error has even as $N \rightarrow \infty$.

The main drawback to determining the advantages of (1) relative to single scattering theory is that the Foldy-Twersky integral equation has only been approximately solved for a very limited class of particles. Foldy [1945] obtained an expression for the propagation constant or wavenumber of the average field when the particles are isotropic point scatterers. Twersky [1964] solved (1) for a slab of large diaphanous dielectric spheres, and Brown [1979] obtained the wavenumber of the average field in an infinite volume comprising Rayleigh particles. The latter two solutions were facilitated by the fact that one can approximately relate the field inside a particle to the incident field for Rayleigh and Rayleigh-Gans particles [Jones, 1964; Ishimaru, 1978]. Unfortunately, both Twersky and Brown used approximate expressions for the field $v_s^r \langle \psi(\vec{r}_s) \rangle$ which are not rigorously correct and the impact of these approximations is difficult to evaluate. Twersky used a far-field approximation for $v_s^a \langle \psi(\vec{r}_s) \rangle$ while Brown employed a single component (no depolarization) vector potential representation for $v_s^a \langle \psi(\vec{r}_s) \rangle$. Both these approaches failed to recognize the fact that the integration in (1) encompasses the observation point \vec{r}_a and the previous respective approximations for $v_s^a \langle \psi(\vec{r}_s) \rangle$ are therefore invalid. Thus, there is a very definite need for a more general solution of the Foldy-Twersky integral equation.

In this note an exact solution for the wavenumber of the average field is obtained for an infinite collection of spherical particles. The analysis starts by using an expression for $v_s^a \langle \psi(\vec{r}_s) \rangle$ which is valid regardless of the location of the observation point \vec{r}_a relative to the particle

boundary. This expression involves a principal value integration (over the volume of a single particle) of the product of the average electric field inside the particle and the free space dyadic Green's function [Van Bladel, 1961]. When this expression is substituted in (1) and V is taken to be infinite, the integration over the volume of the particle can be completed. The resulting equation involving an integration over V can be simplified to a determinantal equation through the application of the operator $(\nabla^2 + k_0^2)$. The determinantal equation for the wavenumber of the average field shows that both the average field outside and inside the particle must propagate as plane waves having the same wavenumber. However, in order to solve the determinantal equation for the wavenumber or propagation constant it is necessary to determine the constant relating these two average fields. Because the average fields outside and inside the particles are both plane waves and because the average field outside the particle acts as the incident field on the particle, it is possible to solve the integral equation relating the two fields exactly for spherical particles. The problem of nonspherical particles with all orientations equally likely is presently under study. For spheres, the result is a closed form expression which is valid for any value of $k_0 a$ where k_0 is the free space wavenumber and a is the radius of the spheres. Furthermore, there are no restrictions on the range of values that can be assumed by the complex relative dielectric constant.

For spherical dielectric Rayleigh particles, the present result reduces essentially to the single scattering solution. The exact solution obtained herein for Rayleigh-Gans spheres yields a slightly larger attenuation than

single scattering results due to the inclusion of off-forward scattering. Probably the most important limit is obtained when the fractional volume occupied by the spherical particles and the physical size of the spheres are held constant and the free space wavelength is decreased, i.e. the particles become large in terms of a free space wavelength. In this limit, it is found that the coherent power attenuates as $8/3$ times the geometric cross section of the spherical particle rather than two times as predicted by single scattering theory. Since this is an exact solution of the Foldy-Twersky integral equation under conditions for which it should be an accurate description of the process, the additional 33% attenuation may be representative of multiple scattering effects. It is not possible at this time to be less equivocal about the source of the additional attenuation because the Foldy-Twersky equation is an approximate formulation and the impact of the neglected orders of multiple scattering is largely unknown.

The primary purpose of this note is to present an exact solution of the Foldy-Twersky integral equation and to compare this solution with the results of single scattering theory. Although an exact solution is found, it does not shed any new light on the basic limitations of the Foldy-Twersky representation for the scattering process. Given the degree of difficulty inherent in any analytical approach which attempts to improve upon the Foldy-Twersky formalism, it would seem that this new result might be best tested by experimental techniques.

General Analysis

It is assumed that both the number of particles N inside the volume V

and the volume V are infinite but in such a manner that the ratio $\rho = N/V$ is finite and constant throughout the volume. In the following, (1) will be written as a vector equation although the final result will reduce to a scalar formulation. Corresponding to the geometry in Figure 1, the average scattered field at \vec{r}_a due to a particle or scattering object at \vec{r}_s may be written in the following form regardless of whether \vec{r}_a is inside or outside the particle volume V_p [Van Bladel, 1961];

$$\langle \vec{E}(\vec{r}_a) \rangle = -k_o^2 (\epsilon_r - 1) \int_{V_p} \langle \vec{E}_i(\vec{r}_s + \vec{r}_1) \rangle \cdot \left\{ \overline{\overline{\Gamma}}(\vec{r}_a - \vec{r}_s - \vec{r}_1) + \frac{1}{3k_o^2} \overline{\overline{\Gamma}} \delta(\vec{r}_a - \vec{r}_s - \vec{r}_1) \right\} d\vec{r}_1 \quad (2)$$

where $\langle \vec{E} \rangle$ is the average scattered field outside or inside the particle, $\langle \vec{E}_i \rangle$ is the total average field inside the particle, $\overline{\overline{\Gamma}}$ is the unit dyad, $\delta(\bullet)$ is the delta function, $\overline{\overline{\Gamma}} = P.V. \overline{\overline{G}}$ where P.V. denotes principal value, and

$$\overline{\overline{G}}(\vec{r}_a - \vec{r}_s - \vec{r}_1) = - \left(\overline{\overline{\Gamma}} + \frac{1}{2} \nabla \nabla \right) g(|\vec{r}_a - \vec{r}_s - \vec{r}_1|) \quad (3)$$

$$g(|\vec{r}_a - \vec{r}_s - \vec{r}_1|) = \exp(-j k_o |\vec{r}_a - \vec{r}_s - \vec{r}_1|) / 4\pi |\vec{r}_a - \vec{r}_s - \vec{r}_1|,$$

and an $\exp(j\omega t)$ time convention is assumed. The quantity $\epsilon_r = \epsilon_r' - j\epsilon_r''$ is the complex relative dielectric constant of the material comprising the particles and the particles are assumed to have the same permeability as free space. It should be noted that the free space dyadic Green's function has been used in (2) rather than the "average medium" dyadic Green's function. The correctness of this approach has been established by Twersky [1964] in the case of a sparse collection of particles. Substituting (2) into the vector equivalent of (1) yields the following;

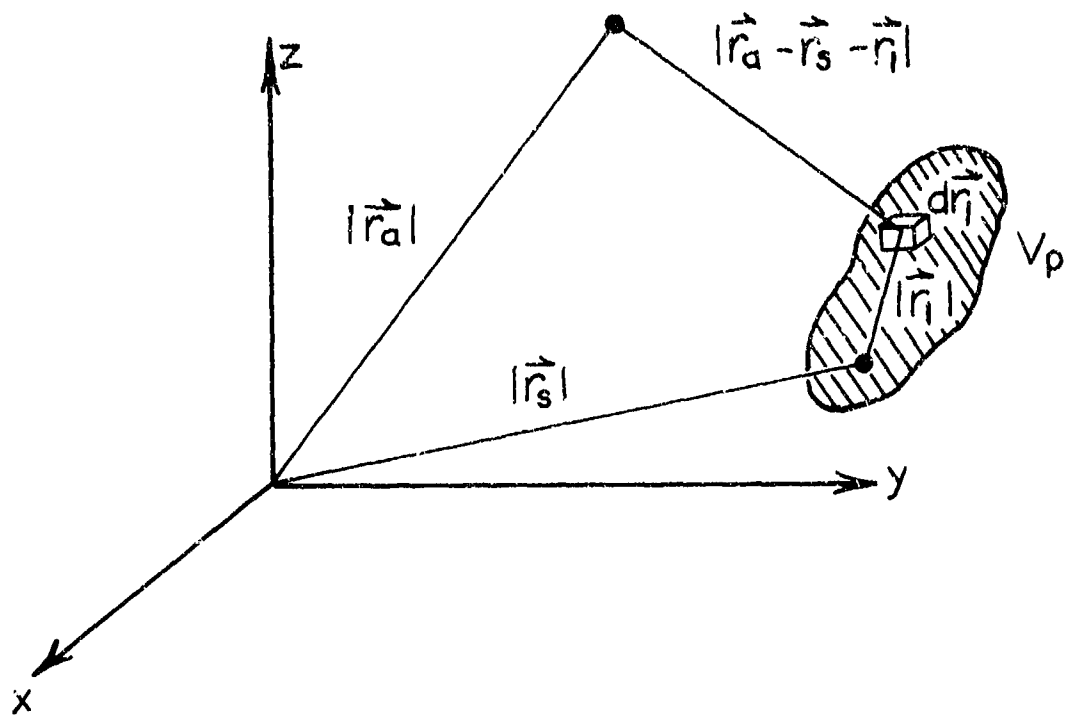


Figure 1. Single particle scattering geometry.

$$\langle \vec{E}_o(\vec{r}_a) \rangle = \vec{E}^i(\vec{r}_a) - k_o^2 \rho (\epsilon_r - 1) \int_V \int_{V_p} \langle \vec{E}_1(\vec{r}_s + \vec{r}_1) \rangle \cdot \left\{ \vec{\Gamma}(\vec{r}_a - \vec{r}_s - \vec{r}_1) + \frac{1}{3k_o^2} \vec{\Gamma} \delta(\vec{r}_a - \vec{r}_s - \vec{r}_1) \right\} d\vec{r}_1 d\vec{r}_s \quad (4)$$

where $\vec{E}^i(\vec{r}_a)$ is the incident field in free space and $\langle \vec{E}_o(\vec{r}_a) \rangle$ is the total average field outside of the particles. Interchanging the \vec{r}_1 and \vec{r}_s -integrations and substituting $\vec{r} = \vec{r}_s + \vec{r}_1$ in the \vec{r}_s -integration yields

$$\langle \vec{E}_o(\vec{r}_a) \rangle = \vec{E}^i(\vec{r}_a) - k_o^2 \rho (\epsilon_r - 1) \int_{V_p} \int_V \langle \vec{E}_1(\vec{r}) \rangle \cdot \left\{ \vec{\Gamma}(\vec{r}_a - \vec{r}) + \frac{1}{3k_o^2} \vec{\Gamma} \delta(\vec{r}_a - \vec{r}) \right\} d\vec{r} d\vec{r}_1 \quad (5)$$

because V is infinite. Since the integrand is independent of \vec{r}_1 , the \vec{r}_1 -integration is trivial and the result is as follows:

$$\langle \vec{E}_o(\vec{r}_a) \rangle = \vec{E}^i(\vec{r}_a) - k_o^2 \rho V_p (\epsilon_r - 1) \int_V \langle \vec{E}_1(\vec{r}) \rangle \cdot \left\{ \vec{\Gamma}(\vec{r}_a - \vec{r}) + \frac{1}{3k_o^2} \vec{\Gamma} \delta(\vec{r}_a - \vec{r}) \right\} d\vec{r} \quad (6)$$

Attention will now be directed toward determining the source-free plane wave solutions of (6) for $\langle \vec{E}_o \rangle$ and, in particular, the propagation constant k for $\langle \vec{E}_o \rangle$. To this end, the operator $(-\nabla \times \nabla \times + k_o^2)$ is applied to both sides of (6) yielding

$$(-\nabla \times \nabla \times + k_o^2) \langle \vec{E}_o(\vec{r}_a) \rangle = -k_o^2 \rho V_p (\epsilon_r - 1) \langle \vec{E}_1(\vec{r}_a) \rangle \quad (7)$$

because [Van Bladel, 1961]

$$(-\nabla \times \nabla \times + k_o^2) \vec{\Gamma}(\vec{r}_a - \vec{r}) = \vec{\Gamma} \delta(\vec{r}_a - \vec{r}) - \frac{1}{3k_o^2} (-\nabla \times \nabla \times + k_o^2) \vec{\Gamma} \delta(\vec{r}_a - \vec{r}) .$$

If the medium comprises spherical particles or if it is isotropic in the mean then (7) reduces to the following result;

$$(-k^2 + k_0^2) \langle \vec{E}_0(\vec{r}_a) \rangle = -k_0^2 \rho_p V_p (\epsilon_r - 1) \langle \vec{E}_1(\vec{r}_a) \rangle \quad (8)$$

where it has been assumed that

$$\langle \vec{E}_0(\vec{r}_a) \rangle = \vec{E} \exp(-j\vec{k} \cdot \vec{r}_a) \quad (9)$$

Equation (8) may, at first glance, appear to be in error because it equates the average exterior field to the average interior field. However, it must be remembered that in the Foldy-Twersky formulation the average exterior field is also the average field incident upon the particle. Since this incident field exists at a point regardless of the presence or absence of a particle, equation (8) is perfectly legitimate. Equation (8) clearly shows that if $\langle \vec{E}_0 \rangle$ is a plane wave then $\langle \vec{E}_1 \rangle$ is also. In short, $\langle \vec{E}_0 \rangle$ and $\langle \vec{E}_1 \rangle$ can differ at most by a complex constant. Equation (8) is different from the result obtained by Brown [1979] because he used a vector potential representation in place of (2) and such an approach does not permit $\vec{r}_a \in V_p$ [Van Bladel, 1961]. Since $\langle \vec{E}_0 \rangle$ is also the average field incident upon the particles, (8) can be approximately solved for Rayleigh or Rayleigh-Gans particles because, for such particles, approximate relationships between the incident and interior fields are known. For nonspherical particles having all orientations equally likely, this approach has definite merit at low frequencies. This result is used in the REV model (see Section 3.2).

To solve (8) for k it is first necessary to determine the complex constant relating $\langle \vec{E}_0 \rangle$ and $\langle \vec{E}_1 \rangle$. To do this one must make use of the fact that $\langle \vec{E}_0 \rangle$ is also the average field incident upon a particle, i.e. it is the source for $\langle \vec{E}_1 \rangle$. It is a reasonably straightforward task to do this

for spheres; however, to illustrate the difficulties involved with nonspherical particles, a more general development will be presented. To simplify matters somewhat, let all of the particles have the same shape, size, and complex dielectric constant; the only random parameters are the particles' respective locations and their orientations. The averages in (8) are over all possible relative particle locations and orientations. (Even in this development, all orientations of a particle are assumed to be equally likely in order to be consistent with the scalar nature of the Foldy-Twersky equation). Let $\langle \vec{E}_1 \rangle_\ell$ and $\langle \vec{E}_0 \rangle_\ell$ be the total field inside a particle and the incident field, respectively, averaged over all possible locations of the particles. Even though these fields have only been averaged over relative locations of particles, they must still satisfy the following integral equation for a single particle with any orientation [Livesay and Chen, 1974] and $\vec{r}_a \in V_p$;

$$\left(\frac{\epsilon_r + 2}{3} \right) \langle \vec{E}_1(\vec{r}_a) \rangle_\ell + k_o^2 (\epsilon_r - 1) \int_{V_p} \langle \vec{E}_1(\vec{r}_o + \vec{r}) \rangle_\ell \cdot \bar{G}(\vec{r}_a - \vec{r}_o - \vec{r}) d\vec{r} = \langle \vec{E}_0(\vec{r}_a) \rangle_\ell \quad (10)$$

The bar through the integral sign denotes the principal value of the volume integral which is defined in a very specific manner, see Van Bladel [1961]. Let the particle rotate about the tip of the position vector \vec{r}_o in passing through all possible orientation angles. Also to simplify matters let $\vec{r}_o = 0$, so (10) becomes

$$\left(\frac{\epsilon_r + 2}{3} \right) \langle \vec{E}_1(\vec{r}_a) \rangle_\ell + k_o^2 (\epsilon_r - 1) \int_{V_p} \langle \vec{E}_1(\vec{r}) \rangle_\ell \cdot \bar{G}(\vec{r}_a - \vec{r}) d\vec{r} = \langle \vec{E}_0(\vec{r}_a) \rangle_\ell$$

Taking the average over all possible particle orientation angles Ω yields

$$\left(\frac{\epsilon_r+2}{3}\right) \langle \vec{E}_1(\vec{r}_a) \rangle + k_o^2(\epsilon_r-1) \left\langle \int_{V_p} \langle \vec{E}_1(\vec{r}) \rangle \cdot \vec{G}(\vec{r}_a-\vec{r}) d\vec{r} \right\rangle_{\Omega} = \langle \vec{E}_o(\vec{r}_a) \rangle \quad (11)$$

where the fact that $\langle \langle \cdot \rangle_{\Omega} \rangle = \langle \cdot \rangle$ has been used. The solution of (11) when the particles have an arbitrary shape is presently under study.

Spherical Particles

For the remainder of this paper the particles will be assumed to be spheres. In this case the limits on the volume integral in (11) are not functions of orientation angle and the averaging is trivial;

$$\left(\frac{\epsilon_r+2}{3}\right) \langle \vec{E}_1(\vec{r}_a) \rangle + k_o^2(\epsilon_r-1) \int_{V_p} \langle \vec{E}_1(\vec{r}) \rangle \cdot \vec{G}(\vec{r}_a-\vec{r}) d\vec{r} = \langle \vec{E}_o(\vec{r}_a) \rangle$$

Since plane wave solutions for $\langle \vec{E}_o \rangle$ are sought, one sets

$$\langle \vec{E}_o(\vec{r}_a) \rangle = (E_x \hat{x} + E_y \hat{y} + E_z \hat{z}) e^{-j \vec{k} \cdot \vec{r}_a},$$

replaces $\langle \vec{E}_1 \rangle$ by $\langle \vec{E}_o \rangle$ using (8), and sets $\vec{r}_a = 0$ to simplify matters.

Following these steps and assuming that neither E_x, E_y nor E_z are zero, the above equation becomes

$$\frac{(\epsilon_r+2)(k^2-k_o^2)}{3k_o^2 \rho V_p (\epsilon_r-1)} - \frac{(k^2-k_o^2)}{\rho V_p} \int_{V_p} \left\{ \left[g + \frac{1}{k_o^2} g_{x_p x_p} \right] + \frac{1}{k_o^2} \sum_{\substack{q=1 \\ q \neq p}}^3 \frac{E_{x_q}}{E_{x_p}} g_{x_p x_q} \right\} \exp(-j \vec{k} \cdot \vec{r}) d\vec{r}$$

$$= 1 \quad p = 1, 2, 3$$

where $x_1 = x$, $x_2 = y$, $x_3 = z$ and the subscripts on g denote partial differentiation with respect to the indicated cartesian variable. To simplify evaluation of the integrals involving the partial derivatives of g , one can take advantage of the fact that the propagation is isotropic in the mean. This means that the polarization and direction of propagation of $\langle \vec{E}_0 \rangle$ can be chosen arbitrarily. For example with

$$\langle \vec{E}_0(\vec{r}) \rangle = E \exp(-jkz) \hat{x} \quad ,$$

the previous equation reduces to the following form;

$$k^2 - k_0^2 = \frac{k_0^2 \rho v_p (\epsilon_r - 1)}{\left(\frac{\epsilon_r + 2}{3}\right) - k_0^2 (\epsilon_r - 1) \int_{V_p} \left[g + \frac{1}{k_0^2} g_{xx} \right] \exp(-jkz) d\vec{r}} \quad (12)$$

If k does not differ appreciably from k_0 , an assumption which can be easily checked in the result, k inside the integral can be replaced by k_0 and (12) becomes a particularly simple equation for k . The integral involving g can be evaluated directly or through the use of the mean value theorem for plane waves [Kara & Keller, 1964], i.e.

$$\int_{V_p} g(r) \exp(-jk_0 z) d\vec{r} = \frac{1}{k_0} \left[\frac{1}{4k_0} \left\{ 1 - \exp(-j2k_0 a) \right\} - j \frac{a}{2} \right] \quad (13)$$

where a is the radius of the spherical particles. The term $g_{xx}(r)$ is given by [Livesay & Chen, 1974]

$$g_{xx}(r) = \sin^2 \theta \cos^2 \phi \left[\frac{d^2 g}{dr^2} - \frac{1}{r} \frac{dg}{dr} \right] + \frac{1}{r} \frac{dg}{dr}$$

where conventional spherical coordinates (r, θ, ϕ) have been used. The ϕ and θ -integrations are straightforward and the result is as follows;

$$\int_{V_p} g_{xx} \exp(-j k_0 z) d\vec{r} = (2\pi)^{3/2} \int_{\eta}^a \left\{ \frac{J_{3/2}(k_0 r)}{(k_0 r)^{3/2}} \left[\frac{d^2 g}{dr^2} - \frac{1}{r} \frac{dg}{dr} \right] + \frac{J_{1/2}(k_0 r)}{\sqrt{k_0 r}} \left(\frac{1}{r} \frac{dg}{dr} \right) \right\} r^2 dr \quad (14)$$

where η is a small number. Using the recurrence relation for Bessel functions to replace $J_{1/2}$ by $J_{3/2}$ and $J_{5/2}$, integrating by parts the term involving $d^2 g/dr^2$, and then taking the limit as $\eta \rightarrow 0$ yields the following;

$$\int_{V_p} g_{xx} \exp(-j k_0 z) d\vec{r} = -\sqrt{\frac{\pi}{2}} J_{3/2}(k_0 a) \exp(-j k_0 a) \left[(k_0 a)^{-3/2} + j(k_0 a)^{-1/2} \right] + \frac{1}{3} \quad (15)$$

Substituting (13) and (15) into (12) produces the desired result for k , i.e.

$$k^2 - k_0^2 = \frac{3k_0^2 \rho V_p (\epsilon_r - 1)}{\epsilon_r + 2 + 3(\epsilon_r - 1) T(k_0 a)} \quad (16)$$

where

$$T(k_0 a) = -\frac{1}{4} [1 - \exp(-j 2k_0 a)] + j k_0 a/2 - 1/3 + \sqrt{\pi/2} \left[J_{3/2}(k_0 a) \exp(-j k_0 a) \cdot \left\{ [k_0 a]^{-3/2} + j [k_0 a]^{-1/2} \right\} \right]$$

which is the desired result. Apart from the replacement of k by k_0 in (12), equation (16) comprises the exact expression for the propagation constant of the average field in a discrete random medium which is sparsely populated with spherical particles and homogeneous in the mean, at least to the accuracy of the Foldy-Twersky representation.

It was previously stipulated that all the spheres in the medium be of the same size. This is overly restrictive and, in fact, the equation for k resulting from (16) can be averaged over all possible particle sizes to account for a diversity of particle sizes; one should realize that $V_p = 4\pi a^3/3$ in (16). It should be noted that such an averaging process may well accentuate the impact of a relatively few large particles, a fact that has been previously noted [Ishimaru, 1978].

Discussion of Results

In the following it will be assumed that ρV_p or the fractional volume occupied by the spherical particles is very small with respect to one. If $2k_0 a \ll 1$, the various terms in T can be expanded in power series about $k_0 a = 0$ and to the order of $(k_0 a)^4$ there results

$$k^2 - k_0^2 \approx \frac{3k_0^2 \rho V_p \left(\frac{\epsilon_r - 1}{\epsilon_r + 2} \right)}{1 + \left(\frac{\epsilon_r - 1}{\epsilon_r + 2} \right) \left[\frac{13}{5} (k_0 a)^2 + j \frac{2}{3} (k_0 a)^3 \right]} \quad (17)$$

Since $0 \leq |(\epsilon_r - 1)/(\epsilon_r + 2)| \leq 1$, and the terms involving $k_0 a$ are small, (17) simplifies to the following form;

$$k - k_0 \approx \frac{3}{2} k_0 \rho V_p \left[\left(\frac{\epsilon_r - 1}{\epsilon_r + 2} \right) + \left| \frac{\epsilon_r - 1}{\epsilon_r + 2} \right|^2 \left(\frac{13}{5} \right) (k_0 a)^2 - j \frac{2}{3} \left| \frac{\epsilon_r - 1}{\epsilon_r + 2} \right|^2 (k_0 a)^3 \right] \quad (18)$$

which is the small particle limiting form of (16). It is interesting to note that unlike the conventional Rayleigh approximation, (18) does not require $k_o a \epsilon_r \ll 1$ but only $k_o a \ll 1$. The reason for this will be discussed shortly.

In view of the conditions stipulated in the development of (18), it is not unreasonable to expect that k should agree with the single scattering result k_s where

$$k_s - k_o = \frac{2\pi\rho}{k_o} \left\{ \text{Re}[f(\hat{i}, \hat{i})] - j \text{Im}[f(\hat{i}, \hat{i})] \right\} \quad (19a)$$

and

$$\frac{2\pi\rho}{k_o} \text{Re}[f(\hat{i}, \hat{i})] = \frac{3}{2} k_o \rho V_p \text{Re} \left(\frac{\epsilon_r - 1}{\epsilon_r + 2} \right) \quad (19b)$$

$$\frac{2\pi\rho}{k_o} \text{Im}[f(\hat{i}, \hat{i})] = \frac{\rho}{2} (\sigma_s + \sigma_a) = \rho \left\{ \frac{4\pi}{3} k_o^4 a^3 \left| \frac{\epsilon_r - 1}{\epsilon_r + 2} \right|^2 + k_o \epsilon_r'' V_p \left| \frac{3}{\epsilon_r + 2} \right|^2 \right\} \quad (19c)$$

$f(\hat{i}, \hat{i})$ is the forward scattering amplitude, σ_s is the scattering cross section, and σ_a is the absorption cross section of a spherical particle [Ishimaru, 1978]. Comparing (18) and (19), one finds that the first term on the right hand side of (18) is equivalent to (19b) and $\rho\sigma_a/2$ while the third term equals $\rho\sigma_s/2$. The second term in (18) is small compared to $(\epsilon_r - 1)/(\epsilon_r + 2)$ so it may be ignored. This comparison shows that if the spheres are Rayleigh-like, the exact solution of the Foldy-Twersky integral equation is identical to the single scattering result. As will be shown, this is in fact a rather obvious result which follows from the form of the Foldy-Twersky integral equation.

The limit of small free space wavelength or large k_o is most interesting. If $2k_o a \gg 1$ and $j k_o a (\epsilon_r - 1) \gg \epsilon_r + 2$, then (16) reduces to the

following form;

$$k - k_0 = \frac{\rho v_p}{a} \left[-j + \frac{2}{(\epsilon_r - 1) * (k_0 a)} - \frac{1}{2k_0 a} \left(1 - e^{j2k_0 a} \right) \right] \quad (20)$$

Both the real part and the absorption dependent term in the right hand side of (20) go to zero as k_0^{-1} . With $v_p = 4\pi a^3/3$ and to the order of k_0^{-1} , (20) becomes

$$k - k_0 \approx -j \frac{4}{3} \rho \sigma_g \quad (21)$$

where $\sigma_g = \pi a^2$ is the geometric cross section of the spherical particle.

The right hand side of (21) is 1/3 larger than the single scattering result, i.e.

$$k_s - k_0 = -j \rho \sigma_g \quad .$$

Equations (18) and (21) represent the low and high frequency asymptotes of the exact solution to the Foldy-Twersky integral equation. This does not mean, however, that (18) and (21) are solutions for the actual process because the Foldy-Twersky equation itself contains certain approximations. The important question is the following; given the Foldy-Twersky equation, its implicit approximations, and its exact solution how does one determine when the solution is a valid representation of the actual process? Since there is no known exact solution for the actual process, it is not possible to provide a complete answer to this question; however, estimates on the validity of the solution can be obtained.

First, it must be realized that the exact solution of the Foldy-Twersky equation comprises the approximate solution of a deterministic boundary value problem. In particular, rather than solving for the average field inside the particle given the incident field, the Foldy-Twersky equation essentially

states that both fields will be plane waves and it is only necessary to solve for the complex constant relating the two fields. This is recognized as the same procedure that is used in the approximate analyses of deterministic scattering by a Rayleigh or Rayleigh-Gans object. This does not mean however that the Foldy-Twersky equation is limited to these types of particles because one must also consider the approximations implicit in the basic equation. For example, in the case of very large particles the solution of the Foldy-Twersky equation should be an accurate representation of the process because the approximations implicit in the equation are satisfied in this case. Conversely, with small but perfectly conducting particles, the Foldy-Twersky equation is probably not accurate. That is, with perfectly conducting small spheres, (18) predicts that the imaginary part of k is equal to $4\pi k_0^4 a^6/3$ whereas single scattering theory yields $5\pi k_0^4 a^6/3$ [Jones, 1961 (pg. 504)]. This disparity results from the well known fact that one cannot use the asymptotic cross section of a small dielectric sphere to obtain the scattering cross section of a small perfectly conducting sphere. In addition, since small conducting spheres scatter strongly in the backscatter direction [Jones, 1961 (pg. 512)], this is exactly the type of situation for which the Foldy-Twersky representation breaks down. For finite conductivity, this problem is not encountered and (18) should be an accurate solution because it agrees with single scattering theory which, in turn, should be valid for small scatterers.

In summary, an attempt has been made to determine when the exact solution of the Foldy-Twersky equation is an accurate representation of the true propagation process. Based upon the reasons given above, it is concluded that (16) is probably accurate for all cases except when the spheres are small with respect to a wavelength and perfectly conducting. In regard to

Rayleigh-Gans spheres, i.e. $k_0 a \gg 1$ and $k_0 a(\epsilon_r - 1) \ll 1$, there is a slight difference between this result and single scattering theory. With $\sigma_s \approx |\epsilon_r - 1|^2 (k_0 a)^2 (\pi a^2) / 2$ [Jones, 1964 (pg. 515)], single scattering theory predicts $\text{Im}(k_s) = -\rho \sigma_s / 2$ whereas the exact solution of the Foldy-Twersky integral equation yields $\text{Im}(k) \approx -\rho |\epsilon_r - 1|^2 (k_0 a)^2 (\pi a^2) / 3$. In a previous approximate solution of the Foldy-Twersky equation [Twersky, 1964] which ignored all scattering except in the forward direction, $k \approx k_s$ was found. Comparing this result with the exact solution gives some idea of the impact of ignoring certain scattering chains.

Numerical Examples

Before concluding, it is instructive to present a few numerical examples for the case of spherical particles. All of these results were computed using the simple expression in (16). Figure 2 illustrates the behavior of $\text{Im}(k/\rho \pi a^2)$ as a function of $k_0 a$ for $\epsilon_r = 1.77$. In single scattering theory, $\text{Im}(k/\rho \pi a^2)$ corresponds to one-half the scattering cross section of a single sphere. In the text above, it was shown that $\text{Im}(k/\rho \pi a^2)$ and the single scattering theory only agree when the spherical particles are Rayleigh and the plot in Figure 2 illustrates this point. In addition to the different asymptote, i.e. $4/3$ rather than 1 , there is a marked difference in the oscillatory behavior also. That is, Figure 2 shows none of the high frequency oscillations that are present in the scattering cross section of a single dielectric sphere due to multiple internal reflections. This is not surprising, however, since there is no reason to expect that the fine scale behavior of a single particle should be evident in a multiple scatter environment. Figure 3 shows the behavior of $\text{Re}[(k - k_0)/\rho \pi a^2]$. Of particular note here is the persistence of the oscillations as $k_0 a$ increases.

As noted previously, the results obtained here are applicable to

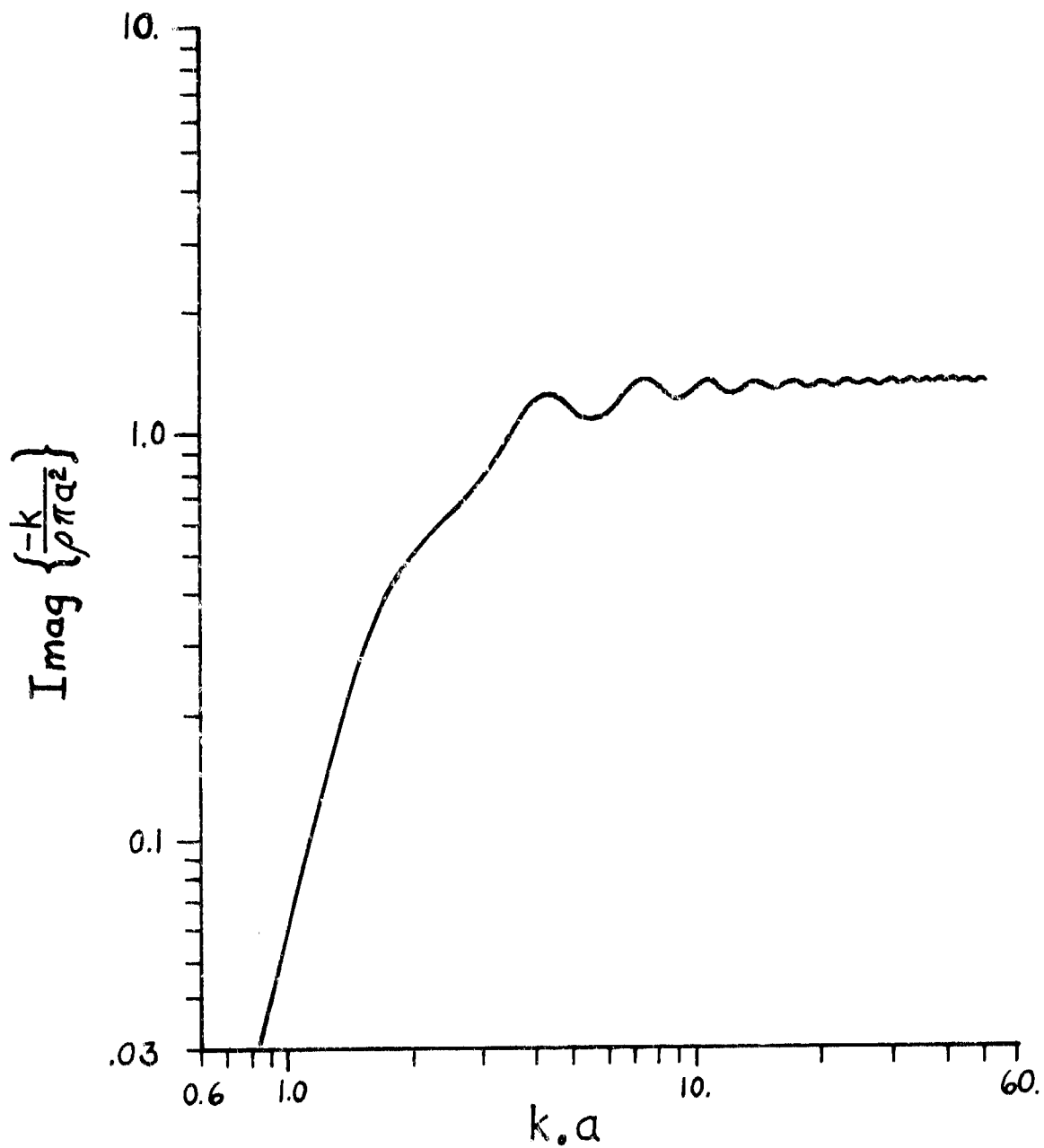


Figure 2. Variation of the imaginary part of the normalized propagation constant of the average field as a function of $k_0 a$ for spherical particles and $\epsilon_r = 1.77$.

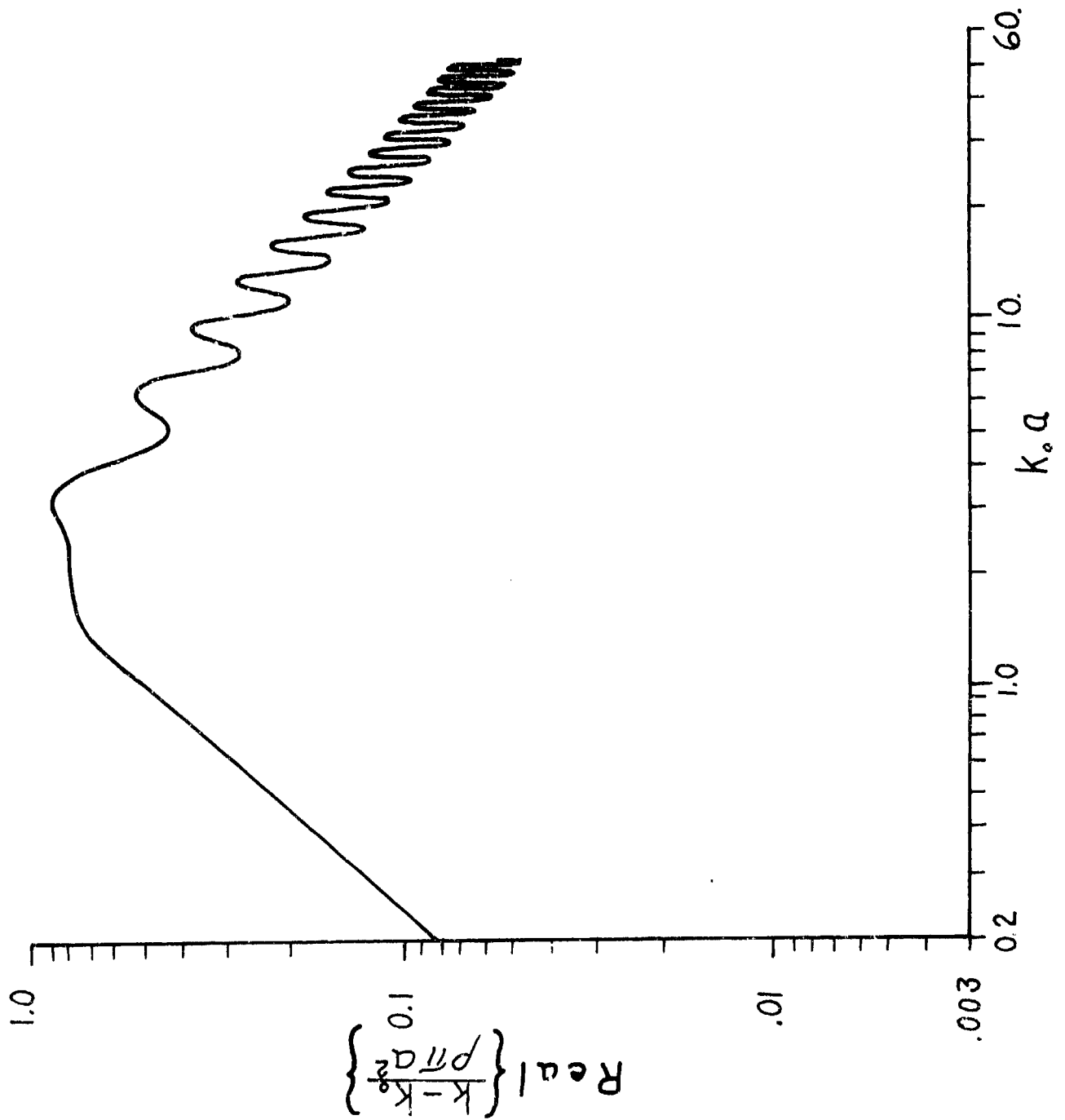


Figure 3. Variation of the real part of the normalized and centered propagation constant of the average field as a function of $k_0 a$ for spherical particles and $\epsilon_r = 1.77$.

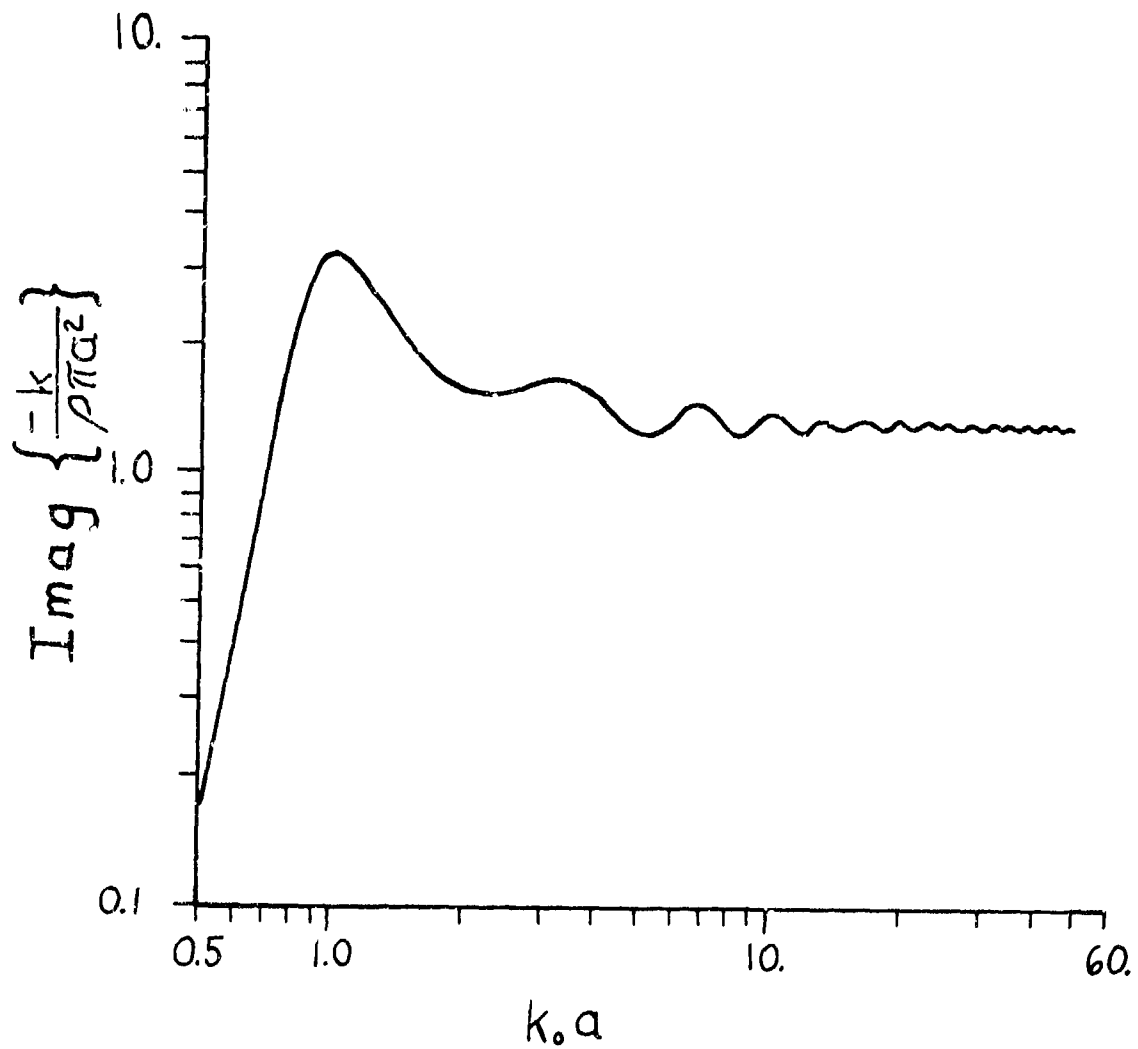


Figure 4. Variation of the imaginary part of the normalized propagation constant as a function of $k_0 a$ for perfectly conducting spherical particles.

perfectly conducting spheres which are not small in terms of a wavelength, i.e. let $\epsilon_r \rightarrow \infty$ in (16) and take $k_0 a \geq 1/2$. Figure 4 is a plot of the quantity $-\text{Im}(k/\rho\pi a^2)$ as a function of $k_0 a$ for perfectly conducting spheres. Here again there is a significant difference between these results and the scattering cross section of a single sphere.

References

1. Beard, C. I., T. H. Kays & V. Twersky (1967), "Scattering by Random Distribution of Spheres vs. Concentration," IEEE Trans. Antennas & Propg., AP-15(1), 99-118.
2. Brown, G. S. (1979), "Coherent Wave Propagation and the Foldy-Twersky Integral Equation," USNC/URSI meeting, Seattle, WA.
3. Foldy, L. L. (1945), "The Multiple Scattering Of Waves," Phys. Rev. 67(2), 107-119.
4. Ishimaru, A. (1978), Wave Propagation and Scattering In Random Media, Vols. I and II, Academic Press, New York.
5. Jones, D. S. (1964), The Theory of Electromagnetism, Macmillian Company, New York.
6. Karal, F. C. and J. B. Keller (1964), "Elastic, Electromagnetic, and Other Waves in Random Medium," J. Math. Phys., 5 (4), 537-547.
7. Livesay, D. E. and K. M. Chen (1974), "Electromagnetic Fields Induced Inside Arbitrarily Shaped Biological Bodies," IEEE Trans. Microwave Theory & Tech., MTT-22 (12), 1273-1280.
8. Twersky, V. (1964), "On Propagation In Random Media Of Discrete Scatterers," Proc. Am. Math. Soc. Symp. on Stochastic Processes in Mathematical Physics and Engineering, 16, 84-116.
9. Van Bladel, J. (1961), "Some Remarks on Green's Dyadic For Infinite Space," IRE Trans. Antennas & Propg., AP-9(6), 563-566.

APPENDIX B

DERIVATION OF A RELATIONSHIP REQUIRED IN SECTION 3.2.2

The purpose of this Appendix is to prove that

$$\langle \sigma_a \rangle = -k_o \langle v_p \rangle \operatorname{Im} \left\{ (\epsilon_r - 1) \langle \vec{\xi} \cdot \hat{e} \rangle \right\}$$

We start by using the definition of $\langle \sigma_a \rangle$, i.e.

$$\langle \sigma_a \rangle = k_o \epsilon_r'' \left\langle \int_{V_p} |\vec{E}_1^1 / E|^2 dV \right\rangle \quad (1)$$

Since

$$\vec{E}_1^1 = \vec{E}_1^0 + \delta \vec{E}$$

and $\delta \vec{E} \ll \vec{E}_1^0$, we have

$$\vec{E}_1^1 \approx \vec{E}_1^0 \quad (2)$$

Substituting (2) into (1) yields

$$\langle \sigma_a \rangle \approx k_o \epsilon_r'' \left\langle \int_{V_p} |\vec{E}_1^0 / E|^2 dV \right\rangle,$$

and since V_p is very small, $|\vec{E}_1^0 / E|^2$ only depends on orientation and

$$\langle \sigma_a \rangle \approx k_o \epsilon_r'' \langle v_p \rangle \left\langle |\vec{E}_1^0 / E|^2 \right\rangle \quad (3)$$

Substituting (29) of Section 3.2.2 into (3) yields

$$\langle \sigma_a \rangle = k_o \langle v_p \rangle \epsilon_r'' \left\{ \langle (\hat{e} \cdot \hat{r})^2 \rangle + \left| \frac{2}{\epsilon_r + 1} \right|^2 \left[\langle (\hat{e} \cdot \hat{e})^2 \rangle + \langle (\hat{e} \cdot \hat{\phi})^2 \rangle \right] \right\} \quad (4)$$

We now proceed to show that

$$\langle \sigma_a \rangle = -k_o \langle v_p \rangle \operatorname{Im} \left\{ (\epsilon_r - 1) \langle \xi_s^+ \cdot \hat{e} \rangle \right\} \quad (5)$$

is equivalent to (4). Expanding (5) yields

$$\langle \sigma_a \rangle = k_o \langle v_p \rangle \left\{ \epsilon_r'' \langle (\hat{e} \cdot \hat{r})^2 \rangle + \operatorname{Im} \left[2 \left(\frac{\epsilon_r - 1}{\epsilon_r + 1} \right) \left(\langle (\hat{e} \cdot \hat{\theta})^2 \rangle + \langle (\hat{e} \cdot \hat{\phi})^2 \rangle \right) \right] \right\} \quad (6)$$

and since $\langle (\hat{e} \cdot \hat{\theta})^2 \rangle$ and $\langle (\hat{e} \cdot \hat{\phi})^2 \rangle$ are real, it only remains to find the imaginary part of the $(\epsilon_r - 1)/(\epsilon_r + 1)$. This is easily done with the following result

$$2 \operatorname{Im} \left\{ \frac{\epsilon_r - 1}{\epsilon_r + 1} \right\} = \epsilon_r'' \left| \frac{2}{\epsilon_r + 1} \right|^2$$

Thus, (6) becomes

$$\langle \sigma_a \rangle = k_o \langle v_p \rangle \left\{ \epsilon_r'' \langle (\hat{e} \cdot \hat{r})^2 \rangle + \epsilon_r'' \left| \frac{2}{\epsilon_r + 1} \right|^2 \left[\langle (\hat{e} \cdot \hat{\theta})^2 \rangle + \langle (\hat{e} \cdot \hat{\phi})^2 \rangle \right] \right\} \quad (7)$$

which is identical to (4) and the proof is complete.

APPENDIX C

ESTIMATION OF MODEL PARAMETERS FROM FOLIAGE STATISTICAL DATA

Introduction

This appendix will describe the development of a procedure for estimating the distribution of fractional foliage volume by its equivalent cylindrical diameter. The REV model parameter $\{\rho V_p\}_{ew}$ is the fractional volume of scattering elements of a given size or less. For a forest, this becomes the fractional volume of foliage (wood, needles) of a given cylindrical diameter or less found within the enclosed forest volume.

The procedure relies on tree growth forms described in the literature. These growth forms are then modeled according to standard summary statistics available from a forest stand table. If the tree models are considered to adequately portray an average tree, a fractional volume estimate is possible for an entire stand of trees.

A prior understanding of the following terms and symbols will be helpful.

<u>Term</u>	<u>Definition</u>
$\{\rho V_p\}$	The fractional volume of scattering elements occupying a total volume; may be further broken down as a distribution function of the element size, i.e. $\{\rho V_p\}_{ew}$ for wood.
Basal area (or $g_{1.3}$)	The cross-section area of a tree trunk found at "breast height", or about 1.3 meters from ground level.
d.b.h.	<u>Diameter breast height</u> . The diameter of the trunk about 1.3 meters from ground.
d.b.h. class (Basal area class)	A d.b.h. (or basal area) size category in which a range of sizes are included for the purpose of classifying trees.

<u>Term</u>	<u>Definition</u>
h	The average forest tree height, sometimes defined as the arithmetic mean of the 100 tallest trees in a stand.
Treewood	All the above ground wood found in a tree.
Stemwood	All wood found in the tree trunk.
Cylindrical or structural diameter	Simply the diameter of a trunk or limb.
Branchwood (or saw-timber)	All wood contained in limbs and trunk with a cylindrical diameter greater or equal to a standard size such as 7 cm.
Forest stand table	A table of summary statistics for a forest stand, usually on a per acre or a per hectare (10,000 m ² .) basis. Included are tree count by d.b.h. (or basal area) class, species present, height information, and various other parameters depending on application.

Total Forest Wood Volume

A total wood volume model will now be developed. Needles and broadleaves will be considered separately in a later section. It is necessary to first determine total volume before finding the volume distribution. Information from Assman [1] will be used to model a conifer form and a deciduous form separately. This information is based on the Spruce (conifer) and the European Beech (deciduous), both common in Central Europe. Assuming that these forms also represent other coniferous and deciduous species, it is possible to use this model for other species.

Singling out an "average" tree, the trunk may be divided into five equal sections from ground up. In Figure 1, h is the average height of the forest and also is the height for this tree. $a_1 \rightarrow a_5$ are the cross-sectional areas of the trunk at each section boundary, spaced $.2h$ apart. The relationship

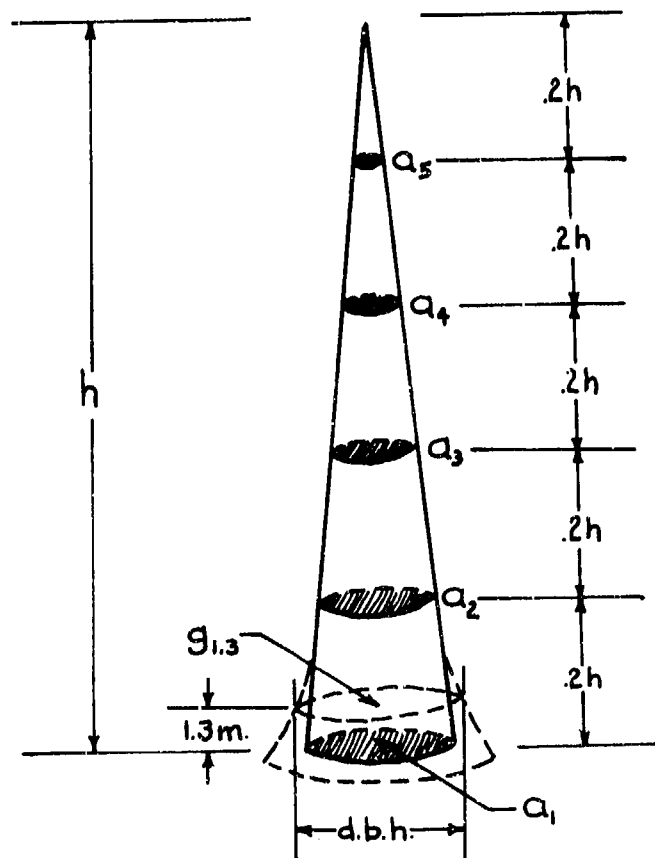


Figure 1. Trunk volume model.

between these areas has been determined for Spruce and is given in [1] (p. 67, Figure 36). Using this information, the relative section areas can be normalized with respect to section area a_2 and are given as follows; $a_2 = 1$, $a_3 = 0.78$, $a_4 = 0.57$, $a_5 = 0.22$. Thus, if a_2 is known, $a_3 + a_5$ can be found by multiplying a_2 by each of these factors.

In Figure 1, the base section or bole of the trunk is shown as a flared shape with the dashed lines. This is a more realistic portrayal of this part of the tree. However, in an effort not to over complicate the model, a conical section will be used. Furthermore, a_1 will be assumed equal to the basal area $g_{1.3}$ even though a_1 is at ground level. This is actually not so inaccurate since the flaring is somewhat exaggerated in Figure 1.

Information from [1] (p. 66, Table 19) shall now be used to derive an expression for a_2 in terms of a_1 (or $g_{1.3}$). Trunk diameter data are given in [1] for different heights of Spruce trees. To utilize these data, a linear fit of mean trunk diameter values was made with the following result. If d_1 and d_2 are the diameters in meters of a_1 and a_2 ;

$$d_2 \approx .78 d_1 + .023$$

Since $a_2 = \pi d_2^2 / 4$,

$$a_2 = \frac{\pi}{4} (.78 d_1 + .023)^2$$

Also, since $d_1 = 2\sqrt{a_1/\pi}$ and $a_1 = g_{1.3}$,

$$a_2 = \frac{\pi}{4} \left(1.56 \sqrt{\frac{g_{1.3}}{\pi}} + .023 \right)^2$$

where $g_{1.3}$ must be in $m.^2$.

Areas a_1 through a_5 are now related to the basal area statistic $g_{1.3}$. Letting $G_{1.3}$ represent the total basal area of a forest stand and A_1 through A_5 the total trunk section areas for the stand; $A_1 = G_{1.3}$, $A_3 = 0.78 A_2$, $A_4 = 0.56 A_2$, $A_5 = 0.22 A_2$, and for $G_{1.3}$ in square meters

$$A_2 = \frac{\pi}{4} \left(1.56 \sqrt{\frac{G_{1.3}}{\pi}} + .023 \right)^2$$

The total trunk volume for a stand can now be calculated from the section areas. The formula for a solid cone with base area A_1 and top section area A_2 is

$$V_1 = \frac{1}{3} (A_1 + A_2 + \sqrt{A_1 A_2}) L \quad (1)$$

where L is the length from base to top. Since the trunk has been modeled as five such cones stacked on top of each other, the total volume is the sum of the five layer volumes. Letting V_{TK} be the total trunk volume for an entire stand of trees the sum of the layer volume formulas yields;

$$V_{TK} = \frac{1}{3} (A_1 + 2A_2 + 2A_3 + 2A_4 + 2A_5 + \sqrt{A_1 A_2} + \sqrt{A_2 A_3} + \sqrt{A_3 A_4} + \sqrt{A_4 A_5}) \cdot (.2h) \quad (2)$$

Branch volume will now be estimated using information from [1]. The conifer in Figure 2 will be based on Spruce data and the deciduous on the European Beech. V_o and V_u are defined as the overhead and underside branch region volumes. For both regions of the conifer and the underside of the deciduous, these volumes are modeled as solid cones. The overhead branch region on the deciduous is a segment of a sphere. In [1], the ratio of l to h

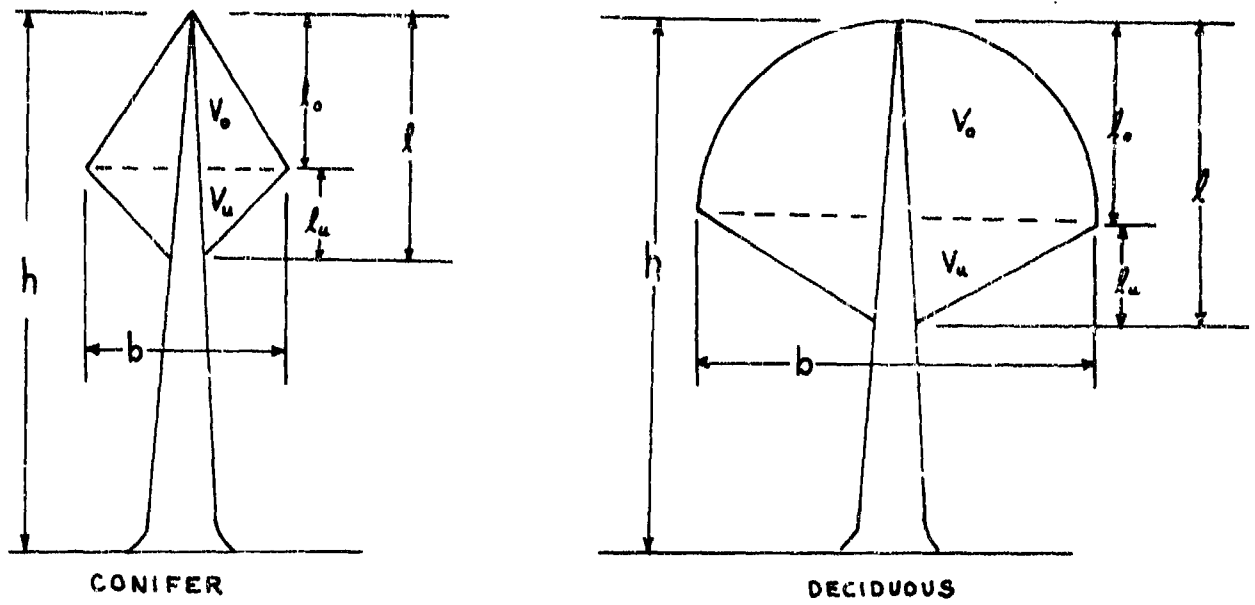


Figure 2. Branch region shapes.

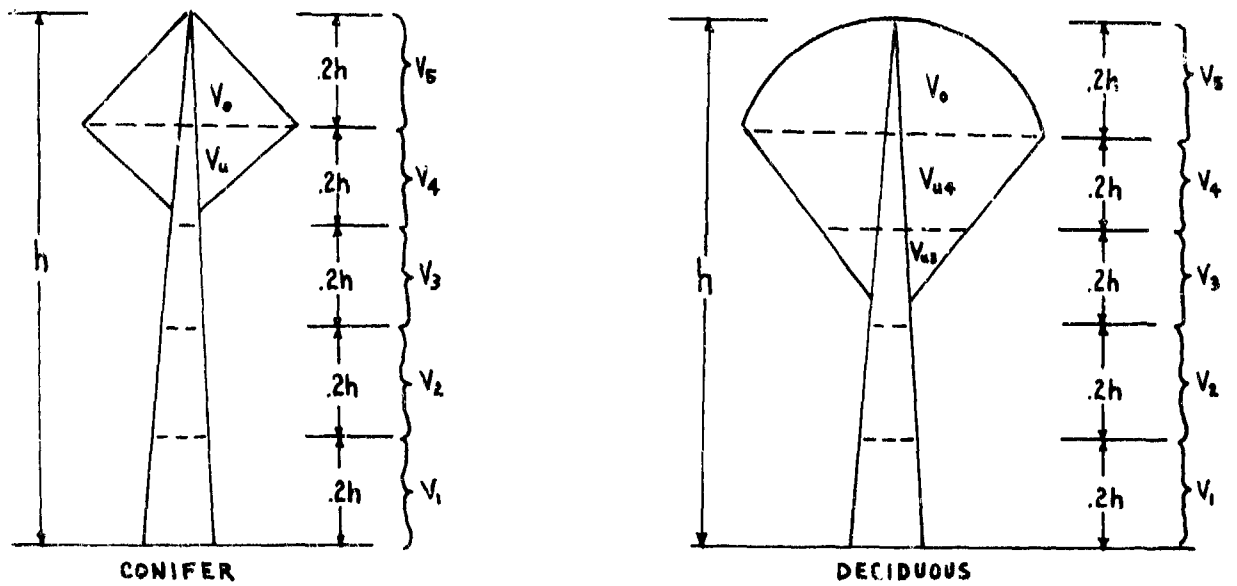


Figure 3. Growth form models.

is about .4 for Spruce and .6 for Beech. The region boundaries will be assumed to be at a height of .8h, i.e., $l_0 = .2h$. Also, l_u will be set equal to .3h for the conifer model and .4h for the deciduous. These values represent some compromise in the original forms given in [1], but conveniently confine the branch regions to the individual layer sections as previously defined. The simplified models are shown in Figure 3. $V_1 + V_5$ are the total volumes of each layer. V_{u4} and V_{u3} are the underside branch region of the deciduous split into two regions, one for each layer.

The branch region volumes are of course not solid wood in reality. They have been defined for the purpose of providing a relative limb volume distribution among section layers. If it is possible to relate the total volume of branches to the treewood (total wood) volume, the branch region volumes can be modeled quantitatively.

In [1], (Figures 39 and 40, p. 76) the percentage stemwood has been estimated according to both d.b.h. and height from data for Spruce. Also, the percentage branchwood has been estimated for Beech. This means that for the conifer Spruce, we have an estimate of the percentage wood volume contained in the trunk. This value is fairly constant and close to 85% for mature trees. The remaining 15% is the percentage volume of branches. Knowing the trunk volume, it is possible to estimate the branch volume from these values. For the deciduous Beech, all that is given is the branchwood, or wood with cylindrical diameter greater than 7 cm. This value is also fairly constant for mature trees and approaches 90%. Due to the growth pattern of many deciduous species, it is usually difficult to make a clear distinction between trunk and branches since the trunk tends to split into several large limbs. Therefore, lacking any better information about its growth form, the deciduous Beech shall be modeled with the trunk model in Figure 1 and the branch region volumes

in Figures 2 and 3 for deciduous. Furthermore, 90% wood volume will be assumed contained in the "trunk" and the remaining 10% in the branches.

Even though a somewhat artificial delineation of trunk and limbs was necessary for the deciduous model, the important consideration is that all the wood present in each layer is accounted for. In fact, the branch region shapes are not really important so long as the volume is distributed and accounted for accurately. Hopefully, this will be true for the deciduous model for at least a first order approximation.

The branch volumes will now be derived. Referring to Figures 2 and 3 it is evident that $V_o = V_u$ for the conifer. Since 85% wood volume is in the conifer trunk, the total treewood volume, V_{TW} is expressed by;

$$V_{TW} = \frac{V_{TK}}{.85} \quad (3)$$

The conifer branch volume is the treewood volume minus the trunk;

$$\begin{aligned} V_o + V_u &= V_{TW} - V_{TK} \\ V_o + V_u &= \frac{V_{TK}}{.85} - V_{TK} \approx .176 V_{TK} \end{aligned} \quad (4)$$

Since V_o and V_u are equal;

$$V_o = V_u \approx \frac{1}{2} (.176 V_{TK}) \approx .088 V_{TK} \quad (5)$$

The deciduous overhead branch region, V_o is found by the formula for a spherical segment volume;

$$V_o = \frac{1}{6} \pi \ell_o \left[3 \left(\frac{b}{2} \right)^2 + \ell_o^2 \right] \quad (6)$$

From [1], b is given to be approximately $.28h$ for Beech. Substituting this and $\ell_o = .2h$ in (6) yields;

$$V_o = \frac{1}{6} \pi (.2h) [3(.4h)^2 + (.2h)^2]$$

$$V_o \approx \frac{1}{6} \pi (.02) h^3 \quad (7)$$

For the underside region volume, the formula for a cone is;

$$V_u = \frac{1}{3} \frac{\pi}{4} b^2 l_u \quad (8)$$

Substituting $b = .28h$ and $l_u = .4h$ in (8) yields;

$$V_u = \frac{1}{3} \frac{\pi}{4} (.28h)^2 (.4h)$$

$$V_u \approx \frac{1}{12} \pi (.03) h^3 \quad (9)$$

Forming the ratio of V_o to V_u given in (7) and (9) yields;

$$\frac{V_o}{V_u} = 1.333 \quad (10)$$

V_o and V_u can be related to the trunk volume in the same manner done for the conifer model. Using the 90% value for the deciduous trunk volume, the total branch volume is given by;

$$V_o + V_u = V_{TW} - V_{TK} = \frac{V_{TK}}{.9} - V_{TK} \approx .111 V_{TK} \quad (11)$$

Using (10) and (11);

$$V_o + V_u = V_o + \frac{V_o}{1.333} = .111 V_{TK}$$

So
$$V_o \approx .063 V_{TK} \quad (12)$$

Also,

$$1.333 V_u + V_u = .111 V_{TK}$$

so
$$V_u \approx .048 V_{TK} \quad (13)$$

It is easy to show with the volume formula for a cone that;

$$V_{u3} = \frac{1}{8} V_u$$
$$V_{u4} = \frac{7}{8} V_u \quad (14)$$

Substituting (13) in (14) yields;

$$V_{u3} \approx \frac{1}{8} (.048 V_{TK}) \approx .006 V_{TK}$$
$$V_{u4} \approx \frac{7}{8} (.048 V_{TK}) \approx .042 V_{TK} \quad (15)$$

This completes the derivation of all the necessary formulas for obtaining treewood volume estimation from basal area. The estimated volume includes as many trees as the basal area value represents, and, if desired, can include only that wood found in any of the five layers. If a forest is a mixture of conifers and deciduous, the volumes could be calculated separately using the basal area for each and the appropriate branch volume expressions. In other words, formula (2) could be used to find the total trunk volume for each type by using the corresponding basal area. Then, branch volumes could be found using the appropriate formula - (4) for conifers, and (11) for deciduous. The sum of the trunk and branch volumes is the total treewood volume for each type and the sum of the conifer and deciduous treewood volumes is the total for the forest stand. This procedure can be simplified by realizing that the trunk volume (2) is directly proportional to $G_{1.3}$. Since we are using the same trunk for conifers and deciduous, only the branch volume expressions require

V_{TK} to represent the individual trunk volumes for each type. The trunk volumes for conifer and deciduous can be simply found from the total trunk volume by taking a proportional part of the total with respect to the basal area values for each type. In other words, if $G_{1.3C}$ is the total conifer basal area and $G_{1.3D}$ is for deciduous, the individual trunk volumes can be found from the following;

$$V_{TKC} = \frac{G_{1.3C}}{G_{1.3C} + G_{1.3D}} V_{TK}$$

$$V_{TKD} = \frac{G_{1.3D}}{G_{1.3D} + G_{1.3C}} V_{TK} \quad (16)$$

where V_{TKC} and V_{TKD} are the coniferous and deciduous trunk volumes, and V_{TK} is found from (2) using the total basal area for all trees. Total treewood volume is now simply found from the sum of all the trunk volume and the branches. If V_{TW} is the total treewood volume, and using (4) and (11) for the conifer and deciduous branch volumes along with (16);

$$V_{TW} = V_{TK} + .176 V_{TKC} + .111 V_{TKD}$$

$$V_{TW} = V_{TK} \left[1 + .176 \frac{G_{1.3C}}{G_{1.3}} + .111 \frac{G_{1.3D}}{G_{1.3}} \right] \quad (17)$$

where

$$G_{1.3} = G_{1.3C} + G_{1.3D}$$

and V_{TK} is the total trunk volume found from (2) using $G_{1.3}$ to find $A_1 \rightarrow A_5$.

A simple example can help illustrate the above. Suppose an acre of forest land is found to contain a total of 60 ft.² trunk basal area and an average height of 65 ft. representing most of the trees. Of the 60 ft.², 40 ft.² are conifers representable by the Spruce conifer model, and the remaining 20 ft.²

are deciduous resembling the Beach. The total treewood volume can be found from (17). We first find A_1 through A_5 .

$$A_1 = G_{1.3} = 60 \text{ ft.}^2$$

$$A_2 = \frac{\pi}{4} \left[1.56 \sqrt{\frac{G_{1.3}}{\pi}} + .023 \right]^2$$

The constants in the parenthesis of the expression for A_2 require $G_{1.3}$ in m.^2 . This means $G_{1.3}$ must first be converted to m.^2 , i.e. $G_{1.3} = 60 \text{ ft.}^2 \approx 5.57 \text{ m.}^2$. The result for A_2 will then be in m.^2 ;

$$A_2 = \frac{\pi}{4} \left[1.56 \sqrt{\frac{5.57}{\pi}} + 0.23 \right]^2 \approx 3.47 \text{ m.}^2$$

A_2 is now converted back to ft.^2 , i.e. $A_2 = 3.47 \text{ m.}^2 \approx 37.35 \text{ ft.}^2$ and

$$A_3 = .78 A_2 = 29.13 \text{ ft.}^2$$

$$A_4 = .56 A_2 = 20.92 \text{ ft.}^2$$

$$A_5 = .22 A_2 = 8.22 \text{ ft.}^2$$

Substituting these values for A_1 through A_5 in (2), we obtain

$$V_{TK} = 1600.58 \text{ ft.}^3$$

From the information given, $G_{1.3C} = 40 \text{ ft.}^2$ and $G_{1.3D} = 20 \text{ ft.}^2$. Substituting in (17) we get;

$$V_{TW} = 1600.58 \left[1 + .176 \left(\frac{40}{60} \right) + .111 \left(\frac{20}{60} \right) \right]$$

$$V_{TW} = 1847.6 \text{ ft.}^3$$

Finally, the fractional volume of treewood in the forest enclosure volume, V_F , is given by;

$$\frac{V_{TW}}{V_F} = \frac{1847.6}{1 \text{ acre} \times h} = \frac{1847.6}{(43,560)(65)} = .000653$$

Notice that the statistic h was not really required for the fractional volume calculation since h in the denominator cancels the factor h in the formula for V_{TK} , (2), and thus V_{TW} .

Volume Distribution By Diameter

The total volume or fractional volume of wood must be further broken down and distributed according to its cylindrical diameter. This provides the parameter $\{\rho V_p\}_{ew}$ required by the REV propagation model. In order to accomplish this task, there must be available additional information concerning the growth form of trees. Essentially, we need to know how wood is distributed in a tree according to its cylindrical diameter on some average basis so that estimates can be extended over an entire stand. Such information could not be located in the literature for any specie of trees and does not appear to be of general interest. The only data which could be of any use whatsoever was found in [1]. This is the branchwood curve which provides a percentage value of treewood volume for all wood with cylindrical diameter 7cm. and greater. Such wood is commonly referred to as saw-timber and comprises that portion of wood with commercial value to saw mills. This means that given a d.b.h. size for a tree, an estimate of all wood volume 7cm. cylindrical diameter and greater can be obtained. This curve has percent volume wood for its y-axis and d.b.h. for the x-axis and is shown in Figure 4 where it is labeled as the 7 cm. curve. It is the same curve referred to earlier for European Beech. Notice that for d.b.h. sizes of about 25 cm. and greater, approximately 90% wood volume is

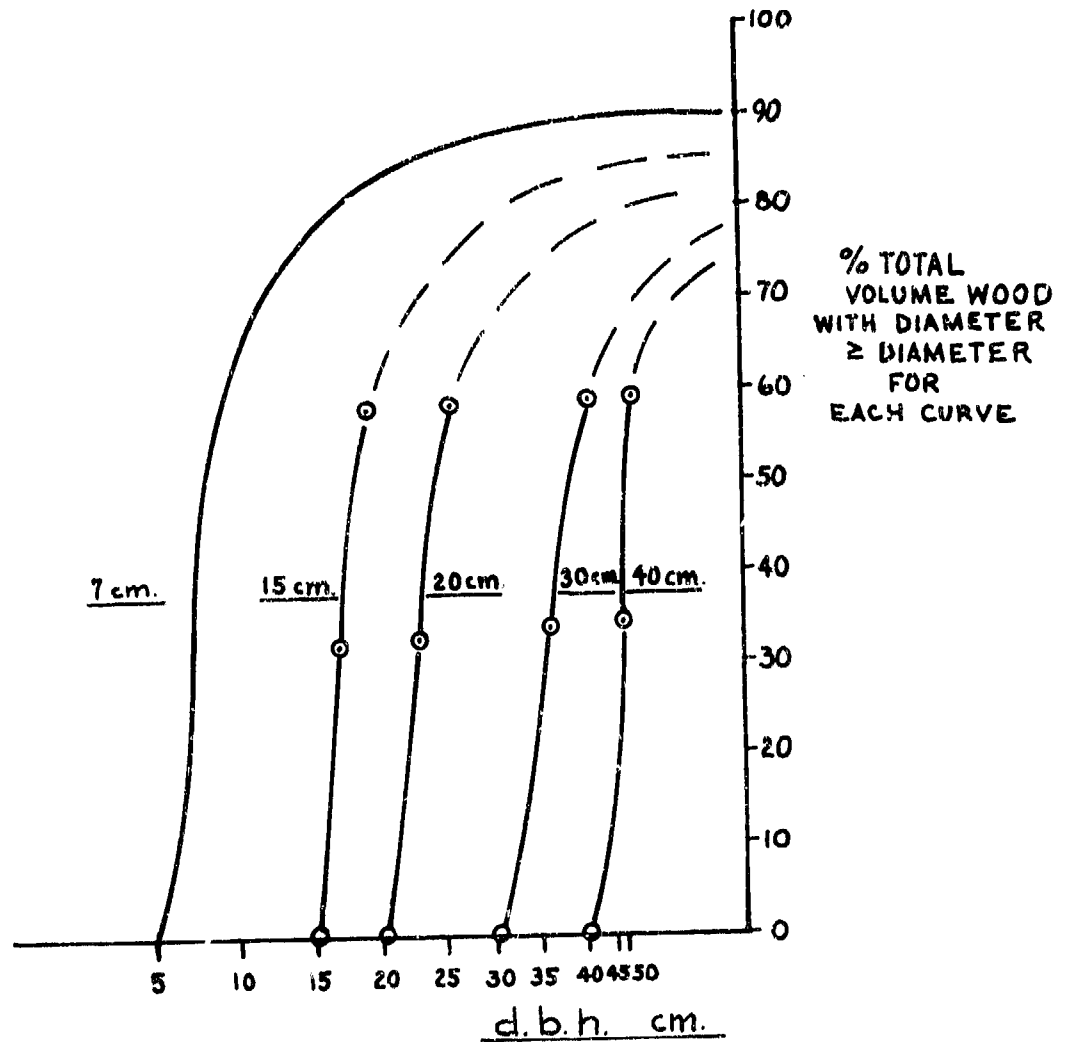


Figure 4. Treewood volume distribution curves. Each curve represents percent volume wood with indicated diameter and larger for d.b.h. size tree. Based on Beech data and model.

contained in tree parts with 7 cm. and larger cylindrical diameter.

If additional curves were available, each representing a different cylindrical diameter, it would be possible to construct a simple distribution function of wood volume according to cylindrical diameter for a given d.b.h. size tree. The percentage volume would of course be found from the intersection of each curve with a vertical line from the d.b.h. axis. Each intersection would provide a volume percentage for each corresponding cylindrical diameter. Each pair of values would be discrete points for a distribution function.

A way to synthesize four additional curves was devised using the wood volume model from the previous section and a fundamental assumption. Referring to the deciduous model in Figure 3, we assume that all wood found in the tree from any level along the trunk between ground and $.4h$, i.e. just before the branches occur, has a cylindrical diameter greater than wood found above that level, and less than wood found below. In other words, we simply assume that the trunk model as proposed is valid, i.e. that the cross-section diameters decrease with increasing height. Furthermore, we assume that up to at least the a_3 cross-section at $.4h$, all branches found growing above have diameters smaller than the trunk. This allows us to assign diameters to sections a_1 , a_2 , a_3 and compute the remaining section areas according to the volume model. The volume of the first layer, V_1 is found and the volume $V_1 + V_2$ as well. Total volume is also computed and a percentage of both V_1 and $V_1 + V_2$ to total volume is found. Since we have assumed that all diameters above d_1 are less than d_1 and all diameters above d_2 are less than d_2 and the same for d_3 , the volume percentages give us the volume of treewood with diameters equal to or greater than the diameters assigned to d_1 , d_2 , or d_3 .

To illustrate how this is done, consider the case for the curve labeled 15 cm. in Figure 4. The first point we obtain for this curve is easy. We

merely assume that a tree with d.b.h. = 15 cm has no wood greater than 15 cm. in diameter. (This is not precisely true, but we have assumed for the volume model that the ground level cross-section a_1 is equal to the basal area $S_{1.3}$. This is the same as saying the ground level diameter d_1 is equal to d.b.h.) So for a 15cm. cylindrical diameter, a 15 cm. d.b.h. tree has 0% volume wood with diameter greater than or equal to 15 cm. This gives us the first point on the curve. Next, we assign the trunk diameter d_2 to be equal to 15 cm. Volume V_1 , the volume of wood in the first layer between ground level and diameter d_2 , is found along with the total treewood volume using the model. This is done by taking the diameter at $d_2 = 15$ cm. and finding a_2 . Then using the relationships between a_2 and the rest of the section areas, a_1 through a_5 are found. V_1 is found by the formula for a conic volume. Total treewood volume, V_{TW} is found according to (17). The ratio $V_1/V_{TW} \times 100$ gives percent volume and d_1 is found from a_1 . Since d_1 is the d.b.h., we have the size tree in which the computed percentage volume of wood has cylindrical diameters 15 cm. and larger. This is the second point on the curve. The third point is found in the same way only now we compute $V_1 + V_2$, the volume between ground and d_3 , when $d_3 = 15$ cm. The ratio of $V_1 + V_2$ and total volume gives the percentage and d_1 (or d.b.h.) is found from a_1 as before. Notice that as the 15 cm. diameter moves up the truck, the model-predicted d.b.h. value increases as would be expected.

Since we are dealing with the deciduous model, we cannot assign the trunk model diameter to any higher level than at a_3 . This is because at a_3 , branches begin to form and the possibility exists of having branches below any level above a_3 with cylindrical diameters greater than the trunk. Therefore, we would violate the assumption that allowed us to compute a volume ratio which gave the percentage volume of wood with diameters greater or equal to the assigned diameter.

Three more curves were formed in exactly the same way. These curves represent cylindrical diameters 20, 30, and 40 cm. Since our assumption breaks down at a_3 , the remaining portions of the curves cannot be found using this procedure. All that could be done here was to guess at the shape of these portions of the curves based only on the shape of the entire 7 cm. curve. Consequently, these portions are shown as dashed lines.

An example shall now be given of the use of these curves in producing a volume distribution among cylindrical diameters. Again the assumption is made that these curves which were developed essentially for a single, average, deciduous tree can be used to make estimations for an entire forest stand. It would have been possible to produce a similar set of curves based on the conifer model but the difference in the synthesized curves would have been very little and certainly within the error bounds. (This is due to the assumption made in the different volume models with the result that the trunks were identical and only the branch regions differed.) Thus, we are dealing with at best a first order approximation and the distinction between conifer and deciduous disappears.

Suppose that from information obtained from a forest stand table, the volume models were utilized to estimate the fractional volume for each of three d.b.h. classes of trees. The results are given in Table I along with the average d.b.h. from each d.b.h. class.

		<u>TABLE I</u>		
		<u>Trees by d.b.h. class</u>		
		<u>1.3 - 13 cm.</u>	<u>13 - 28 cm.</u>	<u>> 28 cm.</u>
Fractional volume	$\frac{V_{TW}}{V_F}$	— .000436	.000418	.000523
Average d.b.h. (cm.)		— 7.	20.	35.

What we should like to determine is what portion or percent of each fractional volume comprises wood with cylindrical diameters less than any given diameter. In other words, what is the fractional volume distribution among cylindrical diameters for each d.b.h. class. This can be found for a few diameter values with the aid of the curves in Figure 4. For example, consider the last d.b.h. class with an average d.b.h. of 35 cm. For this size tree, we can estimate from the curves the percent volume wood with cylindrical diameters greater or equal to 30, 20, 15, and 7 cm. This is shown in Figure 5. Since the parameter $\{pV\}_{p'ew}$ is defined as the distribution of fractional volume among diameters less than any given value, it is necessary to subtract the y-axis percent values from 100 because the scale shown provides a greater than or equal to percentage volume for each cylindrical diameter.

If the same distribution is found for the remaining two d.b.h. classes, it is then only necessary to total the contributions of fractional volume to each distribution diameter from all three d.b.h. classes. In other words, for the 35 cm. average d.b.h. class, we found the distribution of its fractional volume among the 30, 20, 15, and 7 cm. distribution diameters from the curves. Of course for the 40 cm. distribution diameter, 100% of the fractional volume contributes since 100% of the volume of 35 cm. d.b.h. trees is less than 40 cm. cylindrical diameter. Therefore, the total fractional volume .000523 is present in the 40 cm. distribution diameter category. Each of the remaining two d.b.h. classes have partial or total fractional volume contributions among all five distribution diameter categories. The contributions for each distribution diameter category are totaled. The results are then fractional volume totals from the entire forest stand for each distribution diameter. From these data, the distribution function can be constructed. Table II gives these results. Under each d.b.h. class heading, the five fractional volume

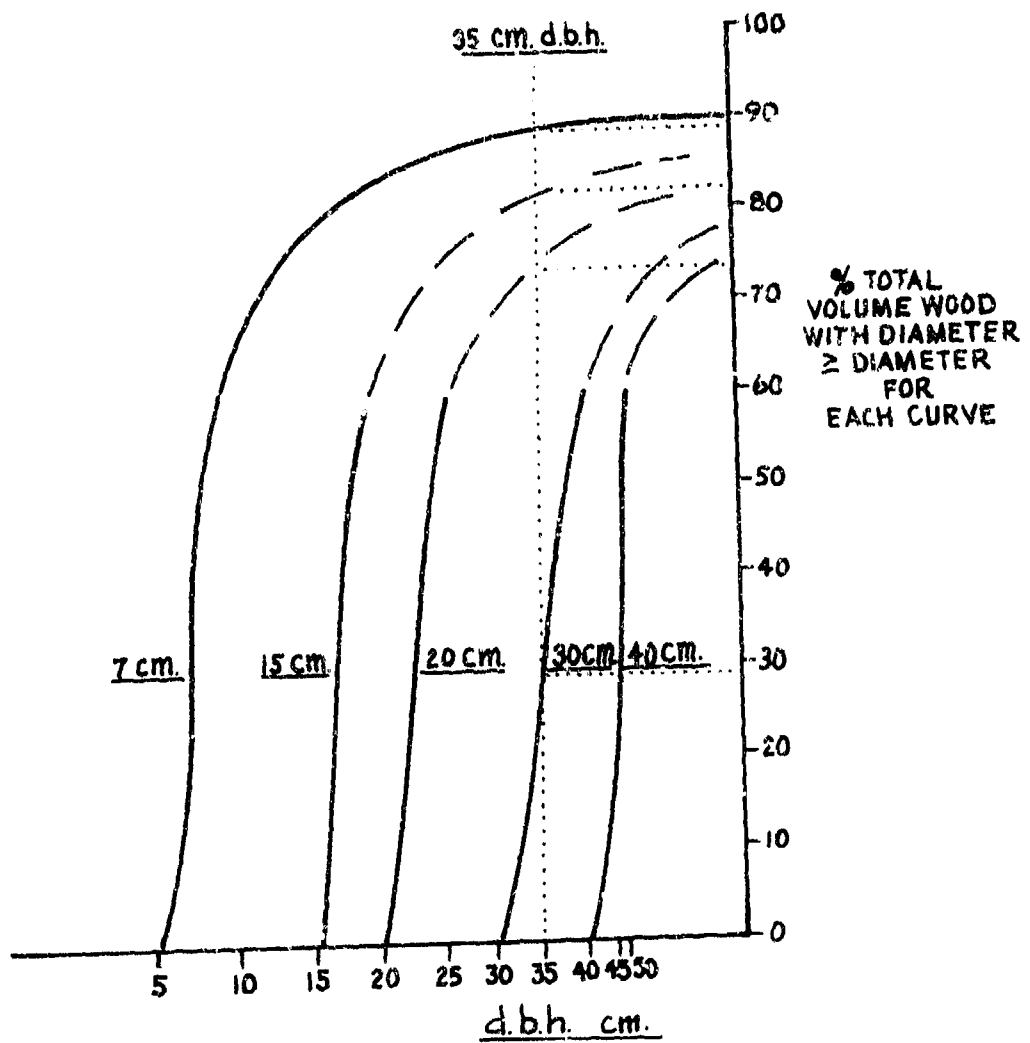


Figure 5. Volume distribution curves showing 35 cm. d.b.h. size example.

contributions are given for each of the five distribution diameters. In the right-hand column, the totals from each d.b.h. class for each of the five distribution diameters is shown.

TABLE II

d.b.h. class	1.3 - 13 cm.	13 - 28 cm.	> 28 cm.	
Average d.b.h.	7. cm.	20 cm.	35 cm.	
Total fractional volume	.000436	.000418	.000523	
<u>Distribution diameters</u>				<u>TOTALS</u>
7 cm.	.000379	.000067	.000058	.000504
15 cm.	.000436	.000159	.000094	.000689
20 cm.	.000436	.000418	.000141	.000995
30 cm.	.000436	.000418	.000371	.001225
40 cm.	.000436	.000418	.000523	.001377

Fractional volume totals for the five distribution diameters can now be used to construct a distribution function. A continuous curve can then be fitted to these data points and is shown in Figure 6. The fractional volume is now identified as $\{pV\}_{P_{ew}}$, the parameter required by the REV propagation model and is defined as the fractional volume of all forest wood with cylindrical diameter less than the distribution diameter on the x-axis.

Volume of Pine Needles

Until now, broadleaves or needles have not been included in the volume estimates. A procedure for estimating the contribution from pine needles will now be developed. It will be found that the same forest stand table statistics can be used as was required in the wood volume models.

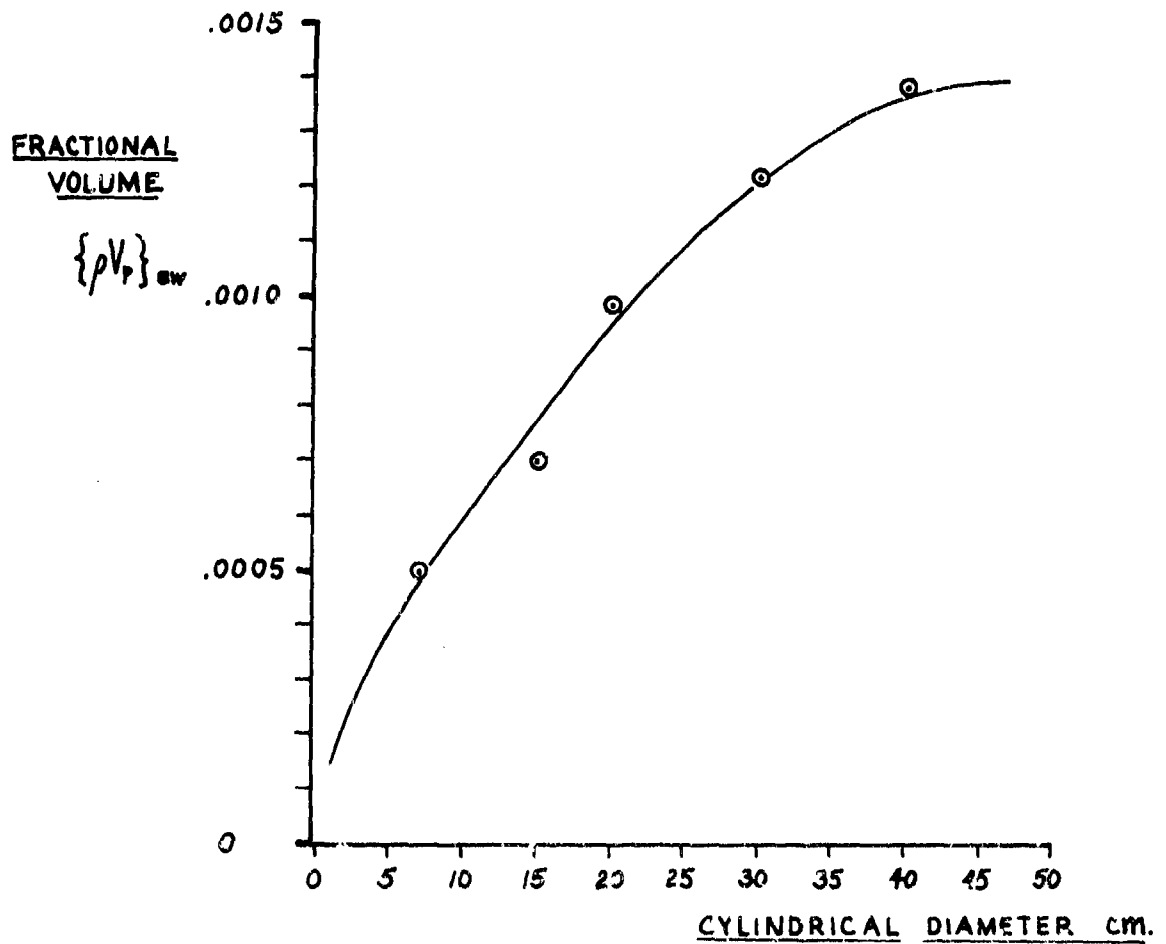


Figure 6. Example (see text) of a fractional volume distribution for a forest stand.

Pine needles might be thought of as comprising the smallest diameter structure of a needle-bearing conifer. Their contribution could then be included in the overall volume distribution. It is not clear, however, where broadleaves would fit in. Nevertheless, it may be necessary to estimate some quantitative parameter for broadleaves so they shall be briefly dealt with at the end.

In published literature, various descriptive quantities of leaves and needles have been modeled for trees and forests. This information is significantly important to timberland ecology. Such quantities have included weight [2], [3], surface area [2], and volume [4]. Kittredge [3] has amassed extensive data from different sites and species and his data shows that weight can be correlated with d.b.h. and will consistently fit a straight-line in log-log space with good correlation. The prediction equation thus assumes the form;

$$\log W = b \log D - a$$

where W = dry weight of leaves or needles and D = d.b.h. Large variance in W was reduced by removing the effect from differences in moisture content by taking the oven-dry weight of the foliage. It seems a rather common practice to mix units of measure in many of these studies. For D in inches and W in kilograms, the range of "a" was .46 → 1.58 while "b" varied from 1.15 → 3.15. Factors which influence the constants were site and species though no significant trend could be established.

Letting the total foliage weight for a stand be W_T and the weight of a d.b.h. class be W_C ;

$$W_T = \sum_{C=1}^N W_C$$

where N is the number of d.b.h. classes for all trees. Solving the logarithmic

regression for W and substituting;

$$W_T = \sum_{C=1}^N 10^{-a} N_C D_C^b = 10^{-a} N_T \langle D^b \rangle .$$

N_C is the number of trees in each d.b.h. class, D_C is the class average, and N_T the total number of trees in the stand. The angle brackets around D^b identify the average of the d.b.h. sizes to the b^{th} power. This last expression might prove useful if a forest can be classified by a known d.b.h. distribution. In that case, $\langle D^b \rangle$ could be determined and would remain constant for any stand with the same d.b.h. distribution.

Reference [2] provides some data by which needle surface area can be estimated from weight. Variation in this relationship is not expected to be great among species. If A_T represents total surface area, it can be expressed in terms of total weight;

$$A_T = \frac{A_n}{W_n} W_T$$

where A_n and W_n are the area and weight of individual needles given in [2].

At this point it is best to mention that surface area is not always defined as the entire physical area of a leaf or needle. Usually it is the stomated surface only which is defined. Stomated area refers to the surface area containing small transpiring openings. For many pine species, however, this is the entire surface of the needle. For broadleaves, it is the underside area only.

Total surface area of all needles is given by;

$$A_T = \frac{A_n}{W_n} 10^{-a} N_T \langle D^b \rangle .$$

It remains to utilize information provided by Kozlowski and Schumacher [4] in which area and volume of pine needles are correlated. Data provided were representative of particular species and it is not known how applicable the results are to other species. The technique for acquiring the data is described and seems neither difficult or very time consuming for small samples.

Before embarking on a project to acquire additional area-volume correlation data, it is well to recall the original goal of the model - to produce needle volume estimates from stand table statistics. An alternative to converting weight to area and area to volume is to simply convert weight to volume using dry-weight density information. Such information is not difficult to obtain directly and should remain fairly constant among given species at certain times of the year. Published values of needle density could not be located in literature, however it is likely that some examples do exist.

The information contained in [4] was actually concerned with the inverse problem of finding area from volume (since volume samples are easier to obtain in survey work). However, the correlation appears quite high in the examples given so there is not expected to be any problem inverting the results. The inverted straight-line expression thus becomes;

$$V_T = c + d(A_T - e)$$

where V_T is total volume, A_T total area, and c , d , and e are constants for species. Values for the constants are given for Loblolly pine which is a 3-needle per fascicle specie with entire surface area stomates (fascicles are clusters of needles joined at the base). Substituting the expression for A_T ;

$$V_T = c + d \left[\frac{A_n}{W_n} 10^{-a} N_T \langle D^b \rangle - e \right]$$

Values of the constants are given below in Table III.

TABLE III
(From Reference [3])

a	b	Trees	Location	Site Index (Standard height) (ft.)	Age (yrs.)
0.46	1.15	Ponderosa pine	California, 5,000 feet	20-39	24-69
0.73	1.67	Ponderosa pine	California, 4,000-5,000 feet	20-76	5-69
0.53	1.47	White pine	Vermont	90	24
1.22	2.09	White pine	Switzerland	72-87	21-70
1.15	2.32	White pine	Vermont	47	28
0.91	1.96	Douglas fir	Switzerland	80-110	20-45
0.94	2.56	Red pine	Vermont	43	28
1.58	2.87	Jack pine	Minnesota	45	37
1.16	3.15	Jack pine	Vermont	54	14

(All values of a and b are for D in inches.)

$$\begin{aligned}
 c &= .0621 \text{ cm.}^3 && \text{(Loblolly pine)} \\
 d &= .014108 \text{ cm.} && \text{(Loblolly pine)} \\
 e &= 6.078 \text{ cm.}^2 && \text{(Loblolly pine)} \quad [4]
 \end{aligned}$$

$$\frac{A_n}{W_n} = 1.24 \times 10^5 \text{ --- } 1.35 \times 10^5 \text{ cm.}^2/\text{kg.} \quad [2]$$

The result for V_T is in cubic centimeters if D is in inches and all of the constants used as given. As with the wood volume model, it is only necessary to divide V_T by the total volume enclosing forest stand space to obtain volume density.

Information for estimating broadleaf volume could not be found. References [2] and [3] contain one-sided area and weight data, but volume was not

considered. The same procedure for obtaining needle volume estimates could be applied to broadleaves, but area-volume correlation information is lacking. As with needles, a preferable alternative would be to estimate volume directly from weight using density. A rough estimate could be made, however, if one-sided area is found and multiplied by an estimated thickness. Leaf thickness probably does not vary considerably for most species and a range of .01 - .03 cm. should include many types. Constants which might be used to estimate one-sided broadleaf area are $a = 1.36$ [D in inches (live oak)] and $b = 2.66$ [3], and from [2]

$$\frac{A_n}{W_n} = 8.77 \times 10^4 - 1.53 \times 10^5 \frac{\text{cm.}^3}{\text{kg.}} \quad (\text{oak})$$

REFERENCES

- (1) Assman, E., The Principles of Forest Yield Study, Pergamon Press, New York, 1970.
- (2) Rothacher, J. S., Blow, F. E., Potts, S. M., "Estimating the Quantity of Tree Foliage in Oak Stands in the Tennessee Valley," J. of Forestry, 52, pp. 169-173, November, 1954.
- (3) Kittredge, J., "Estimation of the Amount of Foliage of Trees and Stands," J. of Forestry, 42, pp. 905-912, 1944.
- (4) Kozłowski, T. T., Schumacher, F. X., "Estimation of Stomated Foliar Surface of Pines," Plant Physiology, 18, pp. 122-127, 1943.

APPENDIX D

DIELECTRIC PROPERTIES OF TREES AT RADIO FREQUENCIES

Dielectric Properties of Wood

Although dielectric measurements for living wood are scarce, some data has been compiled over the years by wood technologists for cut and dried wood. It is expected that the greatest difference between lumber and living wood (relative to dielectric properties) is moisture content. To a lesser extent the suspension of sap and wet nutrients within the wood cells of living trees affect the electrolytic nature and resistance to electric conduction. Also, the majority of cut lumber represents inner regions of tree stems away from the thin outer living sheath with its abundance of mineral enriched water and sap. With these limitations in mind, however, a study of the dielectric properties of living wood can at least begin by considering the results for cut wood.

C. Skaar [1] reported one of the earliest studies of the dielectric properties of cut wood. Although his range of frequencies was limited to 2 - 15 MHz, (indeed the method of measurements employing a simple parallel plate capacitor structure could not have supported very high frequency accuracy - however, the method excelled in "textbook" clarity as a near exact replica of pure theory) the study revealed several of the most significant physical parameters affecting the electric properties of all wood.

It was found that moisture content decidedly exerts the most influence on dielectric properties (Figure 1). The dielectric constant increases substantially as the moisture content increases. Skaar also found that denser samples displayed larger dielectric constant values (Figure 2). Another interesting finding was that orientation of the electric field direction with respect to wood grain altered the polarizability of the sample, and therefore the dielectric

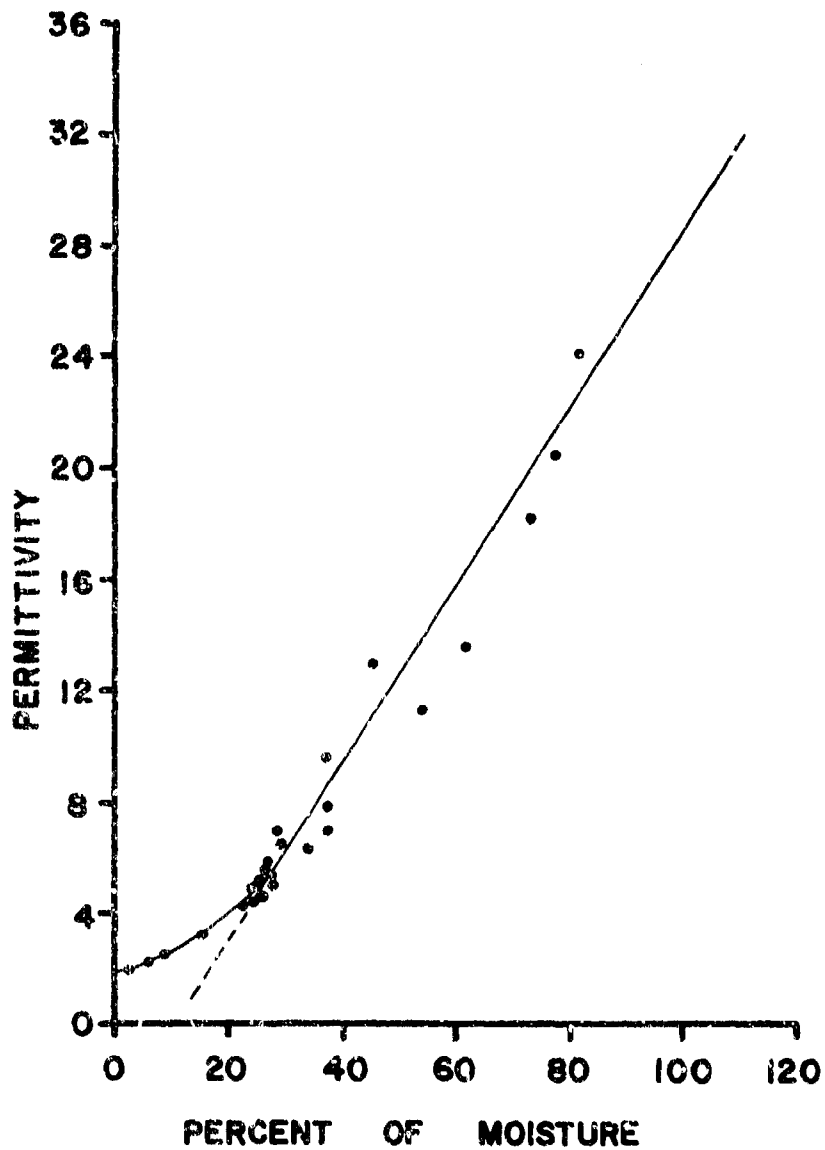


Figure 1. Effect of moisture content on the dielectric permittivity of wood showing linear trend past approximately 30% moisture (by dry weight). The frequency was 2 MHz; from [2].

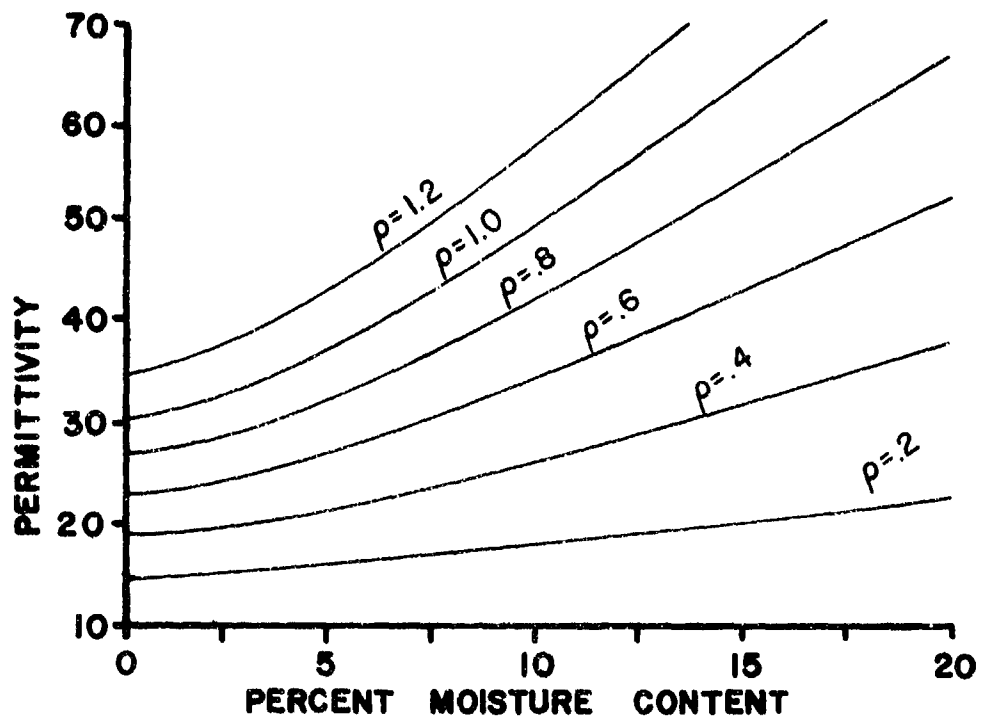


Figure 2. Effect of moisture content and density on the dielectric permittivity of wood. The frequency was 15 MHz; from [2].

constant. With field lines parallel to the grain, greater values were achieved. A suggested explanation of this phenomena was that the alignment of cellulose chain molecules and their bound water molecules in wood fibers is such that freedom to polarize is greatest in a longitudinal direction to the grain.

Wood technologists were interested in the electrical properties of wood as they relate to radio frequency heating and curing of glue joints and the design and construction of wood moisture meters. A later report by Yavorsky [2] gathered information from several sources. It was by then apparent that the dielectric "constant" was anything but constant and was in fact a widely varying quantity over the frequency spectrum. Moreover, the physical causes at the microscopic level were complicated and not well understood. They seemed to arise from several sources directly related to the macroscopic properties of the wood.

Physical Properties of Wood

Wood, whether comprising the bulk of living trees or cut and stacked in the lumber yard possesses certain physical properties important to determining its dielectric constant and other electrical terms. Wood moisture content μ is defined by wood technologists and forestry professionals in terms of the oven-dry weight of the wood [3];

$$\mu = \frac{W_u - W_o}{W_o}$$

where W_u = weight of green (moist) wood

W_o = weight after oven-drying

Using this definition as a percentage ($100 \times \mu$), it can be seen that values over 100% are possible, and indeed are often encountered in living wood.

The density, or specific gravity (weight per unit volume), is usually defined as $\rho = W_o/V_g$ where V_g is the volume of green wood. The reason V_g is the green wood volume is that wood swells with increasing moisture up to about 30% moisture and then its volume remains fairly constant.

To obtain some idea of reasonable moisture content values for living wood, 38 common hardwood species and 26 common softwoods were analyzed statistically from data found in the U.S.D.A. handbook of wood [4]. Normal distributions were produced and shown on the graph (Figure 3). As can be seen, hardwoods exhibit little variation (on the average) throughout the sapwood (outer layer) to heartwood (core) regions. Typical moisture content values are around 80%. Softwoods (conifers), however, display a marked transition in moisture from the outer sapwood layer - usually 1.5 to 5.1 cm. thick - to the inner, drier heartwood.

Density of specific gravity values vary considerably (from 0.25 to 1.25) for all species in the world [3]. However, the more common species, especially those found in temperate climates, fall within a more narrow spread of 0.3 - 0.7 [4]. These values are applicable to lumber or living wood since the manner in which density is defined precludes changes in moisture content from affecting density values once V_g is established. To find the actual density (including the water) for a moist sample of wood one uses the following;

$$\text{actual density} = \rho(1 + \mu) \quad .$$

Care must be taken when reviewing reports dealing with any property of wood affected by these parameters. The author's exact definition should be known as sometimes different definitions are used. This, for example, occurs with data reported by Broadhurst, [5] as compared to others; [1], [2], etc.

In a sampling of common living trees a certain correlation between ρ and μ occurs which influences dielectric properties. Referring to Figure 4

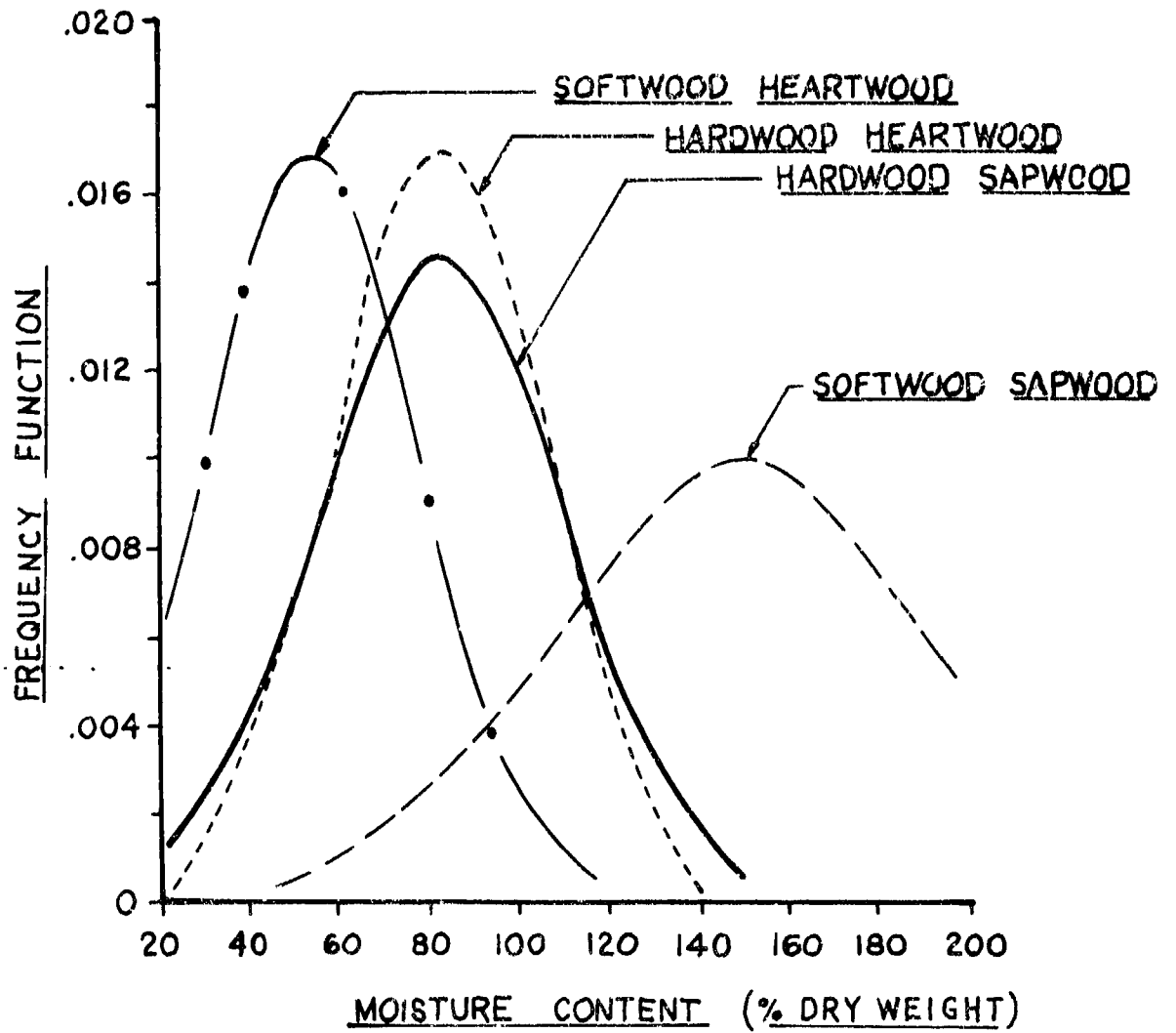


Figure 3. Normal distributions of typical dry weight moisture content for 38 hardwood and 26 softwood species.

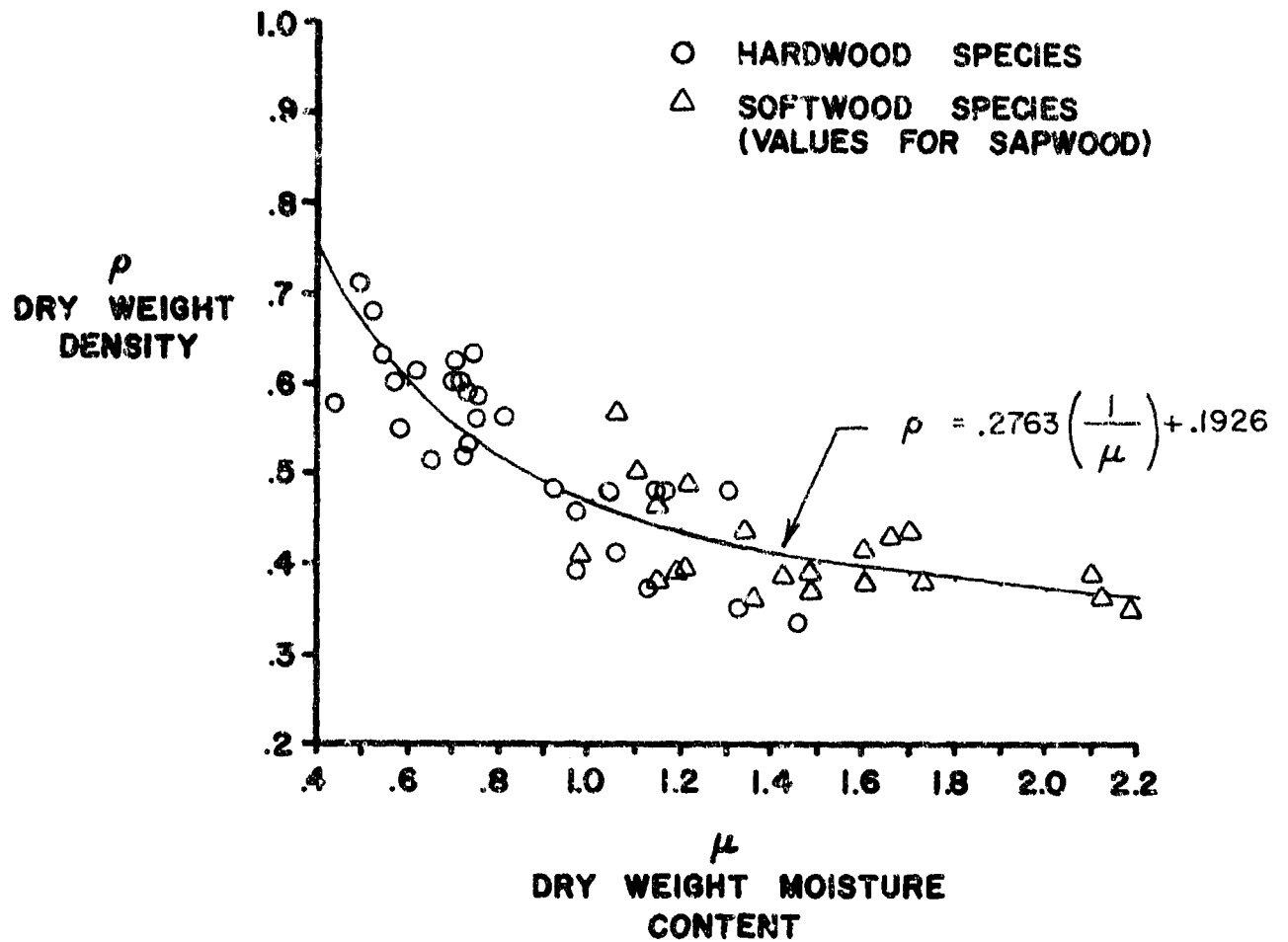


Figure 4. Inverse relationship between dry weight density and moisture content for a wide variety of common trees.

an inverse relation between ρ and μ is shown. Certainly it is reasonable to suppose the denser woods to be less capable of containing water. A given volume packed with more woody material usually has a smaller cross section of water conduit openings. This is important when regarding an "average" forest. Since ρ and μ both affect the dielectric constant similarly their inverse relation will tend to limit the range of dielectric constant values in different species. Trees with normally high moisture content such as softwoods typically have relatively low densities. The effect of the high moisture content will be partly offset by the lower density. Nevertheless a spread of dielectric constants can be expected since the effects of μ and ρ are not equal.

Dielectric Polarization and Conduction

There are four types of polarization in materials: interfacial, dipolar, atomic, and electronic. They are distinct in the physical processes they involve and in their range of influence over the frequency spectrum.

Interfacial polarization occurs in heterogeneous materials (such as wood) in which dissociated ions are present but partly constrained to interfacing boundaries within the material. This type of polarization usually produces the largest polarizing fields, but is limited to low frequencies. Beyond a certain cutoff, the ions simply do not have time to drift to the interfacial borders within a period.

Dipolar polarization can extend well into radio frequencies. This is a more common type in dielectrics and is explained in terms of molecular dipoles. This type has been extensively explored and described by Debye [6] and many others since.

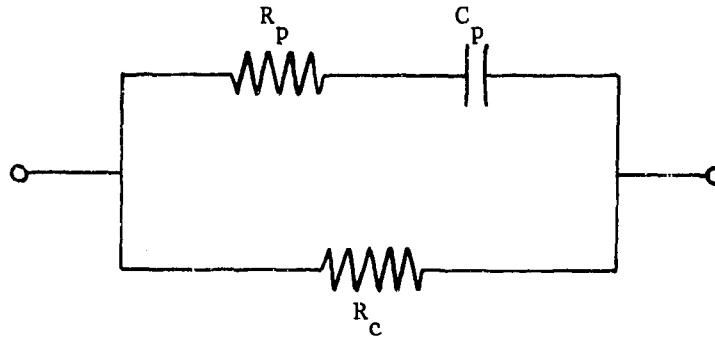
The last two types, atomic and electronic, extend well into optical frequencies. Their respective contributions to overall polarization, however, is usually small.

The complex dielectric constant quantitatively relates polarization and conduction effects to field quantities inside and outside a body. It is usually written as:

$$\epsilon = \epsilon' - j \epsilon''$$

where ϵ' is the ordinary electric field permittivity that occurs in Coulomb's Law as a property of the medium. The so-called loss factor ϵ'' actually arises when dealing with lossy media in harmonic fields. It accounts for a conductivity term in Ampere's Law and represents the in-phase conduction losses. Strictly speaking, it also is meant to include losses arising from polarization phenomena.

One way to represent polarization and conduction is to model the material as a circuit analog with lumped parameter elements. Polarization results from the displacement of charge concentrations within a material and any movement of charge constitutes a current. If for the moment this displacement is considered frictionless, it will exactly coincide with the rate at which the external electric field changes. This is equivalent to a 90° out-of-phase "displacement current" and is represented as a pure capacitor in the circuit. Since polarization is not frictionless or without loss, a certain resistance to the displacement current arises. This is representable as a pure resistance in series with the capacitor. The net result is a current partially in-and out-of-phase to the drive field. Direct current conduction by free charge carriers in the material results from the driven field and flows in-phase. It can be represented by a pure resistance parallel to the series resistor and capacitor. The equivalent circuit is shown below.



In the diagram, R_p is the polarization loss element, C_p the polarization displacement current element, and R_c the direct conduction path element. Obviously, their values are dependent on the physical properties of the material and frequency.

At the macroscopic level, a resultant current flows in the direction of the instantaneous electric field. This current is a phasor quantity resulting from the in and out of phase components whose magnitudes are directly proportional to ϵ'' and ϵ' respectively.

Permittivity of Wood

James [7] has devised a reasonable model expression for ϵ' of wood. The model includes the effects of each polarization type as a function of frequency. The constants of his formula are actually functions of all the physical parameters affecting dielectric properties. They are, however, generally unknown. The utility of the model is that given several data points at different frequencies, a continuum of ϵ' throughout all frequencies may be projected by fitting the model to the data points. The model is of the following form;

$$\epsilon' = a + b/(1 + f/f_0) + c/f^\lambda$$

where a represents electronic and atomic polarization effects, b implies dipolar effects in which f_0 is the center frequency in the range of influence, and c denotes interfacial effects in which λ differs slightly from 1.0.

Some overlapping is implied between polarization types in that each constant may include the effects of other types with similar relaxation times. (Relaxation time describes the time required to polarize or depolarize and thus determines the frequency range of influence.) The model seems to fit the extent of data taken by James for his report [7] quite well (Figure 5).

The model predicts one feature of ϵ' for wood which is born out by experimental evidence. At a certain frequency and beyond, ϵ' becomes more or less constant as the effect of c diminishes. This seems to occur around 20 MHz [5], [7]. It is expected that this nearly constant characteristic of ϵ' will continue to at least 5 - 8 GHz; but beyond that, ϵ' is expected to decrease. This feature proves very useful in predicting ϵ' values over a range of frequencies to 10 GHz. Since most radar applications will involve frequencies higher than 20 MHz, the ϵ' values need only be considered dependent on physical parameters.

It remains to determine actual values for ϵ' in living wood. Skaar [1] found (see Figure 1) that ϵ' increases very nearly as a linear function of μ (ρ held constant) for values of μ beyond 20 - 30%. This implies that given at least two data points in the linear region, intermediate values for ϵ' may be interpolated using a straight-line fit. If data were available at, for example, 25% and 130% moisture content, a line could be drawn and intermediate values for ϵ' estimated. Values of μ typical to living wood of the same density may then be used to predict ϵ' . If data at frequencies 20 MHz or higher are available, a spread of probable ϵ' values can be estimated for species of trees of the same density.

In order to produce a spread of ϵ' values for all trees, it is necessary to have representative data for high and low density species. It is useful to split the species into two groups: hardwoods and softwoods (very often,

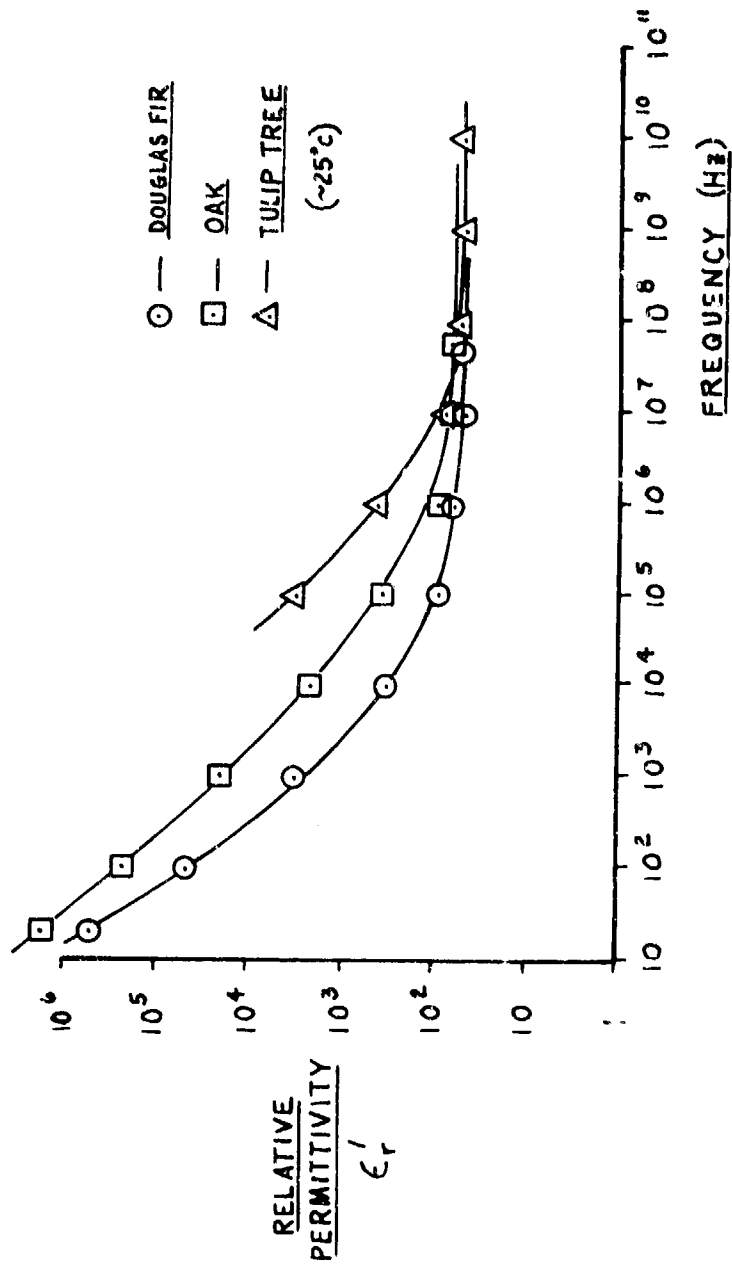


Figure 5. Permittivity data and model fit. The electric field is parallel to the wood grain. ○, □ - ref. [7]. △ - ref. [5].

a forest will be dominated by either type). In his report, James selected Douglas Fir and Oak. These represent medium-density softwoods and a moderately high density hardwood. Using his data which extends to 50 MHz, a spread of ϵ_r' for both hardwood and softwood sapwood was produced (Figures 6,7). These curves are based on a plus or minus one-sigma (standard deviation) spread about the mean value of μ for hardwood and softwood. While this may seem too narrow, it must be remembered that the inverse density relation to moisture content will tend to narrow the spread. In other words, though a few species should fall outside this range of μ values, the effect of their inverse density will cause ϵ' values to lie within a narrower spread. Nevertheless, these values only represent estimates which rest upon several assumptions. Ultimately, they should stand the test of additional experimental data comparisons.

Loss Factor of Wood

The variation of the loss factor with the physical properties of wood is more difficult to predict. A greater disparity seems to exist between cut wood [7] and a sample from a living tree branch [5]. This suggests that the suspended fluids in living wood may not entirely regain their conduction properties when moisture is simply added back to dry wood samples. It implies that the outer living sapwood layer in trees may exhibit values of ϵ'' that are not as accurately given by sampling cut wood from various regions of the stem.

The loss factor represents all the electromagnetic energy losses in a material. Sometimes, only one type of loss is considered in high frequency

* ϵ_r' is defined as the relative permittivity: $\epsilon_r = \frac{\epsilon}{\epsilon_0} = \frac{\epsilon'}{\epsilon_0} - j \frac{\epsilon''}{\epsilon_0} = \epsilon_r' - j \epsilon_r''$
 where ϵ_0 = permittivity of free space.

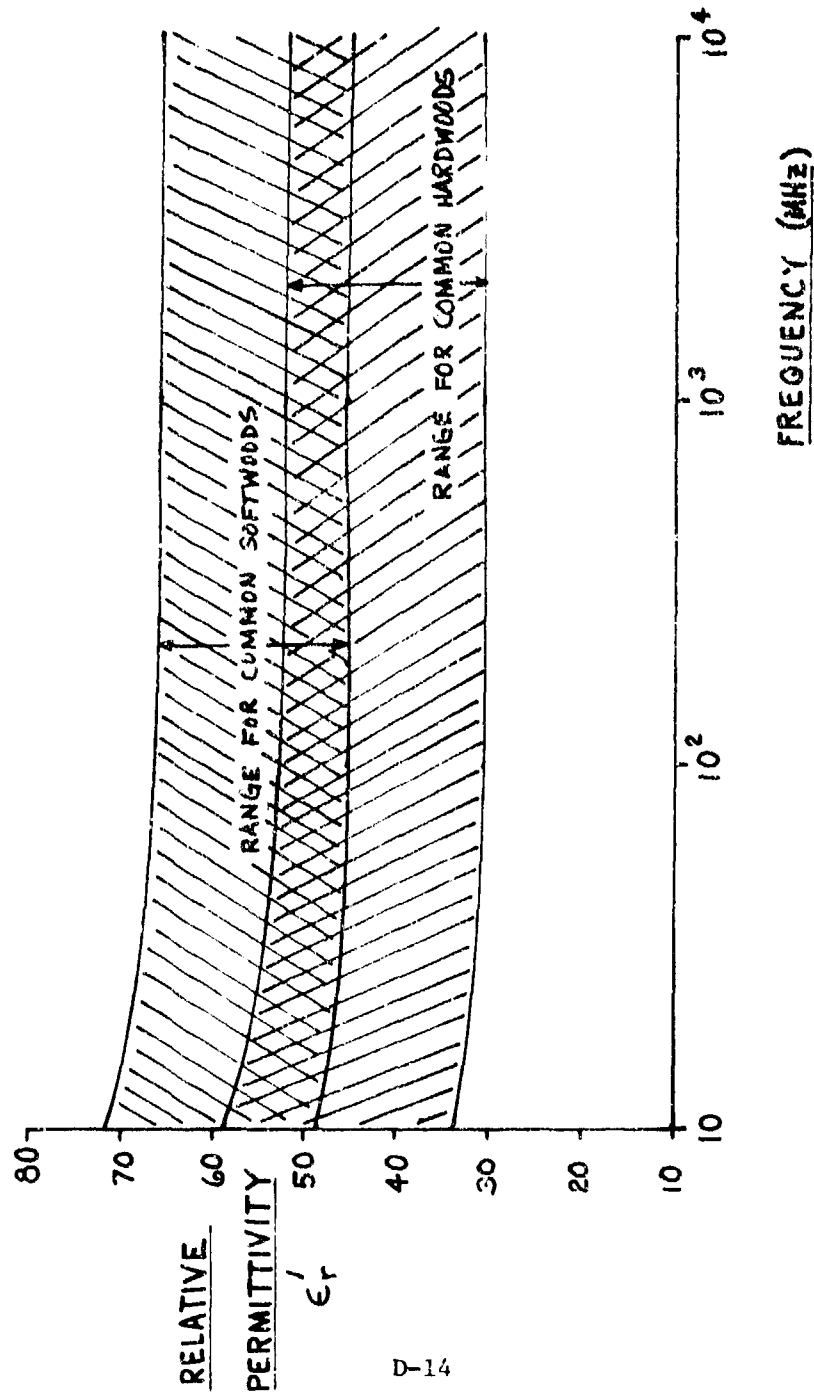


Figure 6. Range of ϵ_r for common species of live (green) trees at 25°C. The electric field is parallel to the wood grain.

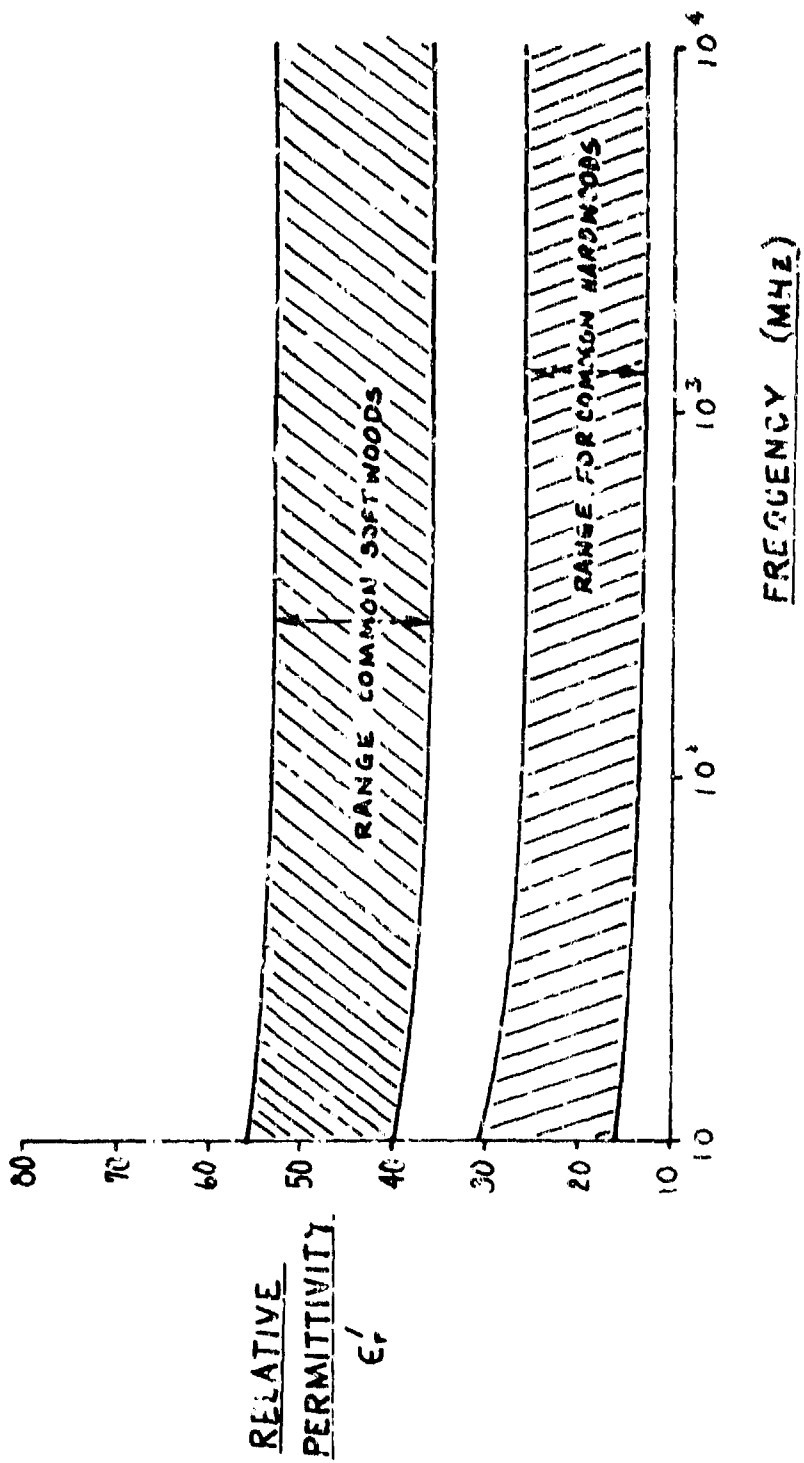
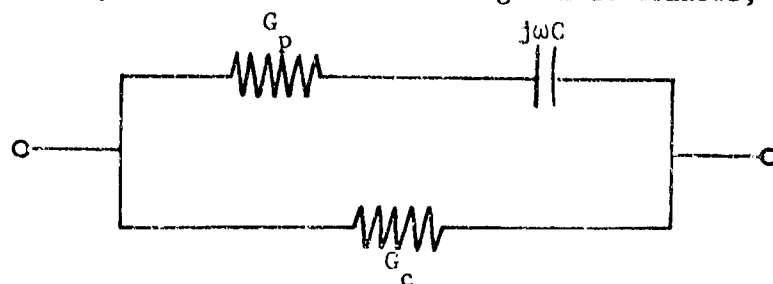


Figure 7. Range of ϵ_r for common species of live (green) trees at 25°C. The electric field is perpendicular to the wood grain.

models for wood or leaves; this is usually the loss from dipolar polarization. In leaves and wood, water is assumed to dominate so a type of mixing formula is generally used based on the estimated volume of water in a unit volume of material [8]. However, conduction and other losses are not represented by this model and data has shown that their effect extends into the radio frequencies [5], [7]. An attempt shall be made to derive a mathematical model for the loss factor in wood accounting for each dominant loss phenomena.

Representing the circuit analog introduced in above paragraphs by its element admittances, the total admittance is given as follows;



$$Y = G_c + \frac{j\omega C G_p}{G_p + j\omega C} = G_c + \frac{G_p (\omega C)^2}{G_p^2 + (\omega C)^2} + j \frac{G_p^2 \omega C}{G_p^2 + (\omega C)^2} \quad (1)$$

The admittance of a lossy dielectric may also be expressed in terms of its free-space capacitance C_o defined as follows;

$$Y = j\omega \epsilon_r C_o = (\epsilon_r'' + j \epsilon_r') \omega C_o \quad (2)$$

where C_o is the capacitance prior to inserting the dielectric material having a complex relative dielectric constant ϵ_r . Solving (2) for ϵ_r'' yields

$$\epsilon_r'' = \frac{1}{\omega C_o} \text{Real} [Y] \quad (3)$$

For the circuit analog with admittance given by (1),

$$\epsilon_r'' = \frac{1}{\omega C_o} \left[G_c + \frac{G_p (\omega C)^2}{G_p^2 + (\omega C)^2} \right] \quad (4)$$

or in terms of the original polarization resistance R_p :

$$\epsilon_r'' = \frac{G_c}{\omega C_o} + \frac{(C/C_o)\omega R_p C}{1 + (\omega R_p C)^2} \quad (5a)$$

or

$$\epsilon_r'' = \frac{G_c}{\omega C_o} + \frac{(C/C_o)\omega \tau_p}{1 + (\omega \tau_p)^2} \quad (5b)$$

where τ_p is the time constant $R_p C$.

Equation (5b) may be recognized as representing a conduction loss (the first term) and a Debye relaxation loss having a relaxation time constant τ_p (the second term). Furthermore, the factor C/C_o may be identified as ϵ_s' , the static or dc relative permittivity, by writing ϵ_r' from (2) as follows;

$$\epsilon_r' = \frac{1}{\omega C_o} \text{Imag}(Y) = \frac{C/C_o}{1 + (\omega R_p C)^2} \quad (6)$$

where $\epsilon_s' = \epsilon_r'$ for $\omega = 0$ or $\epsilon_s' = C/C_o$.

The conductance of a given volume of material can be expressed in terms of the conductivity of the material as $G_c = A\sigma/d$, where A is the cross sectional area, d is the thickness, and σ is the conductivity of the medium. Similarly, the capacitance of the same volume without the material may be written as $C_o = A\epsilon_o/d$ where ϵ_o is the free space permittivity. Thus, we can write $G_c/C_o = \sigma/\epsilon_o$ and substituting this relation in (6) yields

$$\epsilon_r'' = \frac{\sigma}{\omega \epsilon_o} + \frac{\epsilon_s' \omega \tau_p}{1 + (\omega \tau_p)^2} \quad (7)$$

The fact that the loss factor approaches infinity at frequencies approaching zero is a consequence of isolating this term from the admittance expression (2). Since the admittance must become a constant at dc, the $1/\omega$ term is required to cancel the ω term in (2). This may also be understood by considering

the loss tangent which is the angle between a purely reactive (or out of phase) current and the actual current. Since $\tan \delta = \epsilon''/\epsilon'$,

$$\delta(\omega \rightarrow 0) = \lim_{\omega \rightarrow 0} \tan^{-1}(\epsilon''/\epsilon') = 90^\circ$$

which is synonymous with having a finite, dc current entirely through the by-pass conductance G_c in the circuit analog. In practice, however, (7) must be limited to non-zero frequencies.

In order to apply (7) to natural wood, some modifications are in order. First it must be realized that the simple circuit model represents only a single relaxation time. From the limited available data, however, it is evident that a somewhat broad spread of relaxation time constants are found in wood. These correspond to the presence of several different molecular dipoles. Secondly, it is not possible to directly apply values taken for the parameters σ and ϵ_s' from wood to equation (7). The reasons are the conductivity term in (7) also must account for large interfacial polarization charge conduction in this model, and the actual static permittivity of wood is much larger than ϵ_s' in (7) since ϵ_s' is only due to one polarization type of molecule.

It may be possible to identify most or all Debye-type relaxation dipoles and represent each by additional relaxation loss terms in the model. Indications are, however, [5], [10], that in very moist wood (such as in living trees) free water dipoles predominant while much smaller contributions come from bound water and cellulose constituents at lower frequencies. Consequently, the time constant τ_p in (7) shall be assigned values for free water while a slight frequency dependent factor kf^m will be introduced to account for the spread of slower dipole contributions at lower frequencies. Actually, this latter idea was used by James [7] in his model for loss tangent although he refers to a slight frequency dependence of the resistance of wood.

Introducing the factor kf^m into the conduction loss term on the right hand side of (7) yields

$$\epsilon_r'' = \frac{\sigma kf^m}{\omega \epsilon_0} + \frac{\epsilon_s' \omega \tau_p}{1 + (\omega \tau_p)^2}$$

where $0 \leq m \ll 1$. With $A = \sigma k / 2\pi \epsilon_0$, the above equation becomes

$$\epsilon_r'' = \frac{A}{f^{1-m}} + \frac{\epsilon_s' \omega \tau_p}{1 + (\omega \tau_p)^2}$$

or more simply

$$\epsilon_r'' = \frac{A}{f^{1-m}} + \frac{B(f/f_c)}{1 + (f/f_c)^2}$$

where f_c is the critical or relaxation frequency of water. Using a non-linear least-squares fitting routine to the data from [5], A was found to depend upon the dry-weight moisture content μ and grain orientation as follows;

$$A_c = (1.29 + 0.15\mu) \times 10^9$$

for a combinations of orientations of the grain relative to the electric field⁹ and

$$A_p = (3.49 + 0.15\mu) \times 10^8$$

for the grain perpendicular to the electric field. Actually, the 0.15 coefficient was simply assumed for A_p since only one sample was given for that

⁹Use of the term "combination of orientations" is due to the manner in which samples in [5] were prepared. Wood was sliced from the outer branch layer and this results in a combination of parallel and perpendicular grain orientation.

orientation case. The fitting routine also yielded 0.041 for m and B was found to be represented as follows;

$$B = 43.4 + 8.1 \mu$$

for both orientation cases. Finally, (7) becomes

$$\epsilon_r'' = \frac{A}{f \cdot 0.959} + \frac{B(f/f_c)}{1 + (f/f_c)^2} \quad (8)$$

where

$$A = \begin{cases} A_c & \text{for a combination of orientations} \\ A_p & \text{for perpendicular orientation} \end{cases}$$

and

$$f_c \approx \begin{cases} 20 \text{ GHz for summer} \\ 10 \text{ GHz for winter} \end{cases}$$

This model, as it stands, fits data reported in [5] very well (Figure 8). Its widespread applicability is still uncertain. Moisture content values for several species are given in [4] and may be tested with the model to verify the constants. This certainly is an area in need of more relevant research and experiment before confident loss factor values for living trees can be used in microwave forest penetration studies.

One suspected improvement in (8) is in the form of the second term in the expression. Dielectric mixtures usually do not exhibit the ideal characteristics this term describes. Generally, a broader spread of time constants will flatten the curve somewhat and even shift the peak predicted by f_c depending on the proportions of the mixture. In this case, f_c may be somewhat dependent on μ as well as temperature even at the higher moisture contents found in living trees. A modification to the Debye dielectric constant expression described by Von Hippel [9] might provide the desired spreading and a μ -dependent f_c may also improve its accuracy. However, these modifications

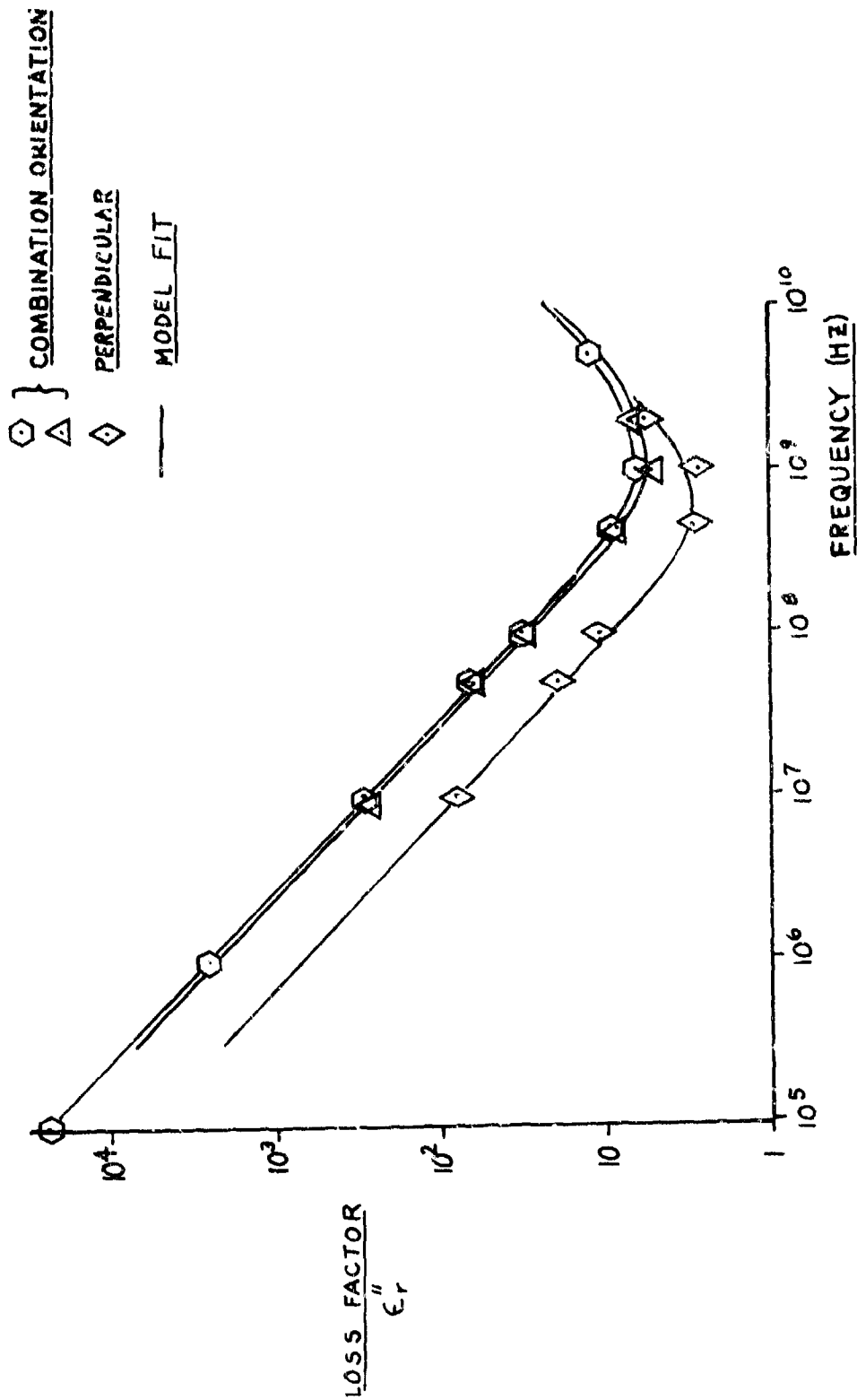


Figure 8. Loss factor data and model fits based on μ -values and field-grain orientation. Data from ref. [5].

require a range of data at Gigahertz frequencies which are not available at present.

A value of 10 GHz was suggested for f_c in winter based upon the drop in the critical relaxation frequency of free water for temperatures near 0°C. In addition, some change in the constants for A and B may be anticipated but no quantitative estimates can at present be given. Ordinarily, values for μ can also be expected to drop in winter months for most species [11].

When air temperatures remain below 0°C, nearly all but 25 - 30% of the dry-weight moisture content freezes in trees [1]. The dielectric constant, both permittivity and loss factor, can be expected to drop significantly. Since both conduction and relaxation will be affected, the overall loss factor should change and in particular, the steep rise in the loss factor curve beginning around 10^9 Hz may disappear altogether.

As mentioned in the footnote, it was not possible to obtain purely parallel orientation loss factor data from [5]. This was a consequence of both the measurement technique and the sample cutting preparation. In fact, it is actually impossible to orient wood so that its grain is purely parallel to the electric field lines with any method which employs a coaxial transmission line sample holder, as was the case in [5]. The suitability of these data and the associated model depends entirely upon the application of the loss factor estimates. It is believed that the so-called "combination" case would most nearly be suitable for propagation and attenuation analysis in forests.

Improved Estimate For B in the Loss Factor

As noted in Figure 8, there is a distinct paucity of data above 1 GHz with which (8) can be compared. Thus, we did not have a great deal of confidence in the expression for B obtained from fitting (8) to the data from [5],

i.e. $B = 43.4 + 8.1\mu$. To overcome this problem and, in a sense, to check the Rayleigh-Effective Volume (REV) propagation model, we used the data from [13] and the REV model to improve our estimates of B .

The data given in [13] is easily converted into attenuation per unit length γ as a function of the dry weight of the intervening foliage \tilde{W}_0 , i.e. $\gamma = \beta \tilde{W}_0$ where β is the proportionality constant given in [13]. Assuming that the transmission path was sufficiently long that the received power was determined only by the absorption due to the intervening foliage, the REV model predicts the following attenuation per meter (see (59) of Section 3.3);

$$\gamma = \frac{8.686}{6} k_0 \epsilon_r'' v_{ew} \quad (\text{dB/m}) \quad (9)$$

where $k_0 = 2\pi/\lambda_0$, λ_0 is the free space wavelength, and v_{ew} is the effective fractional volume of the intervening foliage. The effective fractional volume is determined by those foliage components having a diameter to wavelength ratio of less than one half. The effective fractional volume is related to the dry weight of this volume of foliage, \tilde{W}_0 , by the specific gravity of the foliage ρ , i.e. $v_{ew} = \tilde{W}_0/\rho$. It should be noted that \tilde{W}_0 is the dried weight of only those foliage components having a diameter of less than roughly one half a free space wavelength (≈ 0.5 inch in this case). Thus, (9) can be written as follows;

$$\gamma = \beta \tilde{W}_0 = 1.45 k_0 \left(\frac{\tilde{W}_0}{\rho} \right) \epsilon_r'' \quad (10)$$

or solving (10) for ϵ_r'' yields;

$$\epsilon_r'' = \frac{\rho \beta}{1.45 k_0} \quad (11)$$

The experiments reported in [13] were conducted on Virginia Pine which has a specific gravity of $\rho = 0.448$ [3]. Since β is known from the correlations reported in [13], it is possible to estimate ϵ_r'' . Furthermore, we can determine the moisture content μ of the foliage measured in [13]. A summary of these results are given in Table I.

TABLE I

	Winter 1973	Spring 1973	Summer 1973	Summer 1974	Winter 1976
μ	NA	NA	1.57	1.56	1.0
ρ	.448	.448	.448	.448	.448
ϵ_r''	12.11	14.57	15.99	17.53	7.01
f(GHz)	10	10	10	10	12.25

The loss factor values computed using (11) and shown in Table I appear to be very reasonable in their correlation with moisture content. Although the moisture content data for the Winter and Spring of 1973 were not available, the season itself suggests that the lower ϵ_r'' values are the result of a drop in μ which is typical of some pines for that time of year [11].

We will now use the results of Table I, i.e. ϵ_r'' as a function of the product $\mu\rho$, to refine our estimates of the factor B in equation (8). To do this, we note that the general expression for ϵ_r can be modified to account for a distribution of relaxation time constants centered about τ_p by introducing the exponent α [9] as follows^⑥;

^⑥We only consider the Debye or second term in (8) since the first term is negligible in the neighborhood of f_c .

$$\epsilon_r = \epsilon_r' - j\epsilon_r'' = \epsilon_\infty' + \frac{\epsilon_s' - \epsilon_\infty'}{1 + (j\omega\tau_p)^{1-\alpha}} \quad (12)$$

where ϵ_∞' is the optical limit permittivity, ϵ_s' is the static or dc permittivity and $0 \leq \alpha \leq 1$. Solving (12) for ϵ_r'' yields

$$\epsilon_r'' = \frac{(\epsilon_s' - \epsilon_\infty')(\omega\tau_p)^{1-\alpha} \sin\left[\frac{\pi}{2}(1-\alpha)\right]}{1 + 2(\omega\tau_p)^{1-\alpha} \cos\left[\frac{\pi}{2}(1-\alpha)\right] + (\omega\tau_p)^{2(1-\alpha)}} \quad (13)$$

and substituting $B = \epsilon_s' - \epsilon_\infty'$ and $f/f_c = \omega\tau_p$ gives

$$\epsilon_r'' = \frac{B(f/f_c)^{1-\alpha} \sin\left[\frac{\pi}{2}(1-\alpha)\right]}{1 + 2(f/f_c)^{1-\alpha} \cos\left[\frac{\pi}{2}(1-\alpha)\right] + (f/f_c)^{2(1-\alpha)}} \quad (14)$$

which is comparable to the second term in (8). Using $f_c \approx 20$ GHz for summer and $f_c \approx 10$ GHz for winter along with the results in Table I provides three "data" points to estimate B and α as a function of $\mu\rho$. In addition, we also know ϵ_r'' for 100% dry wood ($\mu\rho=0$) and water ($\mu\rho=1$) from data. Thus, using a non-linear least squares fitting algorithm, we determine the best-fit values of B and α (as a function of $\mu\rho$) which agree with (14) and the known values of ϵ_r'' . The results of this computation for B are shown in Figure 9; we consistently obtained $\alpha=0.1$ in the fitting procedure. The continuous curve in Figure 9 is a polynomial approximation to the five points and it has the following form;

$$B = 0.07 + 29.5(\mu\rho) - 4.8(\mu\rho)^2 + 63(\mu\rho)^3 \quad (15)$$

Substituting (15) and $\alpha=0.1$ in (14) and then replacing the second term in (8) by this result yields the following expression for the loss factor of wood;

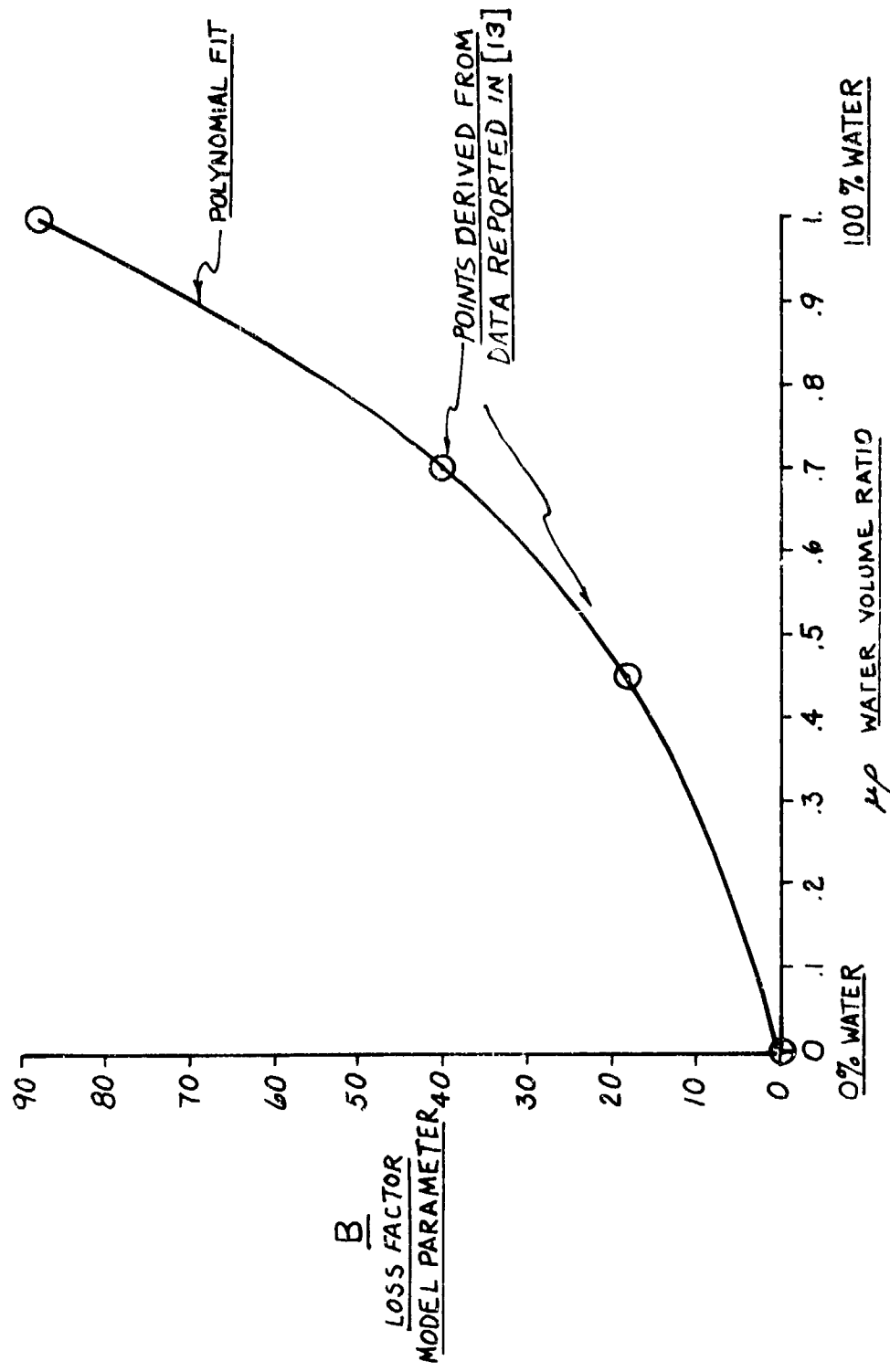


Figure 9. Modified loss factor model parameter B as a function of water volume percentage in wood and with $\alpha = 0.1$.

$$\epsilon_r'' = \frac{A}{f^{0.96}} + \frac{[0.07 + 29.5(\mu\rho) - 4.8(\mu\rho)^2 + 63(\mu\rho)^3] (f/f_c)^{0.9}}{1 + 0.3129(f/f_c)^{0.9} + (f/f_c)^{1.8}} \quad (16)$$

where

$$A \approx \begin{array}{ll} 1.5 \times 10^9 & \text{for a combination of orientations} \\ 3.7 \times 10^8 & \text{for perpendicular orientation} \end{array}$$

and $f_c = 20$ GHz for summer and 10 GHz for winter. Equation (16) is plotted in Figure 10 along with data from [5] and [13]. For the frequency range of interest to this study, the (f/f_c) dependent part of the second term of (16) is reasonably well approximated by $(f/f_c)/[1 + (f/f_c)^2]$ as noted in equation (57) of Section 3.2.4. Of particular note in Figure 10 is the fact that the two high frequency data points from [5] are in close agreement with (16) even though they were not used in obtaining (15) or (16). The fact that we can use the Rayleigh-Effective Volume (REV) propagation model to convert attenuation data into estimates of ϵ_r'' at 10 GHz must necessarily indicate that it is a reasonable description of the attenuation process.

Dielectric Constant For Leaves

The mathematical models used in the preceding sections were developed according to the observed influence of the physical properties of wood. Assumptions regarding the structure and constituents of wood were not so restrictive as to preclude applying these models to leaves. In fact, it is found that permittivity and loss factor data for leaf samples from living plants and trees closely resemble similar data for wood, both in magnitude and overall trend. This suggests that those properties of wood which are dominant in polarization and conduction are to be found in leaves. This is reasonable since the internal composition of leaves and their cells is not drastically different from wood.

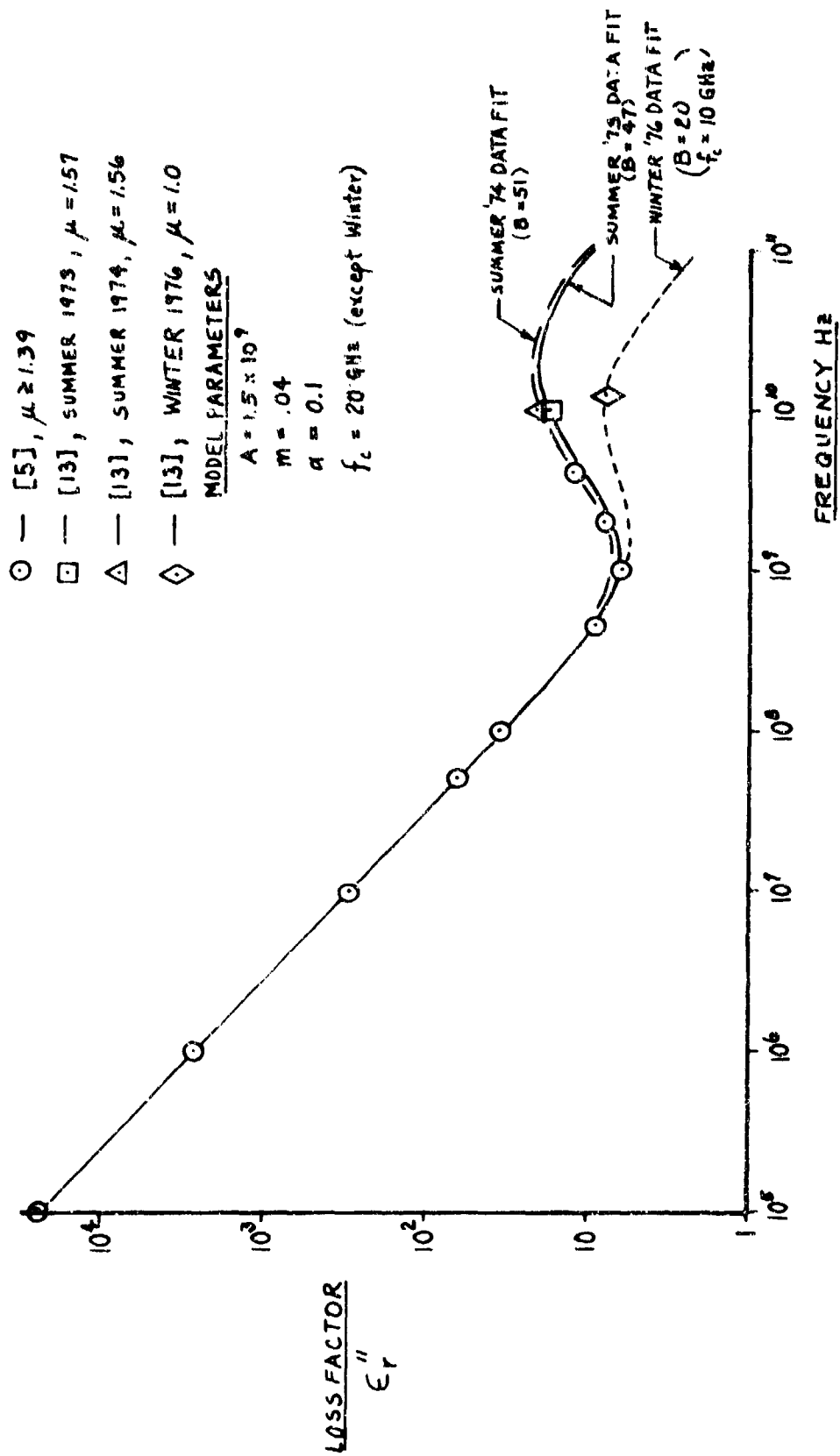


Figure 10. Modified loss factor model fits to derived data points from [13] plus data from [5].

The only identified source of experimental dielectric constant data for leaves taken at radio frequencies was Broadhurst [5]. In that report, data are presented for Tulip tree leaves along with data from a variety of plant leaves. The tulip tree data falls approximately in the middle of all other leaf data reported. In an effort to provide an estimated spread of values, data for both the highest and lowest cases were fit with the mathematical models to provide a continuum of curves and smooth out the experimental error. These results are presented in Figures 11 and 12. While the mean squared error in the fit is somewhat larger than encountered with wood, it appears that the data itself deviates randomly from a continuous curve in greater amounts than the wood data suggesting larger experimental errors.

Conclusion

The information presented here are estimates and should undergo further substantiation and possible refinement. At present, the scarcity of experimental data preclude further extensions of the models. The permittivity values shown are, however, expected to be reasonably accurate and representative of a variety of common trees for both orientation cases. Loss factor values can at present only be viewed as possibly "typical", but not necessarily covering the extent of variation found in common trees. The same is true for the leaf data fits. Since effective loss factor values largely influence propagation and attenuation through forests, more experimental effort should be undertaken in order to better understand and predict this quantity. In particular, the ability to accurately predict the loss factor curve minima might lead to optimum frequency selection for maximum penetration by radar systems. This is where an accurate model expression can help since it is not feasible to experimentally determine the dielectric constant over all frequencies for each variety of tree with different physical properties.

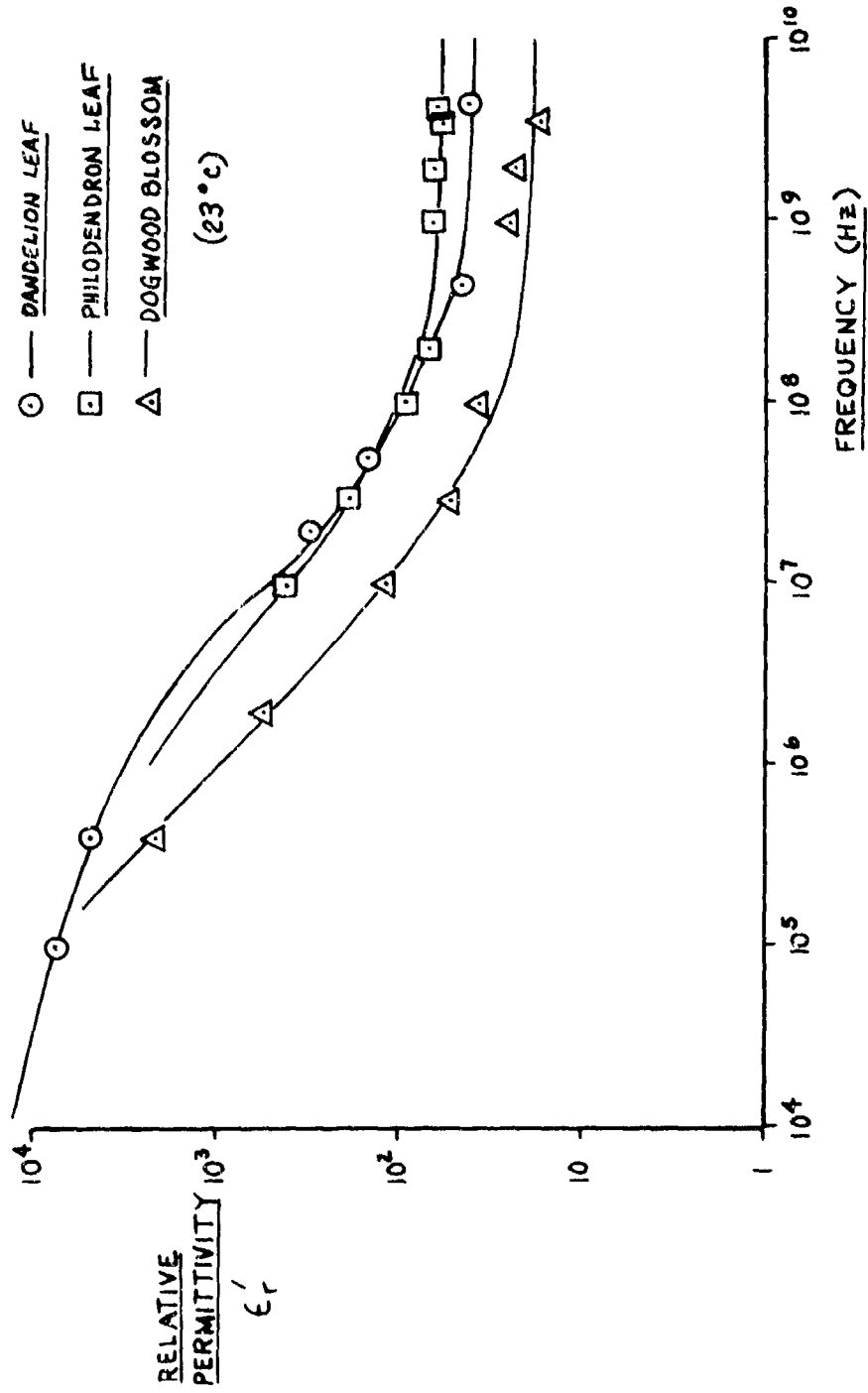


Figure 11. Selected permittivity data for leaves connected by model fit showing extremes in range. Other samples fall within boundaries. Date from ref. [5].

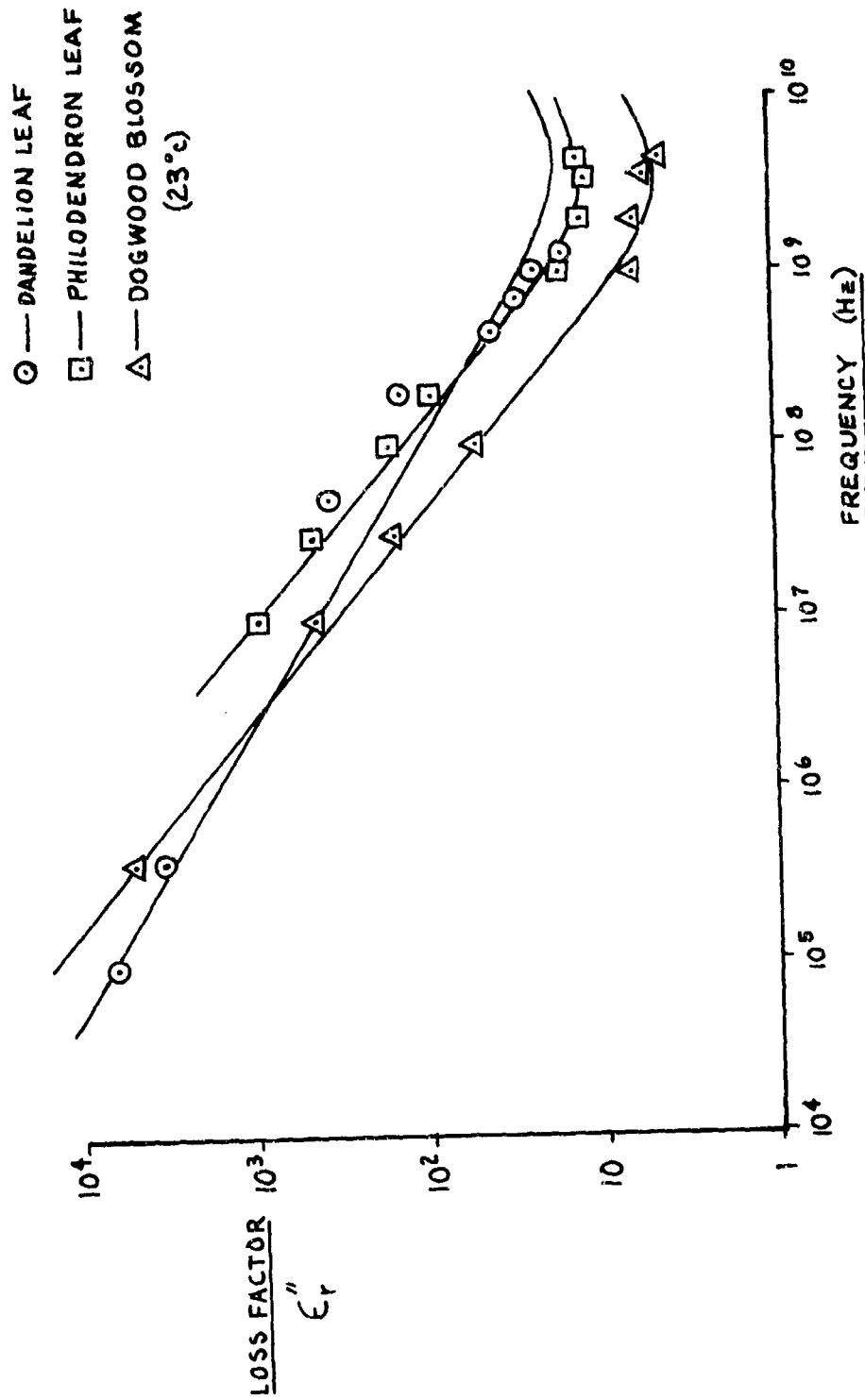


Figure 12. Selected loss factor data for leaves showing extremes in range. Other samples fall within boundaries. Data from ref. [5].

REFERENCES

1. Skaar, C., "The Dielectric Properties of Wood at Several Radio Frequencies," Tech. Bulletin 69, N. Y. State College of Forestry, Syracuse, N.Y., 1949.
2. Yavorsky, J. M., "The Electrical Properties of Wood," N. Y. State College of Forestry, Syracuse, N.Y., 1951.
3. Kollmann, Côté, Principles of Wood Science and Technology. Springer, Verlag, 1968.
4. Wood Handbook. (U.S.D.A. Agr. Handbook No. 72, rev.), U. S. Dept. Agriculture Forest Products Laboratory, 1974.
5. Broadhurst, M. G., "Complex Dielectric Constant and Dissipation Factor of Foliage," National Bureau of Standards Report 9592, 1970.
6. Debye, P., Polar Molecules, Dover Publications, New York, 1945.
7. James, W. L., "Dielectric Properties of Wood and Hardboard: Variation with Temperature, Frequency, Moisture Content, and Grain Orientation," USDA Forest Service Research Paper FPL 245, U. S. Dept. of Agr. Forest Service, Forest Products Lab., Madison, WI., 1975.
8. Fung, A. K. and F. T. Ulaby, "A Scattering Model for Leafy Vegetation," IEEE Transactions on Geoscience Electronics, Vol. GE-16, No. 4, October, 1978.
9. Von Hippel, A., Dielectrics and Waves, John Wiley & Sons, Inc., New York, New York, 1954.
10. Trapp, W., and Pungs, L, "Einfluss von Temperatur and Feuchte auf das dielektrische Verhalten von Naturholz im grossen Frequenzbereich (Influence of Temperature and Moisture on the Dielectric Behavior of Natural Wood in the High Frequency Range)," Holzforschung, Vol. 10, pp. 144-150, 1956.

REFERENCES (Cont'd.)

11. Gibbs, R. D., "Patterns in the Seasonal Water Content in Trees," Part I, 3 of The Physiology of Forest Trees, (K. V. Thimann, ed.), Ronald Press, New York, 1958.
12. Scholander, P. F., "The Rise of Sap in Lianas," Part I, 1 of The Physiology of Forest Trees, Ronald Press, New York, 1958.
13. Stutzman, W. L, F. W. Colliver, and H. S. Crawford, "Microwave Transmission Measurements for Estimation of the Weight of Standing Pine Trees," IEEE Transactions on Antennas and Propagation, Vol. AP-27, pp. 22-26, January, 1979.

APPENDIX E

DIELECTRIC CONSTANT MEASUREMENT METHODS WITH APPLICATION TO GREEN WOOD AT GHz FREQUENCIES

Low Frequency Range, (0 - 10 Hz) [1]

At very low frequencies, the usual method of measuring the dielectric constant is to insert a material sample between a parallel plate holder. After a charge-up from a fixed voltage or dc source, the current vs. time during discharge is recorded. The leakage (steady-state) current is also determined and subtracted from the total current giving the polarization current. The polarization current-time curve is then normalized and compared to known curves representing low frequency polarization parameters. These parameters represent a theoretical, complex dielectric constant distribution due to low frequency polarization mechanisms. Low frequency dielectric constant values for the material may then be obtained from this distribution.

Medium Frequency Range, (10 - 10⁶ Hz) [1], [2]

For audio to radio frequencies, capacitance bridges such as the Schering Bridge are almost exclusively used. The capacitance of a sample held between parallel plates is read and compared to the geometric (or free space) capacitance of the holder when empty. The ratio gives the relative permittivity directly. The dissipation factor, or loss tangent, can be read from settings on commercial bridges.

High Frequency Range, (10⁵ - 10⁸ Hz) [1], [2], [3]

At higher radio frequencies, resonant circuits are used. These comprise a standard inductor and capacitor connected to a micrometer electrode sample holder which accurately measures the plate separation. The circuit is tuned to resonance, first with the sample inserted then when left out of the holder,

by adjusting the micrometer setting. The capacitance of the sample can then be determined by an expression which relates it to the calibration and geometric capacitances [1]. The resistive or loss component is found by various methods. Basically, they involve either retuning to resonance by adding known resistance when the sample is disconnected, or measuring the width at the half-power points of the voltage resonance curve (the more common method).

Efforts to extend the frequency range of resonant circuit measurement methods resulted in development of the re-entrant cavity sample holder [1]. This holder in effect distributes inductance and part of the capacitance in the cavity. Further frequency increases above around 800 MHz, however, encounter other problems related to the smaller wavelength. Non-uniform fields begin to form in the radial direction from the sample holder electrode axis and this complicates interpretation of the capacitance values. At higher frequencies, radiation and coupling losses become a significant part of total loss making dielectric loss difficult to distinguish.

Microwave Frequencies [1], [4], [5], [6]

Lumped circuit parameter techniques are no longer suitable at centimeter and millimeter wavelengths. Instead, a variety of transmission line methods have been developed and are usually tailored to accommodate certain aspects of the material. In these methods, dielectric values are indirectly obtained by observing the effect of a material sample placed in the transmission path. Ordinarily, non-magnetic ($\mu \approx \mu_0$) materials are assumed. Consequently, any scheme which produces an accurate measure of either the propagation constant or the wave impedance of the material may be used. From either of these wave parameters, the complex dielectric constant can be determined.

Methods which measure the material impedance require placing a sample within a coax transmission line or waveguide. The sample usually fills the

entire cross section, introducing a discontinuity in the line. The guide is then terminated and a slot detector positioned in front of the sample as in Figure 1. Given a known termination impedance Z_L , the waveguide impedance Z_0 , and the standing wave ratio determined by the slot detector, the dielectric constant of the sample can be found. This procedure, however, involves a non-analytic expression which must be graphically or numerically solved and is sometimes multi-valued. The ambiguity must then be resolved by either a repeat experiment with a different sample length or by an a priori estimate of the results. This method has been described as best suited for low to medium loss materials [1].

When high-loss materials such as water, moist soil, etc. are to be measured, alternative methods are usually employed. These methods essentially measure the attenuation and phase constant of the material [1], [4], [5]. This can be done by making incremental changes in the sample length and noting the jump in attenuation and the phase shift due to the change. This scheme would involve a configuration similar to that shown in Figure 2. Liquids are particularly well suited for this method since the sample length is easy to change - in some cases without disassembling the apparatus. This method has been called the "long-sample" or "infinite-sample method" since the sample must be long enough to damp out backward reflected waves. If the damping is not sufficient, a standing wave in the sample will occur that is dependent on the length, thus affecting the measurements. The reflection from the front is held constant and does not affect the relative incremental measurements.

One modification of the long-sample method [7] dispenses with the requirement that the sample length be changed. Instead, reflection measurements from a single length are compared to measurements from a shorted waveguide at the boundary. Nomograms to aid in the associated calculations are available [7]

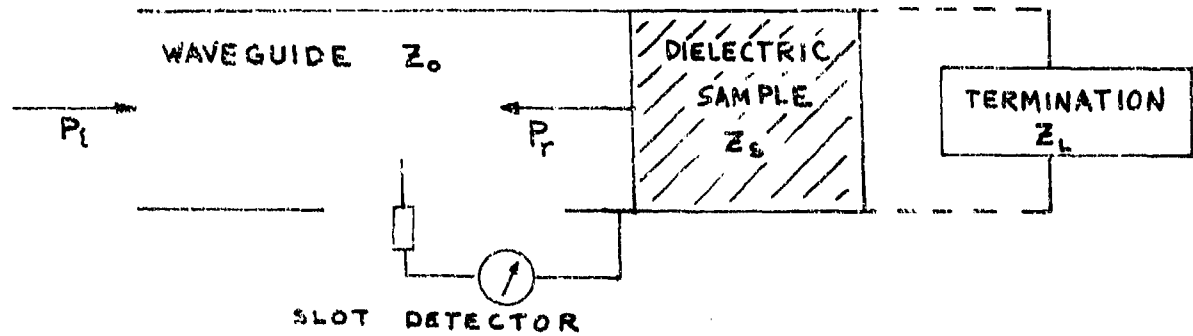


Figure 1. Impedance measurement method set-up.

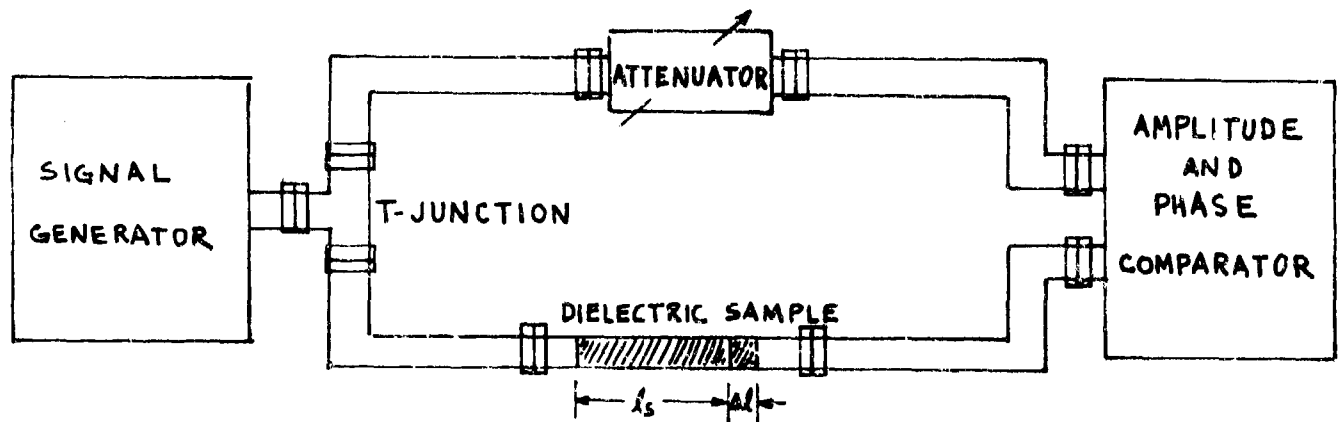


Figure 2. Propagation constant measurement method set-up.

but would have to be extended to cover the typically larger green wood loss factor values. This method is probably not as accurate as the incremental measurement method but undoubtedly is faster.

Before discussing specific applications to green wood, one last method will be introduced, particularly since it was used in the only identified source in which dielectric measurements of green wood were reported [8]. This is the "thin-sample method" and uses coax transmission cable, a slotted line detector, and a coax sample holder [6]. The method is an impedance measuring procedure and requires the sample to be thin enough to justify an approximation in the working expressions. In practice, this may limit samples to less than 1 mm. thickness. Since coax is used, the cut-off wavelength is infinite and the apparatus is suitable for much lower frequency bridge or resonant circuit measurements as well. In that case, the capacitance and conductance are measured for the entire holder and transformed to the sample by the appropriate line impedance expression.

Dielectric Constant Measurements of Green Wood, (.1 - 1 GHz)

This range of frequencies represents a difficult range in which to measure high-loss materials such as green wood. Most of the range is too high for resonant, lumped parameter circuits and yet below 1 GHz, distributed parameter hollow waveguides become too large to be practical. This tends to reduce the choice of a transmission line to coax and limits the available methods. Conventional "Short-sample" reflection methods are considered not as precise with high-loss material [1]. Attempts to employ a "long-sample" technique are not practical due to the difficulty in fabricating long sample sections to fit a coax holder. The "thin-sample" method avoids these difficulties. An objection raised with this method, however, is academic rather than systematic. Wood is known to have an anisotropic dielectric property with respect to direction of

the grain [2]. Since orientation of the electric field lines is radial from the center for coax propagating in the normal TEM mode, it is impossible to cut annular sections of wood which uniquely realize all three grain orientations. Only the radial grain alignment can be strictly realized with a transverse, cross-section cut. All other cuts end up with combination of longitudinal and tangential, or all three (see Figure 3). The experimenter wishing to distinguish the orientation effect on the dielectric constant will find the thin-sample method inadequate for this reason. However, if an application of the results is not strictly dependent on the orientation distinction, the method may be suitable.

One other difficulty encountered with the thin-sample method is the effect of an air gap between the sample and the inner and outer conductor surfaces. For high-loss materials, even the presence of very small air spaces constitutes a series impedance somewhat comparable to the sample impedance. The net result is a larger impedance than that due to the sample alone. A few methods for overcoming this problem have been tried. One is to actually calculate the air-gap effect and modify the working expressions to account for it [6]. This necessitates rather accurate measurements of the gap for each sample and the assumption that it is effectively uniform. Another method is to fill the sample holder with a known high-loss medium such as water and re-evaluate the impedance/admittance expressions for the new medium [7]. With the high-loss medium now filling the gap, the error is reduced. A disadvantage here, however, is a possible interaction of the sample with the medium. In the case of green wood, moisture content must be closely monitored and kept close to its natural state. When most any wood is submerged in water - even moist, green wood - the water is likely to be absorbed. There is also the possibility of a liquid such as water producing a leaching effect on the

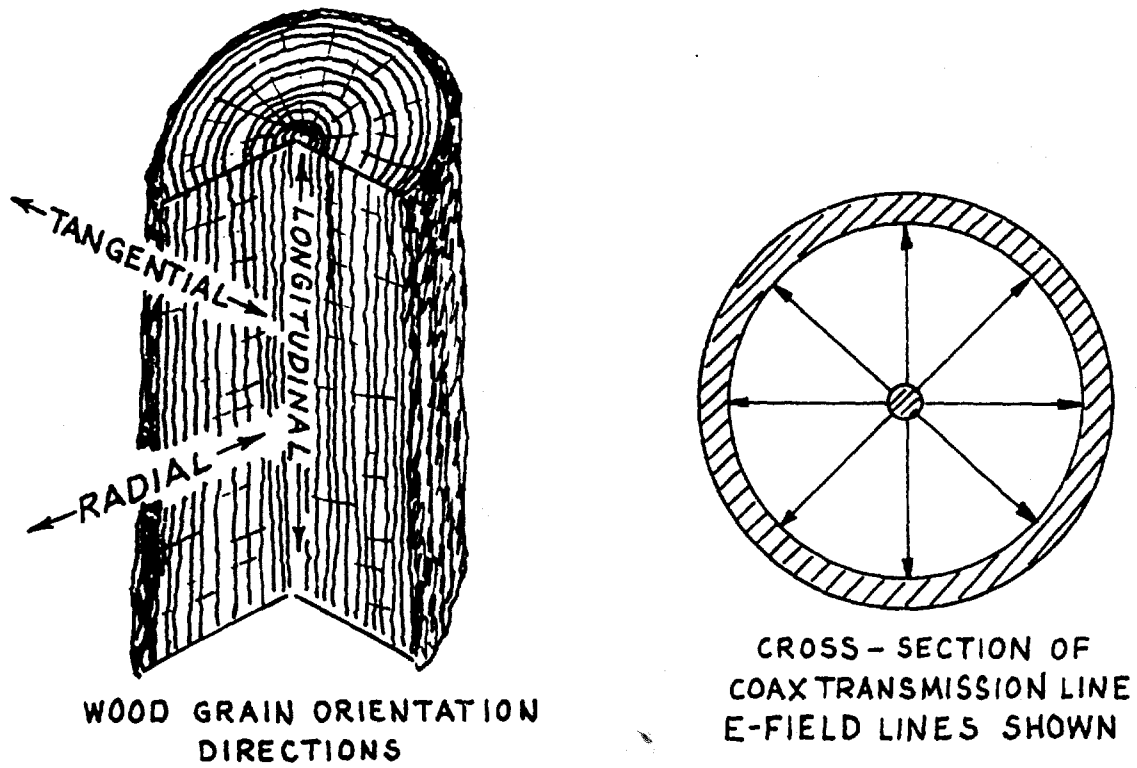


Figure 3. Wood grain directions compared with coax E-field lines direction.

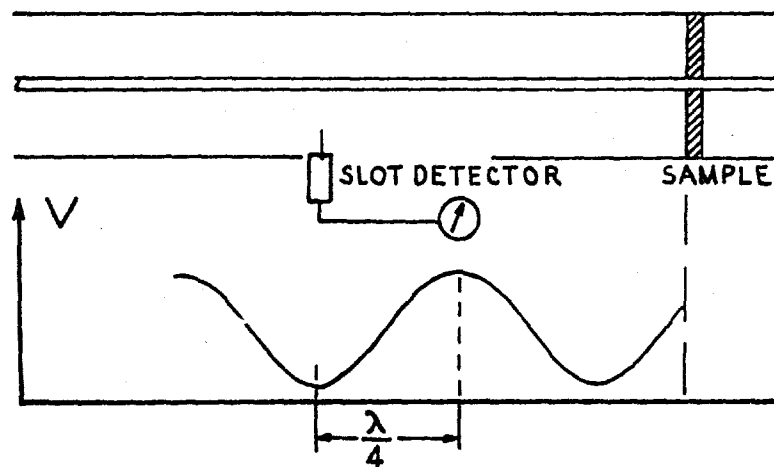


Figure 4. "Thin-Sample" method set-up and standing wave.

various soluble salts and minerals found in wood. If the sample were submerged long enough, its conduction and loss properties could be affected.

Since the difficulty lies in the imperfect contact, perhaps a more direct approach would correct the error sufficiently. By cutting and shaping the sample to as near the inside coax dimensions as possible, and enhancing electrical contact to the conductor surfaces with a thin coating of silver impregnated grease or gel, it would seem doubtful that any significant error would remain.

It should be mentioned that very thin samples will probably require the use of a supporting plug section. The material for the plug should be chosen to be virtually "transparent" at these frequencies. Polystyrene foam has been used successfully for this purpose [8].

In Figure 4, the sample is shown inserted in a coax line. The detector probe must travel at least one-quarter wavelength to determine the standing wave ratio necessary in the calculation of dielectric constant. This places a lower frequency limit on slotted line measurements at around .4 GHz for most equipment. Consequently, it would be necessary to employ a resonant circuit impedance method for the lower frequencies. The derived sample capacitance and conductance values would then be used to find permittivity and loss factor [8].

Dielectric Constant Measurements of Green Wood (1 - 40 GHz)

Between 1 - 4 GHz, coax experiences the onset of a higher propagation mode and this restricts use of the slotted line used in preceding measurements. The experimenter interested in observing most of the anomalous dispersion effect from water in green wood will need to carry out measurements to at least 35 - 40 GHz at room temperature. This will require the use of hollow waveguides and a different measurement method. It is, however, advantageous to

extend use of the coax method to as high a frequency as possible before encountering unacceptable error. This will eliminate the need for some of the larger waveguide sizes.

To cover the range from 4 - 40 GHz, several waveguide sizes must be selected. Actually, by using about five sizes, all frequencies can be covered under dominant mode conditions. This is probably not necessary since the general shape of the anomalous dispersion region of a material highly dominated by water is fairly easily modeled. (This topic is covered in Appendix D.) Only a distributed sampling of frequencies should be needed to construct a continuous curve throughout this region. At even higher frequencies, the dielectric constant of green wood is expected to become nearly constant and settle into its optical value.

When using hollow waveguide, the "long-sample" technique should be considered since it works better for high-loss materials. Milling sections of rectangular wood samples should not be difficult although moisture content must be closely monitored and kept at the natural state. The use of humidior storage and avoidance of prolonged exposure to dry air would be recommended. The problem of contact fit is not as critical as in the thin-sample method although the sections should fill the waveguide as completely as possible. If using the incremental cut and measure procedure, it is obviously easier to begin with the longest length and make cuts from there.

Equipment requirements, in addition to the waveguide, are a CW signal generator, variable attenuator, and a means of measuring amplitude and phase difference. The latter requirement can be realized with a two-channel vector voltmeter although it will probably be necessary to down-convert the signal to within the frequency range of the meter. A network analyzer supplemented with frequency extending test units can alone provide all the equipment requirements of this method, but its cost may be prohibitive.

Conclusion

Measurement of the dielectric constant of natural, green wood in the .1 - 40 GHz range will require several different test set-ups and methods. This may explain the apparent lack of reported data at these frequencies. But with increasing interest in UHF and microwave propagation through forest models, this information will be a required need.

These recommendations were based primarily upon tried and successful past techniques as reported in literature. This does not suggest that more modern or as yet untried methods are unsuitable. Such methods, however, tend to specialize in the materials they are used for which usually comprise very low-loss dielectrics. It would be highly desirable to investigate the development of in situ techniques for forest trees. This would eliminate the cutting and storage aspect and provide measurements in the intended natural, undisturbed state.

REFERENCES

1. Von Hippel, A. R., (ed.), Dielectric Materials and Applications, John Wiley & Sons, Inc., New York, 1954.
2. James, W. L., "Dielectric Properties of Wood and Hardboard: Variation with Temperature, Frequency, Moisture Content, and Grain Orientation," USDA Forest Service Res. Paper FPL 245, USDA Forest Products Lab., Madison, WI., 1975.
3. Peterson, R. W., "The Dielectric Properties of Wood," F.P.L. Tech. Note No. 16, Forest Products Laboratory of Canada, 1960.
4. Straiton, A. W., "Measurement of the Dielectric Properties of Soils and Water at 3.2 cm Wavelength," J. of Franklin Institute, 246, pp. 13-20, 1948.

REFERENCES (Cont'd.)

5. Collie, C. H., et al., "The Dielectric Properties of Water and Heavy Water," Proc. Physical Society (London), 60, pp. 145-160, 1948.
6. Conrad, E. E., et al., "Extension of the 'Thin-Sample Method' for the Measurement of Initial Complex Permeability and Permittivity," J. of App. Physics, 27, No. 4, pp. 346-350, 1956.
7. Gardiol, F. E., "Nomograms Save Time In Determining Permittivity," Micro-waves, pp. 68-70, November, 1973.
8. Broadhurst, M. G., "Complex Dielectric Constant and Dissipation Factor of Foliage," NBS Report 9592, 1970.

APPENDIX F

THE MEASUREMENT OF APPLICABLE FOLIAGE STATISTICS

Required Measurements

A set of statistics best describing a forest in quantitative terms is found in a complete forest stand table. This information is basic in forest management and necessary in any analysis concerned with a certain forest stand.

The propagation attenuation model for a forest medium requires several of these statistics. First, a count of trees per unit area is basic to the required fractional volume parameter. These data are usually categorized into trunk diameter classes. It is common to measure diameter at "breast height", (d.b.h.). In more extensive tables, the tree count may be further broken down by species. However, it is only necessary for the attenuation model to distinguish broad-leaved or needle-bearing types. From the count per area and tree type, the total wood volume may be estimated using tree-form volume models [1] (see Appendix C).

Total leaf volume is generally not available from stand tables. However, this quantity may be estimated for given trunk diameters (d.b.h.) using available leaf area and volume models [2, 3, and 4]. Total leaf volume may then be projected from the tree-count data. This kind of information is also of interest in forest management and research efforts since it has direct bearing on watershed properties.

More recently, it was found necessary to provide a further categorization of wood and leaf (biomass) data for the propagation attenuation model. It is required to know the distribution of volume according to its structural diameter. In other words, what percentage of total wood volume comprises components equal to or less than a given diameter. In practice this would be

determined for a range of discrete diameter class sizes. There is no clear way to categorize hardwood leaves by diameter, however, so this volume must be handled separately.

It is not a normal practice for forest surveys to provide this kind of wood volume distribution. There is, however, a fairly common practice of classifying wood as "saw timber". This amounts to providing estimates of the wood volume for all wood having a diameter greater than a standard such as 7 cm.

Measurement Difficulty

With knowledge of modern mensuration techniques and experienced personnel, a forest stand table can be readily generated. Different levels of statistical significance can be realized depending on the particular sampling scheme used. It is even possible that a 100% survey may be accomplished if the area of interest is not too great.

Data describing biomass volume versus diameter is not commonly obtained. The same techniques used in saw timber surveys, however, could be extended to include a wide range of diameter classes. The difficulty lies in the tedious and time consuming effort this would require on a wide scale. Before this is done, a preliminary study is recommended to determine the accuracy in assuming a common growth form for a given specie. If an acceptable estimate of the volume distribution for a given specie can be made based on tree-height, or possibly d.b.h., then a great deal of survey work is eliminated. It is possible, however, that such an assumption would require certain environmental stipulations as well. In other words, the volume distribution of wood may be too highly site dependent for each specie. It is well known that the site impacts tree growth considerably. The question is how much it alters the basic form of a specie and, consequently, its distribution of wood volume.

Techniques for Obtaining Wood Volume Vs. Diameter

Two procedures for gathering wood volume data will be mentioned. One is a destructive method and the other non-destructive. The first method is to cut the tree and determine its average green wood density [8]. The tree is then weighed whole or in parts and the volume given as;

$$\text{Volume} = \text{Weight}/\text{Density} \quad .$$

If the tree parts are separated into diameter size classes and then weighed, the volume may be obtained for each of these classes by the same relationship;

$$\text{Volume}_{\text{class}} = \text{Weight}_{\text{class}} / \text{Density}$$

Each of these class volume values would then comprise points on a distribution curve.

An alternative method is non-destructive. Actual hand measurements are taken from limbs with aluminum pole limb calipers. Bark Thickness is determined and subtracted out. The volume of most of the large tree parts is then directly computed. It is of course impractical to measure all the small branches and twigs this way. It may be possible, however, to simply estimate their contribution to the small diameter class or clip and weigh them.

The choice of these techniques may not be arbitrary. In some instances, it may not be possible to cut trees and the non-destructive method is the only recourse. Alternatively, if attenuation test measurements could be scheduled prior to a proposed site clearing, perhaps the cut and weight technique could be considered.

It is interesting to note that the U. S. Forest Service is currently sponsoring studies to test and develop a scheme for acquiring this kind of data from electromagnetic attenuation measurements [5, 6]. This approach is

the inverse of the immediate problem which is to obtain attenuation estimates from forest data.

Work Estimates

Ideally, experimental measurements would be conducted at a recently surveyed site. Examples of such sites would be managed commercial or private timberland and sections of state and national forests. It should be emphasized that recent data - certainly within the past 18 months - ought to be available to accurately describe the current growth status for the site.

If a survey is necessary, an estimate of the work involved in producing a 100% sample stand table for a one-acre stand is one full work day for two experienced men [7]. This is 16 man-hours per acre for a 100% sample. Any of the random sample schemes would require less time in the field, however, the computational time would increase. Site parameters, weather, and other such factors will affect the time required.

The estimate given above is for a standard stand table only and does not include volume distribution data. As mentioned, techniques used in total biomass or saw-timber surveys could be extended to include several diameter class sizes. Again, a two man crew is ordinarily sufficient. No work estimate can be given since the additional effort involved in categorizing several diameter classes is not a normal practice.

REFERENCES

1. Assman, E., The Principles of Forest Yield Study, Pergamon Press, New York, 1970.
2. Rothacher, J. S., Blow, F. E., Potts, S. M., "Estimating the Quantity of Tree Foliage in Oak Stands in the Tennessee Valley," J. of Forestry, pp. 169-173, November, 1954.

REFERENCES (Cont'd.)

3. Kittredge, J., "Estimation of the Amount of Foliage of Trees and Stands," J. of Forestry, 42, pp. 905-912, 1944.
4. Kozlowski, T. T., Schumacher, F. X., "Estimation of Stomated Foliar Surface of Pines," Plant Physiology, 18, pp. 122-127, 1943.
5. Crawford, H. S., "Sampling Weight of Pine Foliage and Twigs by Microwave Signal Attenuation," USDA Forest Service Res. Note SE-225, S. E. Forest Experiment Station, Asheville, North Carolina, July, 1975.
6. Stutzman, W. L., Colliver, F. W., and Crawford, H. S., "Microwave Transmission Measurements for Estimation of the Weight of Standing Pine Trees," IEEE Trans. Antennas & Propg., AP-27, pp. 22-26, January, 1979.
7. Personal Communication Herb Knight, Resource Analyst, S. E. Forest Experiment Station, U. S. Forest Service, Asheville, N. C.
8. Smith, D. M., "Maximum Moisture Content Method For Determining Specific Gravity of Small Wood Samples," U. S. Forest Service, Forest Products Lab. Rep. 2014, 1954.